Jürgen Berje
Physico-Chemical Properties of Mixtures Containing Formaldehyde, Water, and Butynediol
Scientific Report Series Volume 49
2024

Scientific Report Series
Laboratory of Engineering Thermodynamics (LTD)
Rheinland-Pfälzische Technische Universität Kaiserslautern-Landau
P.O. Box 3049
67653 Kaiserslautern
Germany

ISSN 2195-7606
ISBN 978-3-944433-48-6

Physico-Chemical Properties of Mixtures Containing Formaldehyde, Water, and Butynediol

Vom Fachbereich Maschinenbau und Verfahrenstechnik
der Rheinland-Pfälzischen Technischen Universität Kaiserslautern-Landau
zur Verleihung des akademischen Grades

Doktor-Ingenieur (Dr.-Ing.)

genehmigte

Dissertation

von

M. Sc. Jürgen Berje
aus Bremerhaven

Dekan:	Prof. Dr. rer. nat. Roland Ulber
Berichterstatter:	Prof. Dr.-Ing. Hans Hasse
	Prof. Dr.-Ing. Jakob Burger

Tag der mündlichen Prüfung: 24.05.2024

D 386

„It's very hard to talk quantum using a language that was originally designed to tell other monkeys where the ripe fruit is.“

Terry Pratchett

Danksagung

Diese Arbeit entstand während meiner Tätigkeit als wissenschaftlicher Mitarbeiter am Lehrstuhl für Thermodynamik der Technischen Universität Kaiserslautern. Ich möchte an dieser Stelle allen danken, die mit ihrer Unterstützung zum Gelingen dieser Arbeit beigetragen haben.

Ganz besonderen Dank möchte ich meinem Doktorvater Prof. Dr.-Ing. Hans Hasse aussprechen. Für die Aufnahme ins Team, für die wunderschönen Jahre am Lehrstuhl und natürlich für die Zeit, die du in meine Ausbildung investiert hast.

Ich danke Prof. Dr.-Ing. Jakob Burger und Prof. Dr.-Ing. Erik von Harbou für die vielen tollen fachlichen Diskussionen und für ihre Rollen als Berichterstatter bzw. Prüfungskommissionsvorsitzender.

Für die finanzielle Unterstützung des Projekts danke ich der BASF.

Großen Dank an die damals Studierenden, die durch ihre Mitarbeit am Projekt beigetragen haben: Markus Kolano, Natalia Urich, Nikolas Krüger und Ellen Steimers.

Vielen lieben Dank auch an das Laborteam: Kirsten Brunn, Nicole Hevert, Tanja Breug-Nissen, Berthold Mrawek und Julian Peter.

Ebenso lieb möchte ich an dieser Stelle auch dem Sekretariat danken, dass immer alles so reibungslos wie möglich funktioniert hat: Monika Reim, Caro Hofmann, Ilona Stein, Jennifer Bergmann und Marlies Mangold.

Daniel Fröscher danke ich für die herausragende Unterstützung bei IT-Angelegenheiten.

Allen anderen Kollegen, die mich während meiner Zeit am LTD begleitet haben, möchte ich ebenso ganz herzlich für sowohl die vielen fachlichen als auch die vielen sozialen Events danken. Es war eine ganz tolle Zeit mit euch allen!

Hanau, 17.02.2024

Jürgen Berje

Abstract

Liquid mixtures of formaldehyde, water, and butynediol are complex multicomponent systems, since formaldehyde forms oligomers with both water and butynediol. NMR spectroscopy was used to determine the species distribution in these mixtures, and the ^{1}H and ^{13}C-NMR spectra of the ternary system were fully assigned.

Two models of the chemical equilibrium in these mixtures were developed: one based on mole fractions and one based on activities. Both models rely on quantitative ^{13}C-NMR spectroscopic data of the species distribution. The experimental conditions ranged from 293 K to 366 K in temperature, from 0.10 g g^{-1} to 0.27 g g^{-1} in overall formaldehyde mass fraction, and from 0.05 g g^{-1} to 0.50 g g^{-1} in overall butynediol mass fraction.

A predictive model of the physico-chemical equilibrium was derived and validated from the activity-based model of the chemical equilibrium. Vapor-liquid equilibrium measurements in mixtures of formaldehyde, water, and butynediol were conducted at 393 K and 413 K for the validation, with formaldehyde mass fractions from 0.1 g g^{-1} to 0.2 g g^{-1} and butynediol mass fractions from 0.05 g g^{-1} to 0.35 g g^{-1}. Residue curves were computed to illustrate the distillation behavior of the system.

A reaction kinetic model of the reactions of formaldehyde and butynediol was established from ^{1}H-NMR spectra obtained after mixing aqueous solutions of formaldehyde and butynediol, extending the equilibrium model. The experiments were performed in simple NMR tubes, as well as in a special micro-mixer NMR probe. The new reaction kinetic data spanned temperatures from 293 K to 328 K and pH values from 3 to 6. Moreover, the data base of reaction kinetic data for the reactions of formaldehyde and water was expanded to faster kinetics.

Kurzfassung

Mischungen aus Formaldehyd, Wasser und Butindiol sind komplexe Mehrkomponentensysteme, in denen Formaldehyd sowohl mit Wasser als auch mit Butindiol Oligomere bildet. Mit Hilfe der NMR-Spektroskopie wurde die Speziesverteilung in diesen Mischungen bestimmt, und die Signale in den ^{1}H- und ^{13}C-NMR-Spektren des ternären Systems wurden vollständig zugeordnet.

Es wurden zwei Modelle für das chemische Gleichgewicht in diesen Mischungen entwickelt: eines auf der Grundlage von Molenbrüchen und eines auf der Grundlage von Aktivitäten. Beide Modelle wurden auf Basis von quantitativen ^{13}C-NMR-spektroskopischen Daten der Speziesverteilung entwickelt. Die Versuchsbedingungen lagen im Temperaturbereich von 293 K bis 366 K, mit Formaldehydanteilen von 0,10 g g^{-1} bis 0,27 g g^{-1} und mit Butindiolanteilen von 0,05 g g^{-1} bis 0,50 g g^{-1}.

Aus dem aktivitätsbasierten Modell des chemischen Gleichgewichts wurde ein Vorhersagemodell des physikalisch-chemischen Gleichgewichts abgeleitet und validiert. Für die Validierung wurden Dampf-Flüssigkeits Gleichgewichtsmessungen in Mischungen aus Formaldehyd, Wasser und Butindiol bei 393 K und 413 K durchgeführt, mit Formaldehydanteilen von 0,1 g g^{-1} bis 0,2 g g^{-1} und Butindiolanteilen von 0,05 g g^{-1} bis 0,35 g g^{-1}. Es wurden Rückstandslinien berechnet, um das Destillationsverhalten des Systems zu veranschaulichen.

Anhand von ^{1}H-NMR-Spektren, die nach dem Mischen von wässrigen Lösungen von Formaldehyd und Butindiol erhalten wurden, wurde ein reaktionskinetisches Modell für die Reaktionen von Formaldehyd und Butindiol erstellt, das das Gleichgewichtsmodell erweitert und komplettiert. Die Experimente wurden sowohl in einfachen NMR-Röhrchen als auch in einem speziellen Mikromischer-Probenkopf durchgeführt. Die neuen reaktionskinetischen Daten umfassten Temperaturen von 293 K bis 328 K und pH-Werte von 3 bis 6. Darüber hinaus wurde die verfügbare Datenbasis der reaktionskinetischen Daten für die Reaktionen von Formaldehyd und Wasser um schnellere Kinetiken erweitert.

Contents

1 Introduction

Formaldehyde is a highly reactive C1 building block that is widely used in the chemical industry. One of its applications is the synthesis of butynediol, an important intermediate in the C4 value added chain. Butynediol is produced by reacting acetylene with aqueous formaldehyde solution (Reppe chemistry [52]), resulting in a mixture of butynediol, water, and formaldehyde. To purify butynediol, formaldehyde has to be separated from this mixture, usually by distillation. However, this process is complicated by the fact that formaldehyde forms oligomers both with water and with butynediol, affecting the vapor-liquid equilibrium behavior of the system. Therefore, modeling the properties and behavior of this system requires accounting for the oligomerization of formaldehyde. This is essential for designing and optimizing the production processes of butynediol and its derivatives.

Previous works [2, 5, 26, 29, 30, 33, 35, 41, 43, 48, 53] have already established a clear understanding of the reactions between formaldehyde and water. Models exist for calculating the distribution of species in chemical equilibrium, as well as for the time-dependent behavior after disturbing the equilibrium. These models are available based on both mole fractions and activities. While the mole fraction-based models are easy to implement and describe the species distribution in the liquid phase equally well, the activity-based models can be used to describe vapor-liquid equilibria in a thermodynamically consistent manner.

The objective of this work is to develop an understanding of the species present in the ternary system as well as their quantification under equilibrium conditions and after its disturbance. Prior to this study, equilibrium models for reactions of formaldehyde with monoalcohols such as methanol [29, 30, 33, 48] and 1-butanol [18] as well as some equilibrium data for the reactions of ethylene glycol [8] with formaldehyde were available in the literature. Reactions of formaldehyde with butynediol have never been investigated before.

For the quantification of the formaldehyde oligomers, NMR spectroscopy is the preferred method [8, 22, 26, 29, 30, 43, 45, 50, 53, 56, 58] because the species cannot be isolated and the spectrometer does not require calibration, as the signal areas are directly proportional to the number of nuclei responsible for the signals.

This work is structured into five chapters, the first being this introduction and the last being Chapter 5 showing the conclusions that were drawn from the results of this work. Chapter 2 deals with the elucidation of the occuring species in the ternary mixtures of formaldehyde, water, and butynediol. A complete assignment of the signals in the ^{1}H- and ^{13}C-NMR spectra to the components occuring in the system is provided. Based on quantitative ^{13}C-NMR spectra, a model of the species distribution under equilibrium conditions has been developed.

Chapter 3 presents the development of a predictive physico-chemical model of the vapor-liquid equilibrium in ternary mixtures of formaldehyde, water, and butynediol. The model was developed based on the findings in Chapter 2. The model is validated by experiments using a special type of thin-film evaporator. Calculated residue curves are shown which allow conceptual feasibility studies for distillation processes involving formaldehyde, water, and butynediol.

In Chapter 4, the investigations of the reaction kinetics in mixtures of formaldehyde, water, and butynediol are described. The resulting reaction kinetic model is based on ^{1}H-NMR spectra that were taken after mixing a concentrated aqueous formaldehyde solution with an aqueous butynediol solution.

2 Chemical Equilibrium

2.1 Introduction

In this chapter, the studies of the chemical reactions between formaldehyde and butynediol are described. As butynediol is solid at ambient temperature and water-free mixtures of formaldehyde and butynediol are difficult to prepare and to handle, all experiments were performed in the ternary system formaldehyde + water + butynediol. The ^{1}H- and ^{13}C-NMR spectra of these mixtures are elucidated and chemical equilibrium constants for the reactions of formaldehyde with butynediol are determined from quantitative ^{13}C-NMR spectroscopic investigations of the species distribution.

2.2 Chemical reaction system

In the system formaldehyde + water + butynediol, both water and butynediol undergo formaldehyde addition reactions. The reactions occur in acidic, neutral, and basic environment without requiring catalysts. Formaldehyde (FA) and water (W) yield methylene glycol (MG_1) [61]:

$$\underbrace{CH_2O}_{\text{FA}} + \underbrace{H_2O}_{\text{W}} \overset{K_{MG_1}}{\rightleftharpoons} \underbrace{HO(CH_2O)H}_{MG_1} \tag{I}$$

Poly(oxymethylene) glycols (MG_n) are formed in further reactions [61]:

$$\underbrace{CH_2O}_{\text{FA}} + \underbrace{HO(CH_2O)_{n-1}H}_{MG_{n-1}} \overset{K_{MG_n}}{\rightleftharpoons} \underbrace{HO(CH_2O)_nH}_{MG_n} \tag{II}$$

Due to the presence of two hydroxyl groups and the butynylene group in butynediol the addition to the carbonyl group of formaldehyde yields poly(oxymethylene) hemiformals of the general structure

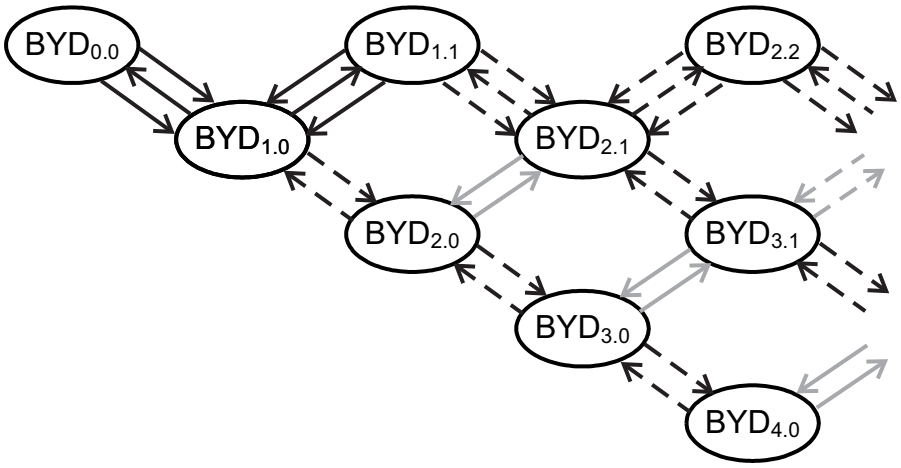

Figure 1: Oligomerization reactions of butynediol with formaldehyde yielding poly(oxymethylene) hemiformal. (—) addition of a vacant butynediol hydroxyl group to formaldehyde, (- -) chain propagation reactions, black arrows: independent set of chemical reactions, gray arrows: dependent reactions.

$$\mathrm{H{-}(OCH_2)_{\mathit{n}}{-}O{-}CH_2{-}C{\equiv}C{-}CH_2{-}O{-}(CH_2O)_{\mathit{m}}{-}H}$$

which are labeled here as $\mathrm{BYD}_{n.m}$. $\mathrm{BYD}_{0.0}$ is butynediol and no oligomer. $\mathrm{BYD}_{n.m}$ and $\mathrm{BYD}_{m.n}$ are the same molecule. In the following the convention $\mathrm{BYD}_{n.m}$ with $n \geq m$ is used to label that species.

Figure 1 shows a mechanistic picture of the oligomerization reactions in the system formaldehyde + butynediol. $\mathrm{BYD}_{0.0}$ can react with formaldehyde on both ends yielding $\mathrm{BYD}_{1.0}$. In the reverse reaction there is only one way to form $\mathrm{BYD}_{0.0}$ from $\mathrm{BYD}_{1.0}$, namely by cleavage of the only $\mathrm{CH_2O}$ group. The number of possible reaction sites for each reaction is shown by the number of arrows. $\mathrm{BYD}_{1.0}$ can react with formaldehyde yielding $\mathrm{BYD}_{2.0}$ or $\mathrm{BYD}_{1.1}$ depending on whether the occupied or the non-occupied end adds to formaldehyde. In the reverse reactions there is one way from $\mathrm{BYD}_{2.0}$ to form $\mathrm{BYD}_{1.0}$, but there are two ways from $\mathrm{BYD}_{1.1}$ to form $\mathrm{BYD}_{1.0}$. This argument can be continued, cf. Figure 1.

Formally two types of reactions are distinguished: 1) the addition of an unoccupied end to formaldehyde (solid arrows in Figure 1) with the general equation

$$\underbrace{CH_2O}_{\text{FA}} + \underbrace{H\text{–}(OCH_2)_n\text{–}O\text{–}CH_2\text{–}C{\equiv}C\text{–}CH_2\text{–}OH}_{\text{BYD}_{n.0}} \xrightleftharpoons{K_{n.0\leftrightarrow n.1}} \underbrace{H\text{–}(OCH_2)_n\text{–}O\text{–}CH_2\text{–}C{\equiv}C\text{–}CH_2\text{–}O\text{–}CH_2\text{–}OH}_{\text{BYD}_{n.1}} \tag{III}$$

and 2) the addition of an occupied end to formaldehyde (dashed arrows in Figure 1) with the general equation

$$\underbrace{CH_2O}_{\text{FA}} + \underbrace{H\text{–}(OCH_2)_{n-1}\text{–}O\text{–}CH_2\text{–}C{\equiv}C\text{–}CH_2\text{–}O\text{–}(CH_2O)_m\text{–}H}_{\text{BYD}_{n-1.m}} \xrightleftharpoons{K_{n-1.m\leftrightarrow n.m}} \underbrace{H\text{–}(OCH_2)_n\text{–}O\text{–}CH_2\text{–}C{\equiv}C\text{–}CH_2\text{–}O\text{–}(CH_2O)_m\text{–}H}_{\text{BYD}_{n.m}} \tag{IV}$$

In these equations, the subscript of the chemical equilibrium constant $K_{n-1.m\leftrightarrow n.m}$ denotes which molecules are involved in the reactions. Obviously n and m can be exchanged so that $K_{n-1.m\leftrightarrow n.m}$ is equal to $K_{m.n-1\leftrightarrow m.n}$.

In the following, a mole fraction-based model for the calculation of the species distribution in the system formaldehyde + water + butynediol is presented. A corresponding activity-based model is given in the Supporting Information. The chemical equilibrium constants of the Reactions (I) to (IV) are expressed using mole fractions x_i:

$$K^x_{\text{MG}_1} = \frac{x_{\text{MG}_1}}{x_{\text{W}} \cdot x_{\text{FA}}} \tag{1}$$

$$K^x_{\text{MG}_n} = \frac{x_{\text{MG}_n}}{x_{\text{MG}_{n-1}} \cdot x_{\text{FA}}} \quad \text{for} \quad n \geq 2 \tag{2}$$

$$K^x_{n.0\leftrightarrow n.1} = \frac{x_{\text{BYD}_{n.1}}}{x_{\text{BYD}_{n.0}} \cdot x_{\text{FA}}} \quad \text{for} \quad n \geq 0 \tag{3}$$

$$K^x_{n-1.m\leftrightarrow n.m} = \frac{x_{\text{BYD}_{n.m}}}{x_{\text{BYD}_{n-1.m}} \cdot x_{\text{FA}}} \quad \text{for} \quad n \geq 2 \wedge m \geq 0 \tag{4}$$

The enumeration chosen here for the reactions of butynediol with formaldehyde (Eqs. (3) and (4)) is complete as there is a complete symmetry between the species, i.e no difference between $\text{BYD}_{n.m}$ and $\text{BYD}_{m.n}$. According to Hess' Law not all of these equations are independent. In Figure 1 one possible choice of independent reactions is indicated. The reactions which are not needed for equilibrium calculations are labeled with gray arrows.

The chemical equilibrium constants $K^x_{n.0\leftrightarrow n.1}$ and $K^x_{n-1.m\leftrightarrow n.m}$ represent equilibria of the types 1) and 2) described above. In the present work only two constants $K^x_{\mathrm{BYD},1}$ and $K^x_{\mathrm{BYD},2}$ will be determined from the experimental data. All $K^x_{n.0\leftrightarrow n.1}$ and $K^x_{n-1.m\leftrightarrow n.m}$ will be related in the following to these two constants. The relation is non-trivial as the number of ways in which a certain compound can be formed may differ for the different reactions, cf. Figure 1.

Generally, chemical equilibrium constants are the ratio of the rate constant of the forward reaction k^+ to the rate constant of the reverse reaction k^-, in this case

$$K^x_{\mathrm{BYD},1} = \frac{k^{+,x}_{\mathrm{BYD},1}}{k^{-,x}_{\mathrm{BYD},1}} \qquad \text{and} \qquad K^x_{\mathrm{BYD},2} = \frac{k^{+,x}_{\mathrm{BYD},2}}{k^{-,x}_{\mathrm{BYD},2}} \tag{5}$$

It is assumed that on the molecular level the rate constants of forward or backward reactions involving BYD species only depend on the type of the hydroxyl group which adds to formaldehyde or is formed by cleavage respectively. That assumption will be justified later by the experiments. For a later comparison with other alcohols containing only one hydroxyl group the chemical equilibrium constants $K^x_{\mathrm{BYD},1}$ and $K^x_{\mathrm{BYD},2}$ are related to a reaction of one hydroxyl group with formaldehyde. As $\mathrm{BYD}_{0.0}$ contains two equal hydroxyl groups, the rate constant for the formation of $\mathrm{BYD}_{1.0}$ from $\mathrm{BYD}_{0.0}$ is twice as large as the rate constant for the formation of $\mathrm{BYD}_{1.1}$ out of $\mathrm{BYD}_{1.0}$ which has only one vacant hydroxyl group. Following the same argument, the cleavage of one formaldehyde from $\mathrm{BYD}_{1.1}$ yielding $\mathrm{BYD}_{1.0}$ is twice as fast as the cleavage of one formaldehyde from $\mathrm{BYD}_{1.0}$ yielding $\mathrm{BYD}_{0.0}$. This results in

$$K^x_{0.0\leftrightarrow 1.0} = \frac{2 \cdot k^{+,x}_{\mathrm{BYD},1}}{1 \cdot k^{-,x}_{\mathrm{BYD},1}} = 2 \cdot K^x_{\mathrm{BYD},1} \tag{6}$$

$$K^x_{1.0\leftrightarrow 1.1} = \frac{1 \cdot k^{+,x}_{\mathrm{BYD},1}}{2 \cdot k^{-,x}_{\mathrm{BYD},1}} = \frac{1}{2} \cdot K^x_{\mathrm{BYD},1} \tag{7}$$

Consequently, the chemical equilibrium constants for the reactions of $\mathrm{BYD}_{n.m}$ with formaldehyde are derived from $K^x_{\mathrm{BYD},1}$ and $K^x_{\mathrm{BYD},2}$ respectively by using prefactors which depend on molecule symmetry. The equations used here for the calculation of the

chemical equilibrium constants in the system formaldehyde + butynediol are as follows:

$$K^x_{n.0\leftrightarrow n.1} = 2 \cdot K^x_{\mathrm{BYD},1} \quad \text{for} \quad n = 0 \tag{8}$$

$$K^x_{n.0\leftrightarrow n.1} = \frac{1}{2} \cdot K^x_{\mathrm{BYD},1} \quad \text{for} \quad n = 1 \tag{9}$$

$$K^x_{n.0\leftrightarrow n.1} = 1 \cdot K^x_{\mathrm{BYD},1} \quad \text{for} \quad n \geq 2 \tag{10}$$

$$K^x_{n-1.m\leftrightarrow n.m} = 2 \cdot K^x_{\mathrm{BYD},2} \quad \text{for} \quad (n-1=m) \wedge (m \geq 1) \tag{11}$$

$$K^x_{n-1.m\leftrightarrow n.m} = \frac{1}{2} \cdot K^x_{\mathrm{BYD},2} \quad \text{for} \quad (n=m) \wedge (m \geq 2) \tag{12}$$

$$K^x_{n-1.m\leftrightarrow n.m} = 1 \cdot K^x_{\mathrm{BYD},2} \quad \text{for} \quad (n-2 \geq m) \wedge (m \geq 0) \tag{13}$$

These considerations can also be transferred to the formation of poly(oxymethylene) glycols in the system formaldehyde + water in Reactions (I) and (II). But as water and all the poly(oxymethylene) glycols are symmetric, the prefactors cancel out. As shown later, a direct comparison of chemical equilibrium constants with the ones of water, butynediol, and other alcohols with one hydroxyl group is however possible.

2.3 Experiments

2.3.1 Chemicals

Aqueous stock solutions of formaldehyde were prepared by dissolving paraformaldehyde (95-100 %, Merck) in ultrapure water at elevated temperature. A detailed procedure is described by Hasse [33]. The ultrapure water was produced by a Milli-Q integral water purification system from MerckMillipore, Darmstadt, Germany. Butynediol (99 %, Sigma-Aldrich) was purified by recrystallization with diethyl ether from ethyl acetate as described by Pyatnitsyna *et al.* [51].

2.3.2 Experimental setup

All experiments were carried out in sealed 5 mm pressure resistant NMR tubes from WILMAD, Vineland, NJ, USA to avoid loss of substance during the experiments. A 399.83 MHz proton resonance frequency NMR spectrometer (Unity Inova 400, Varian, Palo Alto, USA) equipped with a Varian 400 AutoSW PFG 4 nuclei probe head was used to acquire NMR spectra. The temperature measurement in the spectrometer was calibrated by chemical shift difference with methanol and ethylene glycol respectively [7].

Quantitative $^{13}C\{^1H\}$-NMR spectra were acquired with an inverse gated decoupling sequence to avoid the nuclear Overhauser effect. The following acquisition parameters

Table 1: Overall mass fractions of the samples used for the chemical equilibrium measurements.

Sample	$\tilde{x}_{\mathrm{FA}}^{(\mathrm{m})}$ / g g^{-1}	$\tilde{x}_{\mathrm{W}}^{(\mathrm{m})}$ / g g^{-1}	$\tilde{x}_{\mathrm{BYD}}^{(\mathrm{m})}$ / g g^{-1}
I	0.27	0.63	0.10
II	0.21	0.49	0.30
III	0.15	0.35	0.50
IV	0.19	0.76	0.05
V	0.18	0.72	0.10
VI	0.16	0.64	0.20
VII	0.14	0.56	0.30
VIII	0.10	0.40	0.50

were chosen: acquisition time 5 s, relaxation delay 80 s, pulse width 90°, 512 scans or more. The longest T_1-time in the system was determined to be about 9.6 s by inversion recovery experiments and hence well below the chosen relaxation delay.

2.3.3 Sample preparation and experimental program

Ternary mixtures of formaldehyde, water, and butynediol were prepared gravimetrically from an aqueous formaldehyde stock solution and recrystallized butynediol using a precision balance (Mettler Toledo XS603S, Greifensee, Switzerland). The formaldehyde content in the stock solution was determined titrimetrically by the Na_2SO_3 method [61]. About 0.7 ml of the liquid mixture were filled into the NMR tube. Prior to spectra acquisition, the tube was stored in the spectrometer for at least 10 h at the desired temperature to equilibrate the mixture.

Quantitative ^{13}C-NMR spectra were acquired at 293 K, 315 K, 339 K, and 366 K. Overall mass fractions of formaldehyde cover the range from 0.10 g g^{-1} to 0.27 g g^{-1}, mass fractions of butynediol from 0.05 g g^{-1} to 0.50 g g^{-1}. An overview of the studied samples is given in Table 1. The temperature range resulted from experimental limits, the concentration ranges were motivated by the concentrations at which industrial butynediol processes operate.

2.3.4 Peak assignment

For the analysis of the NMR spectra, all hydrogen and carbon signals were assigned. Quantitative ^{1}H- and ^{13}C-NMR spectra were acquired for mixtures with different formaldehyde and butynediol concentrations. These spectra allow a first grouping of signals to

different molecules, especially in the ^{13}C-NMR spectra. The position of the corresponding nuclei in the molecules and the oligomer chain lengths were determined by additional HSQC and HMBC sequences. Furthermore one experiment with formaldehyde-^{13}C,d_2 in D_2O was carried out to establish an assignment of the triple-bonded carbon nuclei. A comprehensive overview of signal assignments is given in Tables 2 and 3.

Table 2: ^{1}H chemical shifts for a mixture of formaldehyde, water, and butynediol ($\tilde{x}_{\mathrm{FA}}^{(\mathrm{m})}$ = 0.27 g g^{-1}, $\tilde{x}_{\mathrm{W}}^{(\mathrm{m})}$ = 0.53 g g^{-1}, $\tilde{x}_{\mathrm{BYD}}^{(\mathrm{m})}$ = 0.20 g g^{-1}, T = 293 K, pH = 6.82, reference: TMSP). An explanation of the nomenclature used for the peak assignment is given in the text.

^{1}H (400.40 MHz)	
δ / ppm	assignment
4.28 (s)	${}^{\beta}\mathrm{H}^{\beta}_{\mathrm{BYD}_{0.0}}$
4.29 (t, ^5J = 1.8 Hz)	$\mathrm{H}^{\beta}_{\mathrm{BYD}_{1.0}}$
4.28-4.30 (m)	$\mathrm{H}^{\beta}_{\mathrm{BYD}_{n.0}}$, $n \geq 2$
4.34-4.38 (m)	${}^{\beta}\mathrm{H}^{\beta}_{\mathrm{BYD}_{n.m}}$, $n, m \geq 1$
4.35 (t, ^5J = 1.8 Hz)	${}^{\beta}\mathrm{H}_{\mathrm{BYD}_{1.0}}$
4.36 (s)	${}^{\beta}\mathrm{H}^{\beta}_{\mathrm{BYD}_{1.1}}$
4.83 (s)	${}^{1}\mathrm{H}_{\mathrm{MG}_1}$
4.85 (s)	$\mathrm{H}^{1}_{\mathrm{BYD}_{n.1}}$, $n \geq 0$
4.88-4.89 (m)	${}^{1}\mathrm{H}_{\mathrm{MG}_n}$, $n \geq 3$
	${}^{n}\mathrm{H}_{\mathrm{BYD}_{n.m}}$, $n \geq 2,\ m \geq 0$
4.89 (s)	${}^{1}\mathrm{H}_{\mathrm{MG}_2}$
4.91 (s)	$\mathrm{H}^{1}_{\mathrm{BYD}_{n.m}}$, $n \geq 0,\ m \geq 3$
4.92 (s)	$\mathrm{H}^{1}_{\mathrm{BYD}_{n.2}}$, $n \geq 0$
4.93-4.96 (m)	${}^{i}\mathrm{H}_{\mathrm{MG}_n}$, $n \geq 3,\ n/2+1 > i \geq 2$
	${}^{j}\mathrm{H}_{\mathrm{BYD}_{n.m}}$, $n \geq 3,\ m \geq 0,\ n > j \geq 2$

A ^{1}H- and a ^{13}C-NMR spectrum of an example mixture containing formaldehyde, water, and butynediol is shown in Figure 2 together with the used nomenclature for the labeling of carbon nuclei. The nomenclature used for the peak assignment is explained in the following, cf. also Figure 2. The superscript α labels carbon in the ethynylene (–C≡C–) group. The superscript β labels methylene groups next to the ethynylene group. Superscript arabic numbers indicate methylene groups in the CH_2O chain on both sides of the ethynylene group. The position of the superscript differentiates the location of the nuclei in $\mathrm{BYD}_{n.m}$. A superscript on the left side stands for the n-side of the molecule, a superscript on the right side for the m-side. These sides are in principle equivalent as exchanging all corresponding indices does not change the molecule. But in unsymmetrical molecules it matters on which side a specific group is located. A detailed discussion of the peak assignment is given in the Supporting Information.

Table 3: ^{13}C chemical shifts for a mixture of formaldehyde, water, and butynediol ($\tilde{x}_{\mathrm{FA}}^{(\mathrm{m})}$ = 0.27 g g^{-1}, $\tilde{x}_{\mathrm{W}}^{(\mathrm{m})}$ = 0.53 g g^{-1}, $\tilde{x}_{\mathrm{BYD}}^{(\mathrm{m})}$ = 0.20 g g^{-1}, T = 293 K, pH = 6.82, reference: TMSP). An explanation of the nomenclature used for the peak assignment is given in the text.

^{13}C (100.68 MHz)			
δ / ppm	assignment	δ / ppm	assignment
52.34	$\mathrm{C}^{\beta}_{\mathrm{BYD}_{n.0}}$, $n \geq 2$	85.05	$\mathrm{C}^{\alpha}_{\mathrm{BYD}_{n.1}}$, $n \geq 4$
52.36	$\mathrm{C}^{\beta}_{\mathrm{BYD}_{1.0}}$	86.13	${}^{\alpha}\mathrm{C}^{\alpha}_{\mathrm{BYD}_{0.0}}$
52.39	${}^{\beta}\mathrm{C}^{\beta}_{\mathrm{BYD}_{0.0}}$	87.41	$\mathrm{C}^{\alpha}_{\mathrm{BYD}_{1.0}}$
56.76	$\mathrm{C}^{\beta}_{\mathrm{BYD}_{n.1}}$, $n \geq 2$	87.75	$\mathrm{C}^{\alpha}_{\mathrm{BYD}_{2.0}}$
56.79	${}^{\beta}\mathrm{C}^{\beta}_{\mathrm{BYD}_{1.1}}$	87.81	$\mathrm{C}^{\alpha}_{\mathrm{BYD}_{3.0}}$
56.83	${}^{\beta}\mathrm{C}_{\mathrm{BYD}_{1.0}}$	87.84	$\mathrm{C}^{\alpha}_{\mathrm{BYD}_{n.0}}$, $n \geq 4$
57.45	${}^{\beta}\mathrm{C}^{\beta}_{\mathrm{BYD}_{2.2}}$	88.27	${}^{1}\mathrm{C}_{\mathrm{MG}_2}$
	$\mathrm{C}^{\beta}_{\mathrm{BYD}_{n.2}}$, $n \geq 3$	88.80	${}^{1}\mathrm{C}_{\mathrm{MG}_3}$
57.48	${}^{\beta}\mathrm{C}_{\mathrm{BYD}_{2.1}}$	88.83	$\mathrm{C}^{2}_{\mathrm{BYD}_{n.2}}$, $n \geq 0$
57.52	${}^{\beta}\mathrm{C}_{\mathrm{BYD}_{2.0}}$	89.06-89.10	${}^{1}\mathrm{C}_{\mathrm{MG}_n}$, $n \geq 4$
57.72-57.85	${}^{\beta}\mathrm{C}_{\mathrm{BYD}_{n.m}}$, $n \geq 3,\ m \geq 0$		$\mathrm{C}^{m}_{\mathrm{BYD}_{n.m}}$, $n \geq 0,\ m \geq 3$
	$\mathrm{C}^{\beta}_{\mathrm{BYD}_{n.n}}$, $n \geq 3$	89.82	${}^{1}\mathrm{C}_{\mathrm{BYD}_{1.0}}$
82.99	${}^{\alpha}\mathrm{C}_{\mathrm{BYD}_{n.0}}$, $n \geq 4$	89.88	${}^{1}\mathrm{C}_{\mathrm{BYD}_{1.m}}$, $m \geq 1$
83.03	${}^{\alpha}\mathrm{C}_{\mathrm{BYD}_{3.0}}$	91.38	${}^{2}\mathrm{C}_{\mathrm{MG}_3}$
83.09	${}^{\alpha}\mathrm{C}_{\mathrm{BYD}_{2.0}}$	91.91	${}^{2}\mathrm{C}_{\mathrm{MG}_4}$
83.33	${}^{\alpha}\mathrm{C}_{\mathrm{BYD}_{1.0}}$	91.94	${}^{2}\mathrm{C}_{\mathrm{BYD}_{3.m}}$, $m \geq 0$
84.28	${}^{\alpha}\mathrm{C}_{\mathrm{BYD}_{n.1}}$, $n \geq 4$	92.08-92.64	${}^{i}\mathrm{C}_{\mathrm{MG}_n}$, $n \geq 5,\ n/2+1 > i \geq 2$
84.32	${}^{\alpha}\mathrm{C}_{\mathrm{BYD}_{3.1}}$		${}^{i}\mathrm{C}_{\mathrm{BYD}_{n.m}}$, $n \geq 4,\ m \geq 0,\ n-1 \geq i \geq 2$
84.38	${}^{\alpha}\mathrm{C}_{\mathrm{BYD}_{2.1}}$	93.00	${}^{1}\mathrm{C}_{\mathrm{BYD}_{2.0}}$
84.62	${}^{\alpha}\mathrm{C}^{\alpha}_{\mathrm{BYD}_{1.1}}$	93.05	${}^{1}\mathrm{C}_{\mathrm{BYD}_{2.m}}$, $m \geq 1$
84.72	${}^{\alpha}\mathrm{C}^{\alpha}_{\mathrm{BYD}_{2.2}}$	93.56	${}^{1}\mathrm{C}_{\mathrm{BYD}_{3.0}}$
84.81	${}^{1}\mathrm{C}_{\mathrm{MG}_1}$	93.61	${}^{1}\mathrm{C}_{\mathrm{BYD}_{3.m}}$, $m \geq 1$
84.96	$\mathrm{C}^{\alpha}_{\mathrm{BYD}_{2.1}}$	93.78-93.84	${}^{1}\mathrm{C}_{\mathrm{BYD}_{n.m}}$, $n \geq 4,\ m \geq 0$
85.02	$\mathrm{C}^{\alpha}_{\mathrm{BYD}_{3.1}}$		

In the present work only the ^{13}C-NMR spectra are used for the quantitative evaluation as ^{1}H-NMR spectra have obvious shortcomings like peak overlaps, baseline distortions (cf. also Figure 2) and structure information (cf. Tables 2 and 3). The ^{1}H-NMR spectra are interesting for quantitative evaluation in reaction kinetic studies as they can be collected faster. As in the present study only equilibria were investigated, only the ^{13}C-NMR spectra were taken into account for the determination of chemical equilibrium constants. The spectra also contain redundant information. Thus, not all peaks were used for the quantification of the reacting species.

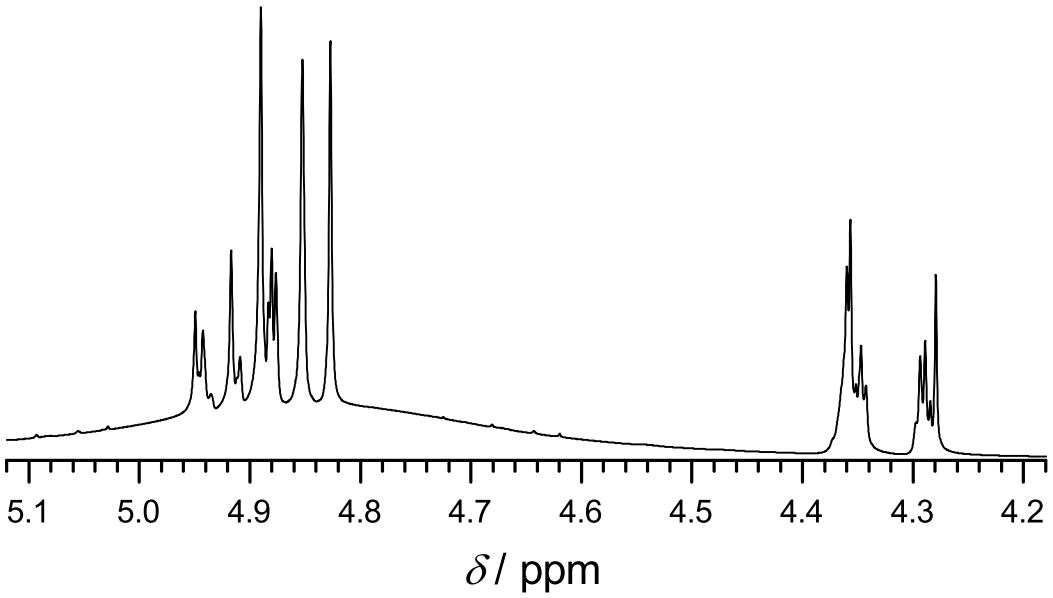

(a)

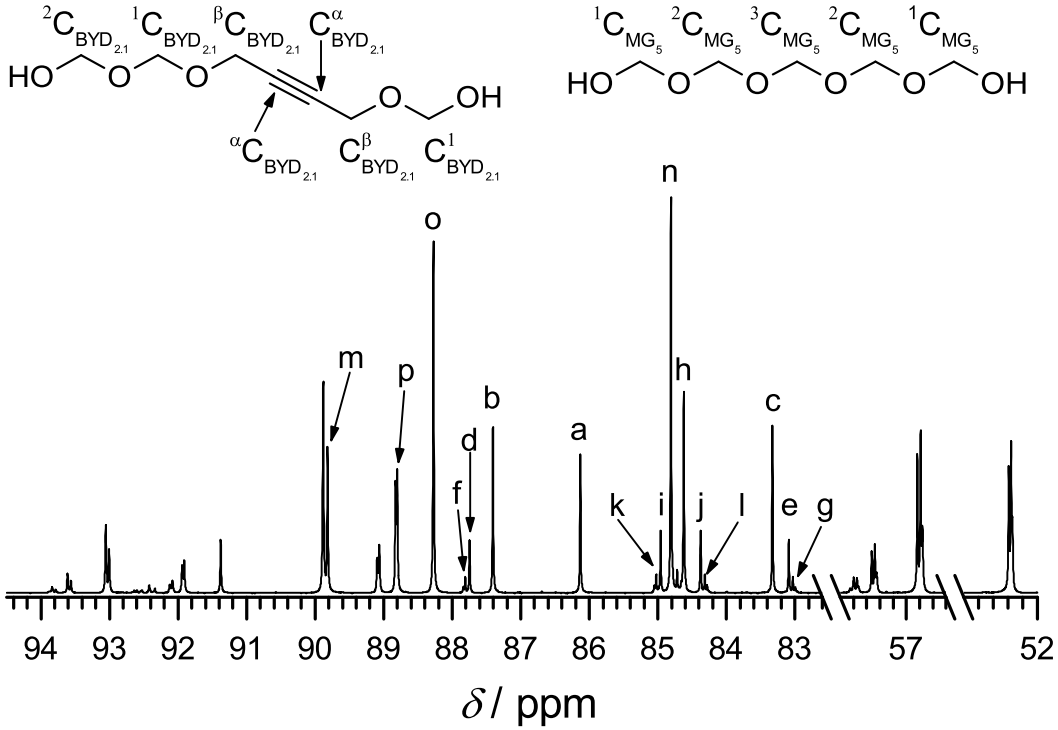

(b)

Figure 2: (a) ^{1}H-NMR and (b) ^{13}C-NMR spectrum and nomenclature for a mixture of formaldehyde, water, and butynediol ($\tilde{x}^{(\mathrm{m})}_{\mathrm{FA}}$ = 0.27 g g^{-1}, $\tilde{x}^{(\mathrm{m})}_{\mathrm{W}}$ = 0.53 g g^{-1}, $\tilde{x}^{(\mathrm{m})}_{\mathrm{BYD}}$ = 0.20 g g^{-1}, T = 293 K, pH = 6.8, reference: TMSP). Only signals used for the modeling of chemical equilibrium constants are labeled: a=$^{\alpha}\mathrm{C}^{\alpha}_{\mathrm{BYD}_{0.0}}$, b= $\mathrm{C}^{\alpha}_{\mathrm{BYD}_{1.0}}$, c=$^{\alpha}\mathrm{C}_{\mathrm{BYD}_{1.0}}$, d= $\mathrm{C}^{\alpha}_{\mathrm{BYD}_{2.0}}$, e=$^{\alpha}\mathrm{C}_{\mathrm{BYD}_{2.0}}$, f= $\mathrm{C}^{\alpha}_{\mathrm{BYD}_{3.0}}$, g=$^{\alpha}\mathrm{C}_{\mathrm{BYD}_{3.0}}$, h=$^{\alpha}\mathrm{C}^{\alpha}_{\mathrm{BYD}_{1.1}}$, i= $\mathrm{C}^{\alpha}_{\mathrm{BYD}_{2.1}}$, j=$^{\alpha}\mathrm{C}_{\mathrm{BYD}_{2.1}}$, k= $\mathrm{C}^{\alpha}_{\mathrm{BYD}_{3.1}}$, l=$^{\alpha}\mathrm{C}_{\mathrm{BYD}_{3.1}}$, m=$^{1}\mathrm{C}_{\mathrm{BYD}_{1.0}}$, n= $\mathrm{C}^{1}_{\mathrm{MG}_{1}}$, o=$^{1}\mathrm{C}^{1}_{\mathrm{MG}_{2}}$, p=$^{1}\mathrm{C}^{1}_{\mathrm{MG}_{3}}$.

2.3.5 Quantitative analysis of the spectra

Quantitative information can be in principle obtained from methylene carbon signals in bound formaldehyde (CH_2O segments), from methylene carbon signals in the butynediol skeleton and from the signals of triple-bonded carbon nuclei. The latter show the best resolution to distinguish the number of CH_2O both to the n- and to the m-side in $BYD_{n.m}$. That means that the chemical shift of the triple-bonded carbon nuclei is influenced by both chains whereas the methylene carbon nuclei rather see what happens on their side of the molecule but know little or nothing about the other side of the molecule.

For the estimation of chemical equilibrium constants, peaks which belong to a single species and preferably do not overlap with other signals were chosen. The peaks used for the estimation procedure are shown and labeled in Figure 2b. Resulting from the discussion above the signals of triple-bonded carbon (peaks a to l) were used for $BYD_{n.m}$. For MG_n the signals of the outer methylene groups (peaks n to p) were used.

Spectra processing was performed with the software MestReNova (version: 8.1.4, Mestrelab Research S.L., Santiago de Compostela, Spain) using automatic phase correction and a third order polynomial for baseline correction. As some signals are slightly overlapping, peak deconvolution (Lorentzian shape) was applied to the spectra.

Preliminary studies with the quantitative ^{13}C spectra showed that the proportionality constants relating peak areas and mole numbers are not the same for all carbon atoms in the BYD-containing products. The signals of α-carbons in $BYD_{n.m}$ are about $10-15$ % larger than those of the β-carbons. The carbons in the groups ${}^{\beta}C_{BYD_{n.0}}$ and ${}^{1}C_{BYD_{n.0}}$ ($n = 1, 2, 3\ldots$) have similar proportionality constants. These results do not depend on the transmitter frequency. It is assumed that the proportionality constants are the same among the same type of carbon atoms, namely methylene or triple-bonded carbon. This argument holds as the signal area ratios of ${}^{1}C_{BYD_{1.0}}$:${}^{1}C_{BYD_{2.0}}$, ${}^{\beta}C_{BYD_{1.0}}$:${}^{\beta}C_{BYD_{2.0}}$, ${}^{\alpha}C_{BYD_{1.0}}$:${}^{\alpha}C_{BYD_{2.0}}$, and $C^{\alpha}_{BYD_{1.0}}$:$C^{\alpha}_{BYD_{2.0}}$ are in good agreement.

Peak area ratios ζ_i were generated among the same type of carbon signals by dividing the peak areas A_i of the labeled peaks in Figure 2b by the peak area of unconverted butynediol $BYD_{0.0}$. The following ratios were determined:

$$\zeta_{\mathrm{BYD}_{1.0}} = \frac{x_{\mathrm{BYD}_{1.0}}}{x_{\mathrm{BYD}_{0.0}}} = \frac{A_\mathrm{b} + A_\mathrm{c}}{A_\mathrm{a}} \tag{14}$$

$$\zeta_{\mathrm{BYD}_{2.0}} = \frac{x_{\mathrm{BYD}_{2.0}}}{x_{\mathrm{BYD}_{0.0}}} = \frac{A_\mathrm{d} + A_\mathrm{e}}{A_\mathrm{a}} \tag{15}$$

$$\zeta_{\mathrm{BYD}_{3.0}} = \frac{x_{\mathrm{BYD}_{3.0}}}{x_{\mathrm{BYD}_{0.0}}} = \frac{A_\mathrm{f} + A_\mathrm{g}}{A_\mathrm{a}} \tag{16}$$

$$\zeta_{\mathrm{BYD}_{1.1}} = \frac{x_{\mathrm{BYD}_{1.1}}}{x_{\mathrm{BYD}_{0.0}}} = \frac{A_\mathrm{h}}{A_\mathrm{a}} \tag{17}$$

$$\zeta_{\mathrm{BYD}_{2.1}} = \frac{x_{\mathrm{BYD}_{2.1}}}{x_{\mathrm{BYD}_{0.0}}} = \frac{A_\mathrm{i} + A_\mathrm{j}}{A_\mathrm{a}} \tag{18}$$

$$\zeta_{\mathrm{BYD}_{3.1}} = \frac{x_{\mathrm{BYD}_{3.1}}}{x_{\mathrm{BYD}_{0.0}}} = \frac{A_\mathrm{k} + A_\mathrm{l}}{A_\mathrm{a}} \tag{19}$$

The MG_n contain no triple-bonded carbon and the methylene signal of $\mathrm{BYD}_{0.0}$ is strongly influenced by other signals. However the CH_2O signal of bound formaldehyde in $\mathrm{BYD}_{1.0}$ suits as a reference since it is quite well separated from other signals and the carbons $^1\mathrm{C}_{\mathrm{MG}_n}$ and $^1\mathrm{C}_{\mathrm{BYD}_{1.0}}$ are chemically very similar. The reference to $\mathrm{BYD}_{0.0}$ is obtained by multiplication with Eq. (14) according to the following equations:

$$\zeta_{\mathrm{MG}_1} = \frac{x_{\mathrm{MG}_1}}{x_{\mathrm{BYD}_{0.0}}} = \frac{A_\mathrm{n}}{A_\mathrm{m}} \cdot \zeta_{\mathrm{BYD}_{1.0}} \tag{20}$$

$$\zeta_{\mathrm{MG}_2} = \frac{x_{\mathrm{MG}_2}}{x_{\mathrm{BYD}_{0.0}}} = \frac{A_\mathrm{o}}{2 \cdot A_\mathrm{m}} \cdot \zeta_{\mathrm{BYD}_{1.0}} \tag{21}$$

$$\zeta_{\mathrm{MG}_3} = \frac{x_{\mathrm{MG}_3}}{x_{\mathrm{BYD}_{0.0}}} = \frac{A_\mathrm{p}}{2 \cdot A_\mathrm{m}} \cdot \zeta_{\mathrm{BYD}_{1.0}} \tag{22}$$

2.4 Modeling

2.4.1 Independent set of reactions

To model the chemical equilibrium in the studied system, a set of independent reaction equations is required. The set of independent reactions which is chosen here was already introduced in the discussion along Figure 1 (black arrows). The chemical equilibrium constants of the dependent reactions are not required for calculations of the chemical equilibrium in the studied mixtures but they can be obtained from the constants reported

here, e.g.

$$\begin{aligned} K^x_{2.0\leftrightarrow 2.1} &= \frac{x_{\mathrm{BYD}_{2.1}}}{x_{\mathrm{FA}} \cdot x_{\mathrm{BYD}_{2.0}}} \\ &= \frac{x_{\mathrm{BYD}_{2.1}}}{x_{\mathrm{FA}} \cdot x_{\mathrm{BYD}_{1.1}}} \cdot \frac{x_{\mathrm{BYD}_{1.1}}}{x_{\mathrm{FA}} \cdot x_{\mathrm{BYD}_{1.0}}} \cdot \frac{x_{\mathrm{FA}} \cdot x_{\mathrm{BYD}_{1.0}}}{x_{\mathrm{BYD}_{2.0}}} \\ &= K^x_{1.1\leftrightarrow 2.1} \cdot \frac{K^x_{1.0\leftrightarrow 1.1}}{K^x_{1.0\leftrightarrow 2.0}} \\ &= 2 \cdot K^x_{\mathrm{BYD},2} \cdot \frac{K^x_{\mathrm{BYD},1}}{2 \cdot K^x_{\mathrm{BYD},2}} \\ &= K^x_{\mathrm{BYD},1}. \end{aligned} \tag{23}$$

This is in agreement with Eq. (10).

The chemical equilibrium constants of the reactions of formaldehyde with water according to Eqs. (1) and (2) are adopted from Hahnenstein *et al.* [30] who give a temperature dependent correlation for their calculation. The results from the present study justify this as shown below. As the reaction mechanism is formulated here in a different way, the chemical equilibrium constants from Hahnenstein *et al.* [30] were converted. The procedure is described in the Supporting Information for the case of the activity-based model. The conversion for the mole fraction based model follows the same arguments and is not repeated here.

2.4.2 Parameter fit

The chemical equilibrium constants $K^x_{\mathrm{BYD},1}$ and $K^x_{\mathrm{BYD},2}$ are fitted to the experimental peak area ratios ζ_i defined by Eqs. (14) to (22). This was done for every experiment individually using the software gPROMS (version: 3.6, Process Systems Enterprise Limited, London, UK). Only species of MG_n with $1 \le n \le 10$ and $\mathrm{BYD}_{n.m}$ with $0 \le n+m \le 10$ are taken into account in the model as oligomers with more CH_2O groups are present only in negligible amounts. In the fit, the deviations between the experimental ζ_i^{exp} and the calculated ζ_i^{calc} are minimized using the maximum likelihood method [6, 23]. For obtaining the calculated peak area ratios, first true mole fractions were calculated from the overall mole fractions $\tilde{x}_i$ of formaldehyde and butynediol and the values $K^x_{\mathrm{BYD},1}$ and $K^x_{\mathrm{BYD},2}$. The latter are varied in the iteration of the fit to improve the value of the goal function. The relation between overall and true mole fractions is given in the Supporting Information. A constant relative variance model was assumed for the experimental signal area ratios.

The temperature dependency of the chemical equilibrium constants $K^x_{\mathrm{BYD},1}$ and $K^x_{\mathrm{BYD},2}$ is described by the van't Hoff equation

$$\ln\ K_i^x(T) = A_i + \frac{B_i}{T/\mathrm{K}} \tag{24}$$

The parameters A_i and B_i were fitted to the ζ_i of all available experiments simultaneously according to the method described above.

2.5 Results and discussion

The peak area ratios determined in the NMR experiments are presented in Table 5 at the end of this section. Ratios of mole fraction-based chemical equilibrium constants can be directly determined from the peak area ratios, e.g.

$$\frac{K_{1.0\leftrightarrow1.1}}{K_{0.0\leftrightarrow1.0}} = \frac{\zeta_{\mathrm{BYD}_{1.1}}}{\zeta^2_{\mathrm{BYD}_{1.0}}} \tag{25}$$

The ratios of $K_{1.0\leftrightarrow1.1}/K_{0.0\leftrightarrow1.0}$, $K_{2.0\leftrightarrow2.1}/K_{0.0\leftrightarrow1.0}$, and $K_{1.1\leftrightarrow2.1}/K_{1.0\leftrightarrow2.0}$ are shown in Figure 3 for all experiments. Their values are approximately 0.25, 0.5, and 2 respectively. Larger deviations occur only when oligomer concentrations are very low, e.g. for $\mathrm{BYD}_{2.1}$ in the samples IV and V, resulting in a low signal to noise ratio. These results confirm the assumption that the constants are dependent on each other, cf. also the discussion along Eqs. (8) to (13).

The results for $K^x_{\mathrm{BYD},1}$ and $K^x_{\mathrm{BYD},2}$ are presented in Figure 4 for both the single fits to the experiments (symbols) and the correlations (lines). The mean absolute percentage deviation ($MAPD$) of the temperature correlation to the single experiment fits

$$MAPD = \frac{1}{N}\sum_{i=1}^{N}\left|\frac{K_i^{\mathrm{single}} - K_i^{\mathrm{correlation}}}{K_i^{\mathrm{single}}}\right| \cdot 100\% \tag{26}$$

where N is the number of experiments are 4 % for $K^x_{\mathrm{BYD},1}$ and 9 % for $K^x_{\mathrm{BYD},2}$. The parameters A_i and B_i of Eq. (24) of the chemical equilibrium constants for the system formaldehyde + water + butynediol are given in Table 4. The standard deviations σ_i of the parameters A and B are obtained by the maximum likelihood method as described for the fit procedure. Between 293 K and 393 K the standard deviations in the chemical equilibrium constants are about 25 % for $K^x_{\mathrm{BYD},1}$ and 75 % for $K^x_{\mathrm{BYD},2}$. The higher value in the deviation of $K^x_{\mathrm{BYD},2}$ is in agreement with the fact that $K^x_{\mathrm{BYD},2}$ is derived from rather small concentrations of longer oligomers.

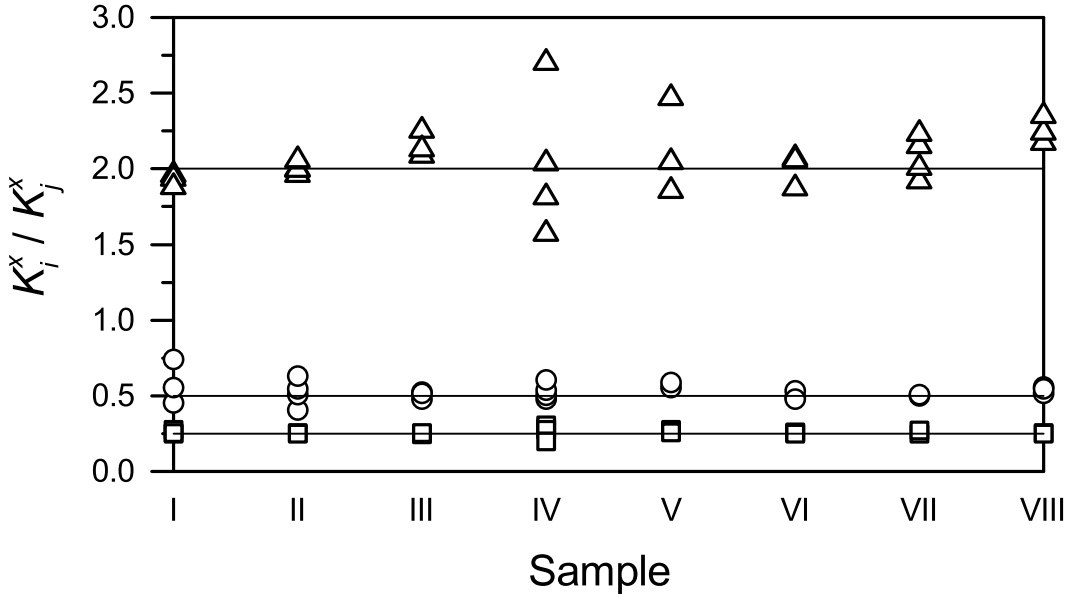

Figure 3: Ratios of mole fraction-based chemical equilibrium constants directly determined from the NMR data: (△) $K_{1.1\leftrightarrow2.1}/K_{1.0\leftrightarrow2.0}$, (∘) $K_{2.0\leftrightarrow2.1}/K_{0.0\leftrightarrow1.0}$, (□) $K_{1.0\leftrightarrow1.1}/K_{0.0\leftrightarrow1.0}$.

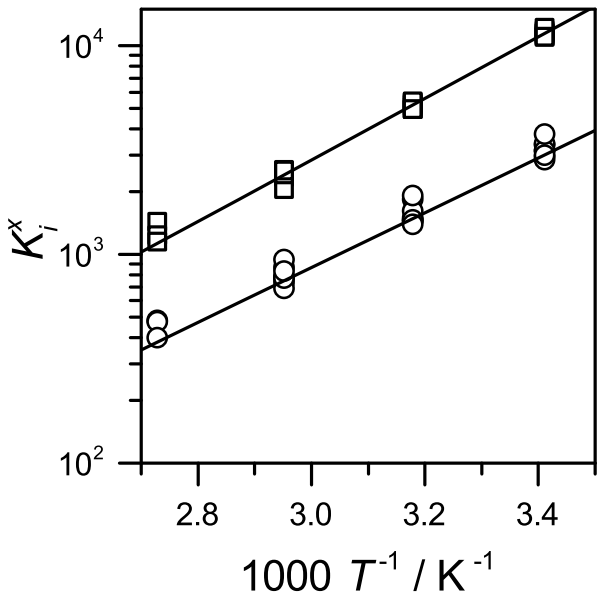

Figure 4: Chemical equilibrium constants from parameter fittings: (□) $K^x_{\mathrm{BYD},1}$, (∘) $K^x_{\mathrm{BYD},2}$, (——) temperature dependent fit.

The rather high values arise from the variances for ζ_i which depend on the quality of the peak deconvolution and the uncertainties in the formaldehyde analytics of the stock solution and the gravimetric sample preparation. The latter ones are negligible since a typical value of the standard deviation of the overall formaldehyde concentration in the formaldehyde stock solution is about ±1 ‰ and the uncertainty in the gravimetric preparation is about ±0.3 ‰. The major contribution comes from the spectra analysis.

For high and well separated peaks the uncertainty in ζ_i is estimated to be about ±5 %. For small peaks and overlapping peaks it even is ±20 % or more. The temperature also influences the quality of the spectra. At high temperatures the signal to noise ratio is lower as the population difference of excited and ground state decreases.

Table 4: Parameters for the calculation of chemical equilibrium constants for the system formaldehyde + water + butynediol according to Eq. (24) and their standard deviations σ.

	A	B/K	σ_A	σ_B/K	$\frac{\Delta h_R}{\text{kJ mol}^{-1}}$	$\frac{\sigma_{\Delta h_R}}{\text{kJ mol}^{-1}}$	Ref.
$K^x_{\text{MG}_1}$	-2.325	2579.0			-21.4		[57]
$K^x_{\text{MG}_2}$	-2.31051	3139.9			-26.1		[30]
$K^x_{\text{MG}_n}$	-2.4334	3039.4			-25.3		[30]
$K^x_{\text{BYD,1}}$	-2.225	3392.6	±0.176	±55.9	-28.2	±0.5	this work
$K^x_{\text{BYD,2}}$	-2.334	3032.4	±0.554	±175.7	-25.2	±1.5	this work

Figures 5a and b show the peak area ratios obtained from the correlations for $K^x_{\text{BYD,1}}$ and $K^x_{\text{BYD,2}}$ over the corresponding experimental peak area ratios. The $MAPD$ of the calculated to the experimental peak area ratios are 2 % for $\zeta_{\text{BYD}_{1.0}}$, 5 % for $\zeta_{\text{BYD}_{2.0}}$, 20 % for $\zeta_{\text{BYD}_{3.0}}$, 6 % for $\zeta_{\text{BYD}_{1.1}}$, 12 % for $\zeta_{\text{BYD}_{2.1}}$, 19 % for $\zeta_{\text{BYD}_{3.1}}$, 4 % for ζ_{MG_1}, 6 % for ζ_{MG_2}, and 14 % for ζ_{MG_3} respectively. The increase of the deviations for components with high CH_2O content also results from the decreasing mole fractions and the lower signal to noise ratio in the NMR spectra. The good agreement for the ζ_{MG_i} justify the adaption of the chemical equilibrium constants from Hahnenstein *et al.* [30] for the reactions of formaldehyde with water.

As an example, Figure 6 shows the experimental and the calculated results for the species distribution in a mixture of formaldehyde, water, and butynediol at 293 K. The bars show the fraction of the overall formaldehyde bound in the different species in MG_n (white) and $\text{BYD}_{n.m}$ (gray). Absolute deviations of the calculation from the experiment range from −2 to +12%. The overall mole fraction of water is about 15 times higher than the overall butynediol concentration. However, approximately half of the formaldehyde is bound to butynediol. The results for the activity-based model are comparable to the mole fraction-based model. For the sake of a better reading they are given in the Supporting Information.

Furthermore, the results from the present study for the reactions of formaldehyde with butynediol are compared to literature data for the corresponding reactions of formaldehyde with other alcohols and water. Figure 7 shows the chemical equilibrium constants for the reactions of formaldehyde with water [30], butynediol, methanol [30] (ME), and 1-butanol [18] (BU) at 293 K. The value of $K^x_{\text{BYD,1}}$ is about 15 % lower than the value of the chemical equilibrium constant $K^x_{\text{BU}_1}$ for the first addition of 1-butanol to form-

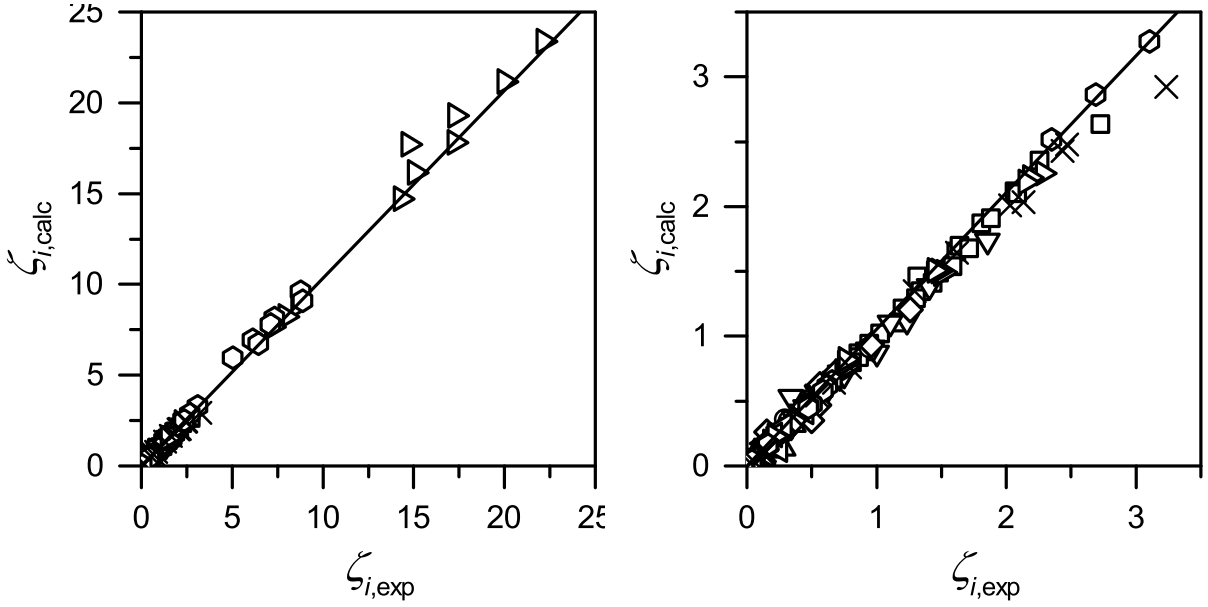

(a) (b)

Figure 5: Calculated vs. experimental peak area ratios. (□) $BYD_{1.0}$, (∘) $BYD_{2.0}$, (△) $BYD_{3.0}$, (▽) $BYD_{1.1}$, (⋄) $BYD_{2.1}$, (◁) $BYD_{3.1}$, (▷) MG_1, (⬡) MG_2, (×) MG_3. (b) Zoom of (a).

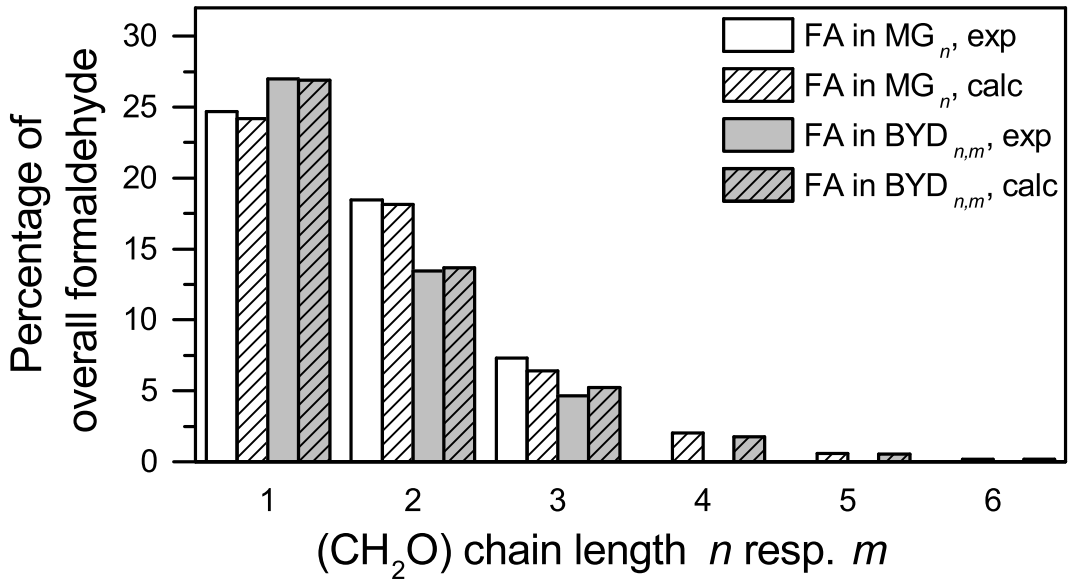

Figure 6: Species distribution in a mixture of formaldehyde, water, and butynediol ($\tilde{x}_{\mathrm{FA}}$ = 0.164 mol mol^{-1}, $\tilde{x}_{\mathrm{W}}$ = 0.784 mol mol^{-1}, $\tilde{x}_{\mathrm{BYD}}$ = 0.052 mol mol^{-1}, T = 293 K).

aldehyde. The fact that butynediol contains two hydroxyl groups doubles this value according to Eq. (8) for the addition of butynediol to formaldehyde so that $K^x_{0.0\leftrightarrow1.0}$ is just 4 % lower than the equilibrium constant $K^x_{\mathrm{ME}_1}$ for the addition of methanol to formaldehyde. On the other side the equilibrium constants of the chain propagation reactions are approximately the same for the reactions of formaldehyde with poly(oxymethylene) glycols and poly(oxymethylene) hemiformals of butynediol, 1-butanol, and methanol. In these reactions the non-reacting side of the molecules has no influence on the chemical equilibrium constant.

The reaction enthalpy $\Delta_\mathrm{R}h$ for Reactions I to IV is estimated from the corresponding chemical equilibrium constants:

$$\Delta_\mathrm{R}h = -B \cdot R \tag{27}$$

where B is the parameter of the temperature correlation in Eq. (24) and R the gas constant. For the chain propagation reactions with formaldehyde and butynediol the reaction enthalpy is −25.2 kJ/mol. The standard deviation is 1.5 kJ/mol. From the literature, values of the reaction enthalpies for the chain propagation reactions in the systems formaldehyde + water [30], formaldehyde + methanol [30], and formaldehyde + 1-butanol [18] are calculated from the converted chemical equilibrium constants (cf. Supporting Information) in the same way. They range between −22.8 kJ/mol and −25.3 kJ/mol. Thus, they are similar to the ones in Table 4. This is expected as the reactions are very similar.

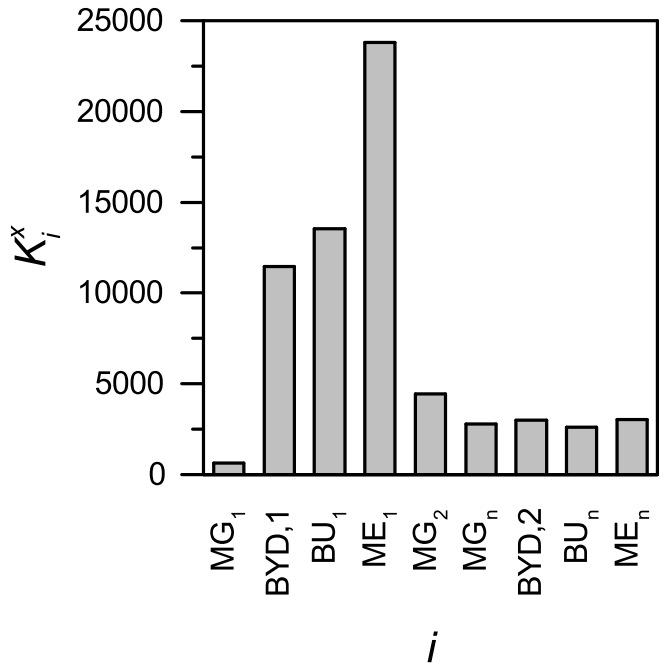

Figure 7: Values of K_i^x for reactions of formaldehyde with water [30], butynediol, methanol [30], and butanol [18] at 293 K.

Table 5: Experimental values of peak area ratios $10^2 \cdot \zeta_i$ from ^{13}C NMR spectroscopic studies of the present work. The definitions of the peak area ratios are given in Eqs. (14) to (22).

		index i								
Sample	T / K	$BYD_{1.0}$	$BYD_{2.0}$	$BYD_{3.0}$	$BYD_{1.1}$	$BYD_{2.1}$	$BYD_{3.1}$	MG_1	MG_2	MG_3
I	293	272.27	94.09	36.23	185.80	125.84	45.78	1724.00	888.76	323.21
	315	225.72	79.42	26.15	140.81	95.85	29.27	1504.32	712.00	243.38
	339	208.51	68.86	18.54	110.46	68.54	21.62	1426.67	646.96	213.32
II	293	171.40	38.66	8.12	75.08	33.19	8.52	149.49	49.91	13.09
	315	158.27	35.37	7.10	62.38	27.86	5.53	151.42	50.43	12.77
	339	143.33	32.41	7.04	51.56	23.25	6.13	147.75	47.72	n.a.
	366	130.30	28.98	7.80	42.08	19.24	4.13	144.86	47.60	n.a.
III	293	90.59	10.85	1.83	20.25	5.06	0.73	17.58	3.17	n.a.
	315	86.23	11.02	2.09	18.47	5.32	n.a.	20.28	3.73	n.a.
	339	80.88	10.91	1.57	16.72	4.81	n.a.	21.47	3.96	n.a.
IV	293	206.42	59.75	25.38	123.45	56.05	12.85	2212.71	877.07	246.90
	315	180.88	55.22	28.20	100.07	55.36	25.53	1999.79	734.91	203.12
	339	161.56	41.53	n.a.	71.68	49.74	n.a.	1726.98	615.13	161.94
	366	131.24	29.17	n.a.	34.24	15.49	n.a.	1470.09	502.63	129.33
V	293	187.91	46.51	16.55	97.02	44.47	13.08	864.60	310.47	79.40

Continued on next page

Table 5 – continued from previous page

		index i								
Sample	T / K	$BYD_{1.0}$	$BYD_{2.0}$	$BYD_{3.0}$	$BYD_{1.1}$	$BYD_{2.1}$	$BYD_{3.1}$	MG_1	MG_2	MG_3
	315	164.04	40.36	8.62	71.87	36.13	15.16	793.36	269.16	67.11
	339	145.64	32.13	7.77	54.31	29.54	n.a.	719.45	234.90	54.02
VI	293	147.88	29.64	5.04	56.15	21.05	4.28	228.03	65.51	13.64
	315	133.94	25.68	4.34	45.35	17.99	4.31	218.22	62.00	13.09
	339	120.12	22.67	4.10	36.31	14.09	3.99	214.84	58.73	12.15
VII	293	117.10	17.93	3.05	34.25	10.06	1.29	73.69	16.56	3.10
	315	102.71	15.29	2.23	26.42	7.88	1.03	76.17	16.79	3.18
	339	94.29	14.01	2.67	22.20	7.09	1.37	75.56	15.98	6.88
	366	85.98	13.54	2.70	20.05	7.04	n.a.	76.25	16.42	n.a.
VIII	293	55.68	4.24	n.a.	7.92	1.31	n.a.	9.73	1.01	n.a.
	315	53.93	4.28	n.a.	7.23	1.28	n.a.	10.88	1.39	n.a.
	339	51.02	4.17	0.65	6.51	1.25	n.a.	13.99	1.68	n.a.

3 Vapor-Liquid Equilibrium

3.1 Introduction

Vapor-liquid equilibrium models for mixtures containing formaldehyde, water, and methanol have been presented in many studies, among others [1–5, 14, 15, 19, 33, 34, 41, 42, 46, 47, 49]. The activity-based model of the chemical equilibrium from the previous study, cf. part A of the Supporting Information, also implicitly contains a model of the physical equilibrium between liquid and vapor phase. The model is predictive since it does not contain any parameters fitted to vapor-liquid equilibrium data with formaldehyde and butynediol.

To the author's knowledge, no experimental vapor-liquid equilibrium data for systems containing formaldehyde and butynediol have been published before this study. Therefore, the vapor-liquid equilibrium in the system formaldehyde + water + butynediol was studied experimentally in this work in a special type of thin-film evaporator which is known to be suited for determining vapor-liquid equilibria of reactive formaldehyde-containing mixtures [1–5, 33, 34, 41, 42]. The data are used for the validation of the predictive model mentioned above.

In Section 3.5, residue curves for the overall ternary system formaldehyde + water + butynediol are presented. These curves allow conceptual feasibility studies for distillation processes involving formaldehyde, water, and butynediol.

3.2 Vapor-liquid equilibrium model

Figure 8 shows a scheme of the vapor-liquid equilibrium model in the system formaldehyde + water + butynediol including the chemical reactions.

The reaction of formaldehyde with water yielding methylene glycol, cf. Reaction (I), takes place both in the vapor and in the liquid phase. Following Maurer [46], it is assumed that no poly(oxymethylene) glycols with $n > 1$ are present in the vapor phase,

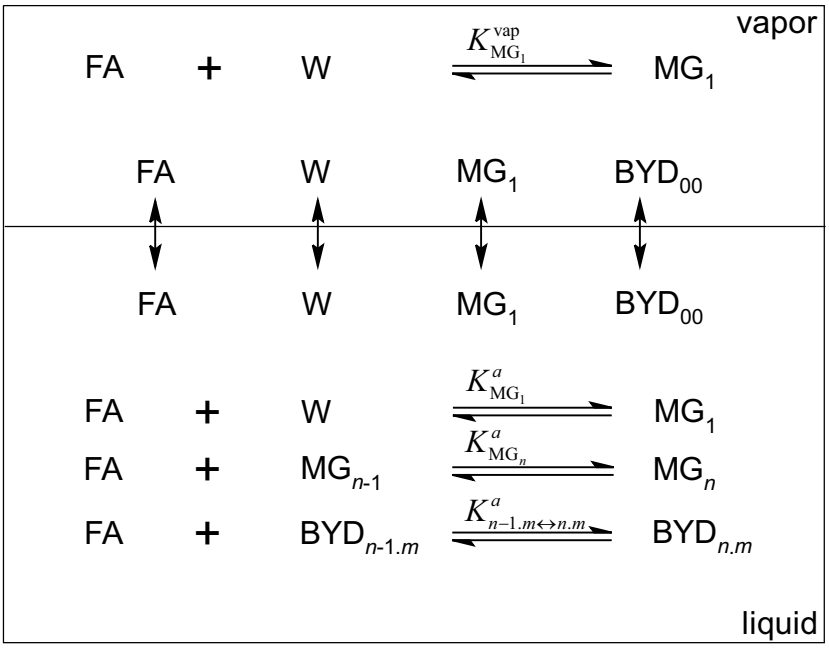

Figure 8: Schematic of the reactive vapor-liquid equilibrium model considering the chemical reactions in the system formaldehyde + water + butynediol.

due to their low vapor pressures. Adapting that argument, only monomeric butynediol ($BYD_{0.0}$) is considered here in the vapor phase. As a consequence, reactions of formaldehyde with butynediol are only considered in the liquid phase.

Activity-based chemical equilibrium constants K^a are used for the calculation of the species distribution in the liquid phase. The equilibrium constants were taken from the results of the preceding study of the chemical equilibrium, cf. part A of the Supporting Information. The phase equilibrium of the components present in both phases is modeled using the extended Raoult's Law

$$p_i^{\mathrm{s}} \cdot x_i \cdot \gamma_i = p \cdot y_i \qquad i = \mathrm{FA}, \mathrm{W}, \mathrm{MG}_1, \mathrm{BYD}_{0.0} \tag{28}$$

where p_i^{s} is the vapor pressure of component i, x_i the true mole fraction of component i in the liquid phase, γ_i the activity coefficient of component i in the liquid phase, p the pressure, and y_i the true mole fraction of component i in the vapor phase. Ideal vapor phase is assumed and the Poynting correction is neglected. As activity-based chemical equilibrium constants are used for describing the liquid phase reactions, the model is thermodynamically consistent. Reaction (I) occurs in both phases. The corresponding chemical equilibrium constants are connected by Eq. (28) following Maurer [46], cf. Eq. (67) in the Supporting Information. The calculation of activity coefficients and pure component vapor pressures is also shown in part A of the Supporting Information.

In the model and the calculations of this work, true concentrations are used. For the presentation of the experimental data and the comparison with the model predictions overall concentrations are used. Mass fractions are used for the latter rather than mole fractions. This facilitates the presentation of the results of the studied mixtures in which butynediol has a much higher molar mass than formaldehyde and water. To differentiate mass fractions in the symbol notation, the superscript (m) is used, e.g. $\tilde{x}_{\mathrm{FA}}^{(\mathrm{m})}$, in contrast to mole fractions where the superscript is omitted, e.g. $\tilde{x}_{\mathrm{FA}}$.

All calculations in this work were performed with the software gPROMS (version: 3.6, Process Systems Enterprise Limited, London, UK) taking into account poly(oxymethylene) glycols up to $n = 10$ and poly(oxymethylene) hemiformals up to $n + m = 10$.

3.3 Experimental

3.3.1 Experimental plan

To remove formaldehyde from aqueous, alcoholic solutions, high temperatures are favorable [47]. However, at temperatures above 423 K decomposition of butynediol can occur [11]. Therefore, the vapor-liquid equilibrium measurements in the present work were carried out at 393 K and 413 K in a concentration range which is interesting for the present applications: $\tilde{x}_{\mathrm{FA}}^{(\mathrm{m})}$ ranging from 0.1 g g^{-1} to 0.2 g g^{-1} and $\tilde{x}_{\mathrm{BYD}}^{(\mathrm{m})}$ from 0.05 g g^{-1} to 0.35 g g^{-1}.

3.3.2 Experimental setup

For the vapor-liquid equilibrium measurements a thin-film evaporator was used which already has been successfully used for the measurements of vapor-liquid equilibria in formaldehyde containing systems [1–5]. Since apparatus and measurement procedure are already well described (see also [33, 34]), just a short outline is given here.

The apparatus consists of a rotating coil which spreads a preheated, equilibrated liquid feed on the inner surface of a stainless steel tube surrounded by a heating jacket. After partial evaporation and equilibration, vapor and liquid phase are separated, cooled down and collected into glass vessels. The temperature was measured with a PT100 thermometer in a siphon for the liquid phase. Nitrogen back pressure was used to regulate the pressure both in the apparatus and the feed vessel. The accuracy of the temperature measurement was ±0.05 K, the accuracy of the pressure measurement is ±0.1 kPa.

To keep the residence time for equilibration high and the disturbance of the chemical equilibrium in the liquid phase low, the following experimental parameters were chosen: feed flow rate below 30 mL h^{-1} (cf. Hasse [33]), rotation rate of the coil 30 rpm, volume ratio of condensed vapor phase to liquid phase about 1:8. The estimated resulting residence time is about 2 min. It is known [34] for the system formaldehyde + water that this residence time is sufficient to reach chemical equilibrium in the vapor phase at the temperatures chosen here. Since the amount of butynediol in the vapor phase is negligible (cf. results), the considerations also hold for the system with butynediol.

3.3.3 Chemicals and sample preparation

Aqueous formaldehyde stock solutions were prepared by dissolving paraformaldehyde (95-100 %, Merck) in ultrapure water at elevated temperature. A detailed procedure is described by Hasse [33]. The overall formaldehyde mass fraction in the stock solution was determined titrimetrically by the Na_2SO_3 method [61]. The ultrapure water was produced in a Milli-Q integral water purification system from MerckMillipore, Darmstadt, Germany. Butynediol (99 %, Acros Organics) was purified by recrystallization with diethyl ether from ethyl acetate as described by Pyatnitsyna *et al.* [51].

Ternary mixtures of formaldehyde, water, and butynediol were prepared gravimetrically from an aqueous formaldehyde stock solution and recrystallized butynediol using a precision balance (Mettler Toledo XS603S). For chemical equilibration the ternary mixtures are stored in the feed vessel of the thin-film evaporator for at least two hours at measurement temperature.

3.3.4 Sample analysis

The overall formaldehyde mass fraction was determined titrimetrically by the Na_2SO_3 method [61]. The overall mass fraction of butynediol was determined by gas chromatography (HP 6890, Hewlett-Packard) with a Rtx®-Wax column (cat.no. 12454, Restek) and a thermal conductivity detector. 200 µL of 1,4-Butanediol (99 %, Acros Organics) were used as internal standard with 1 mL of the sample to be analyzed. The settings are reported in Table 6.

The gas chromatograph was calibrated with mixtures of known composition. Mixtures of water + butynediol and formaldehyde + water + butynediol were used for the calibration. The preparation of these mixtures was performed as described above.

The overall butynediol concentration was determined ten times for each sample. The mean standard deviation of the determined mean value in the liquid phase is

Table 6: Settings of the gas chromatograph.

Injection volume	0.2 µL
Inlet temperature	250 °C
Helium flow rate	0.9 mL min^{-1}
Split ratio	30:1
Temperature program	0.5 min at 100 °C
	20 °C min^{-1} up to 250 °C
	4 min at 250 °C
Detector temperature	250 °C
Reference flow	20 mL min^{-1}
Column + makeup flow	7 mL min^{-1}

±0.0003 g g^{-1}. The relative accuracy of the butynediol concentration is 2 %. The determination of the overall formaldehyde concentration was carried out at least three times for each sample. The standard deviation of the determined formaldehyde mass fraction is about ±0.0001 g g^{-1}. The relative accuracy of the formaldehyde concentration is 3 %. The water content was determined from the summation equation.

3.4 Results and discussion

In general, few butynediol was found in the vapor phase due to its low vapor pressure. In most experiments, the experimental mass fraction of butynediol in the vapor phase just reaches the detection limit of ca. 0.0010 g g^{-1}, in some experiments the amount of butynediol is not measurable. The results of the vapor-liquid equilibrium measurements are given in Table 7. The experiments in which butynediol could not be detected in the vapor phase are flagged with an asterisk. Table 7 also shows the predictions of the model described above. They were obtained by specifying the temperature and the overall liquid composition.

Even though the new experimental data was not used in the model development, a comparison of the model predictions with the new data show excellent agreement. The deviations of the overall mass fraction of formaldehyde in the vapor phase and the pressure are 3.6 % and 0.6 %, respectively. Since butynediol was detected merely at concentrations around the detection limit, the average deviation of the mass fraction in the vapor phase is quite high (19.2 %) compared to the one of formaldehyde. On the other hand, regarding mole fractions, the highest experimental fraction of butynediol in the vapor phase is 6.2 10^{-4} mol mol^{-1} which has a negligible contribution to the total pressure. The deviations in the formaldehyde mass fraction and the pressure reported

Table 7: Vapor-liquid equilibrium in the system formaldehyde + water + butynediol. Comparison of experimental data from the present work with model predictions. $*$ Butynediol not quantified because below detection limit.

T/K	$\tilde{x}_{\mathrm{FA}}^{(\mathrm{m}),\mathrm{exp}}$/g g^{-1}	$\tilde{x}_{\mathrm{BYD}}^{(\mathrm{m}),\mathrm{exp}}$/g g^{-1}	$\tilde{y}_{\mathrm{FA}}^{(\mathrm{m}),\mathrm{exp}}$/g g^{-1}	$\tilde{y}_{\mathrm{FA}}^{(\mathrm{m}),\mathrm{mod}}$/g g^{-1}	$\Delta\tilde{y}_{\mathrm{FA}}$/%	$\tilde{y}_{\mathrm{BYD}}^{(\mathrm{m}),\mathrm{exp}}$/g g^{-1}	$\tilde{y}_{\mathrm{BYD}}^{(\mathrm{m}),\mathrm{mod}}$/g g^{-1}	$\Delta\tilde{y}_{\mathrm{BYD}}$/%	p^{exp}/kPa	p^{mod}/kPa	Δp/% [a]
393.4	0.0102	0.3418	0.0131	0.0125	4.58	0.0019	0.0018	5.26	184.4	186.8	-1.29
393.1	0.0129	0.2212	0.0181	0.0185	-2.02	0.0010	0.0012	-20.00	189.7	190.5	-0.41
393.2	0.0195	0.1068	0.0314	0.0336	-6.89	$*$	0.0006	$*$	198.0	196.5	0.76
393.1	0.0202	0.2167	0.0295	0.0289	2.03	0.0010	0.0011	-10.00	190.9	192.0	-0.56
393.3	0.0301	0.3456	0.0379	0.0361	4.75	0.0015	0.0016	-6.67	184.8	187.3	-1.38
393.2	0.0477	0.2278	0.0687	0.0651	5.29	$*$	0.0010	$*$	194.0	193.7	0.17
393.1	0.0483	0.0504	0.0840	0.0872	-3.81	$*$	0.0002	$*$	202.9	202.4	0.27
392.8	0.0489	0.2228	0.0658	0.0667	-1.37	$*$	0.0009	$*$	191.6	191.7	-0.05
393.2	0.0494	0.0535	0.0870	0.0885	-1.76	$*$	0.0002	$*$	203.5	203.0	0.27
393.2	0.0626	0.1048	0.0959	0.1000	-4.28	$*$	0.0004	$*$	200.3	201.1	-0.38
393.2	0.0932	0.2131	0.1253	0.1225	2.23	$*$	0.0007	$*$	198.5	198.0	0.23
393.2	0.0959	0.1125	0.1390	0.1426	-2.59	$*$	0.0003	$*$	203.4	203.7	-0.14
393.2	0.1193	0.1389	0.1670	0.1651	1.14	$*$	0.0004	$*$	204.5	204.8	-0.13
413.2	0.0092	0.2085	0.0172	0.0177	-3.11	0.0030	0.0021	30.00	350.7	350.2	0.13
413.3	0.0170	0.1105	0.0337	0.0375	-11.28	0.0013	0.0012	7.69	362.4	359.9	0.69
413.3	0.0191	0.3247	0.0320	0.0314	1.98	0.0034	0.0029	14.71	340.8	343.0	-0.64
413.3	0.0442	0.1814	0.0780	0.0831	-6.54	0.0014	0.0015	-7.14	371.1	361.4	2.60
413.2	0.0452	0.1063	0.0957	0.0943	1.43	$*$	0.0009	$*$	372.4	368.6	1.03
413.2	0.0456	0.2866	0.0786	0.0754	4.07	0.0024	0.0022	8.33	352.3	352.0	0.07
413.2	0.0465	0.0532	0.0993	0.1050	-5.70	$*$	0.0005	$*$	377.8	374.3	0.93
413.3	0.0803	0.1905	0.1423	0.1400	1.62	0.0015	0.0012	20.00	371.8	369.4	0.64
413.2	0.0905	0.0949	0.1673	0.1732	-3.53	0.0011	0.0005	54.55	383.4	382.3	0.29
413.2	0.1675	0.1762	0.2610	0.2559	1.95	0.0011	0.0006	45.45	393.1	389.6	0.89

[a] $u(T) = 0.05$ K, $u(p^{\mathrm{exp}}) = 0.1$ kPa, $u\left(\tilde{x}_{\mathrm{FA}}^{(\mathrm{m}),\mathrm{exp}}\right) = 0.03\ \tilde{x}_{\mathrm{FA}}^{(\mathrm{m}),\mathrm{exp}}$, $u\left(\tilde{y}_{\mathrm{FA}}^{(\mathrm{m}),\mathrm{exp}}\right) = 0.03\ \tilde{y}_{\mathrm{FA}}^{(\mathrm{m}),\mathrm{exp}}$, $u\left(\tilde{x}_{\mathrm{BYD}}^{(\mathrm{m}),\mathrm{exp}}\right) = 0.02\ \tilde{x}_{\mathrm{BYD}}^{(\mathrm{m}),\mathrm{exp}}$.

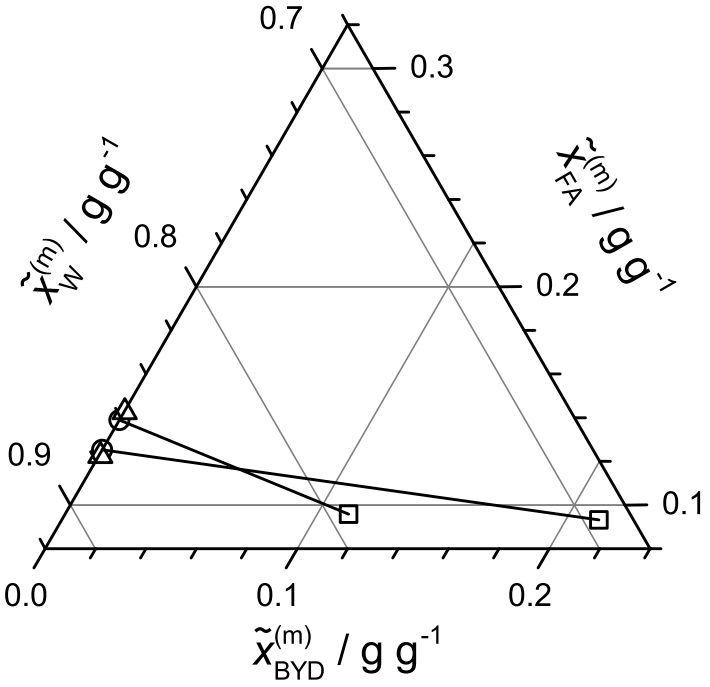

Figure 9: Vapor-liquid equilibrium in the system formaldehyde + water + butynediol at 393 K. (□) liquid phase composition, (∘) experimental vapor phase composition, (△) predicted vapor phase composition, (——) tie line.

here are not higher than the deviations which were observed for the system formaldehyde + water [41]. Thus, changing any parameters of the model was not considered in the present work.

Figure 9 shows the results of two selected experiments at 393 K to illustrate the influence of butynediol in the liquid phase on the formaldehyde mass fraction in the vapor phase.

Squares represent the composition of the liquid phase. They are connected to the composition of the corresponding vapor phase (circles) via tie-lines. The mass fraction of formaldehyde in the liquid phase is approximately the same in both experiments. However, the butynediol fraction differs significantly. The more butynediol is in the liquid phase, the less formaldehyde is in the vapor phase. This is a result of the strong binding of formaldehyde to butynediol which is described very well by the model, cf. the results of the previous chapter.

3.5 Residue curve maps

3.5.1 Introduction

For the illustration of the vapor-liquid behavior in the studied system, residue curves were calculated at constant pressure. The residue curves are the trajectories of the liquid phase composition obtained upon evaporating a liquid mixture slowly in an open still. They are closely related to distillation lines and can be used as an approximation for feasibility studies of distillation processes [62]. Mathematically, a differential-algebraic problem has to be solved which is described by the Rayleigh Equation [27]. In the case of a reactive distillation the equation can be formulated with overall mole fractions [60] according to

$$\frac{\mathrm{d}\tilde{x}_i}{\mathrm{d}\tau} = \tilde{x}_i - \tilde{y}_i \qquad i = \mathrm{FA}, \mathrm{W} \tag{29}$$

where τ can be considered as a dimensionless time. In the overall ternary system formaldehyde + water + butynediol the residue curves are then described by solving the following expression starting at an arbitrary overall composition:

$$\frac{\mathrm{d}\tilde{x}_{\mathrm{FA}}}{\mathrm{d}\tilde{x}_{\mathrm{W}}} = \frac{\tilde{x}_{\mathrm{FA}} - \tilde{y}_{\mathrm{FA}}}{\tilde{x}_{\mathrm{W}} - \tilde{y}_{\mathrm{W}}} \tag{30}$$

3.5.2 Results and discussion

The residue curve maps for the system formaldehyde + water + butynediol at 100 kPa and 400 kPa are shown in Figure 10.

There are two azeotropic points in the binary system formaldehyde + water. The one next to pure formaldehyde is an artifact of the model since at this overall composition formaldehyde is present in very long poly(oxymethylene) glycol chains which crystallize at the given conditions. Neither the formation of a solid phase nor the formation of oligomers with $n > 10$ is considered by the model. In practice the azeotrope replaces pure monomeric formaldehyde in the diagram.

All residue curves start in the other formaldehyde + water azeotrope (unstable node, global low boiler) and end in pure butynediol (stable node, global high boiler). Pure water and the second binary azeotrope are saddles in the diagram. Following the residue curves at 100 kPa starting from a point near the global high-boiling formaldehyde + water azeotrope but at lower formaldehyde concentration, formaldehyde is depleted initially. Coming to higher butynediol concentrations, formaldehyde is however enriched

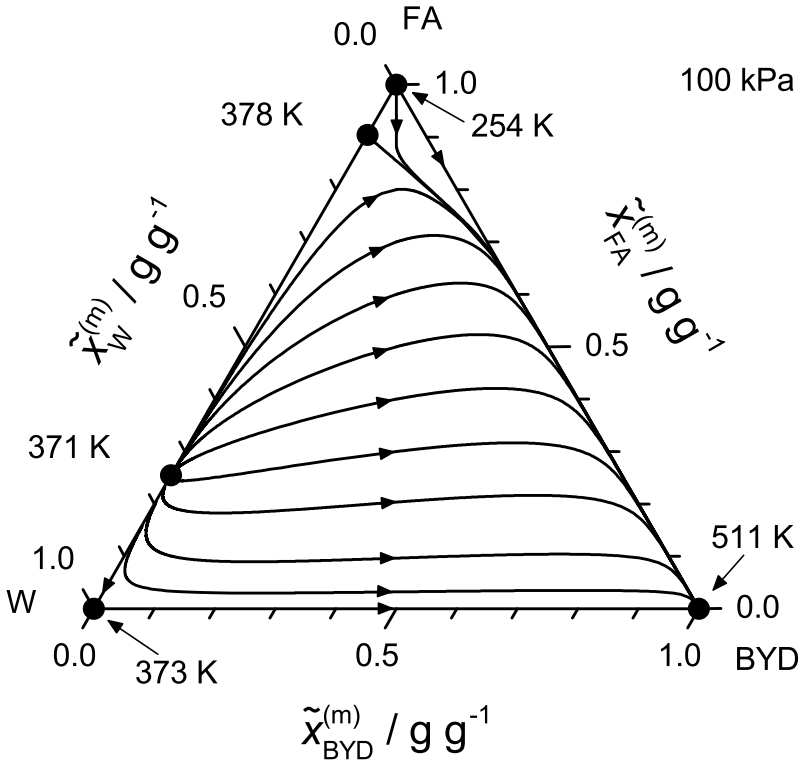

(a)

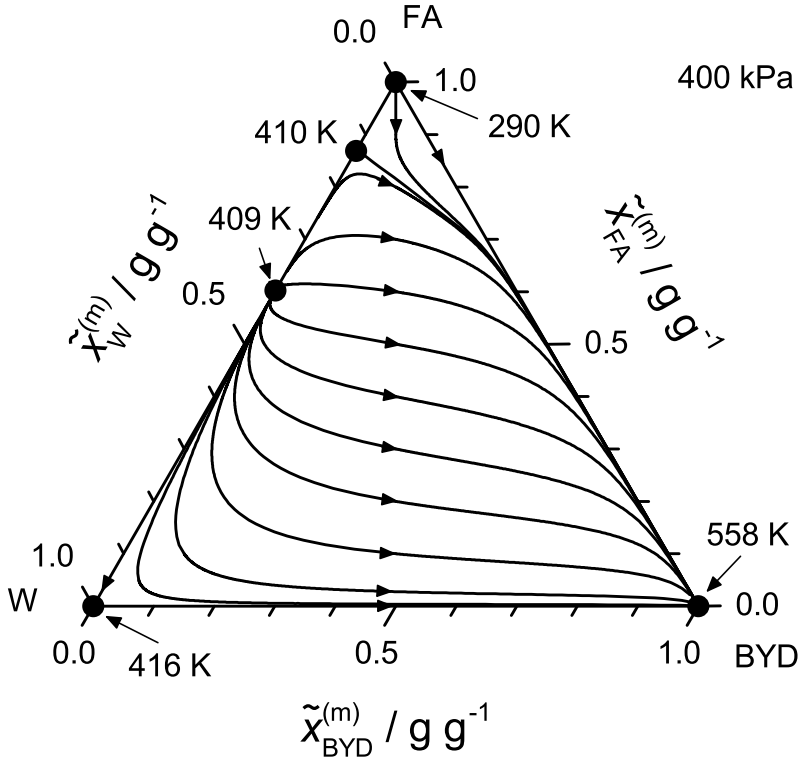

(b)

Figure 10: Residue curve maps for the system formaldehyde + water + butynediol. (a) 100 kPa, (b) 400 kPa. (•) singular point.

again because of the strong formaldehyde binding ability of butynediol [10], cf. also the discussion along Figure 9.

At 400 kPa, and thus higher temperatures, the global high-boiling azeotrope is located at a higher formaldehyde concentration since generally the oligomer chains in the liquid become shorter with rising temperature. Thus, following again residue curves below the unstable azeotrope, the depletion of formaldehyde is even stronger. Following the same argument, formaldehyde is also weaker bound in the poly(oxymethylene) hemiformals with butynediol.

4 Reaction Kinetics

4.1 Introduction

In many processes with formaldehyde-containing mixtures, also reaction kinetic effects play a role [16, 17, 20, 21, 37, 45, 49, 55, 56, 59]. Information on reaction kinetics is only available for the reactions of formaldehyde with water [29, 33, 35, 48], but not for those with butynediol. There is also information on the kinetics of the reactions of formaldehyde with mono-alcohols (methanol [29, 48], 1-butanol [18]), but the reactions with diols, such as butynediol have never been studied before. Recently, Kircher *et al.* [38] have proposed a generalized equilibrium constant for oligomerization reactions of formaldehyde with alcohols, but this approach cannot be extended in a straightforward manner to reaction kinetics.

This chapter finally deals with the experimental determination of the reaction kinetic rate constants for the oligomerization reactions of formaldehyde with butynediol using NMR spectroscopy. Besides kinetic experiments in NMR tubes, some NMR experiments have been carried out using a novel micro-mixer NMR probe [12, 13, 32] that enables to study fast reactions with time constants well below 1 min. The investigations were performed in the system formaldehyde + water + butynediol, as in the chapters before. Therefore, a kinetic model for the reactions of formaldehyde with water is needed for the evaluation of the results.

To keep the presentation in the main part concise, the experiments with the micro-mixer NMR probe are described in the Appendix section of this chapter. The kinetic model of the reactions of formaldehyde with water was taken from Hahnenstein *et al.* [29]. Furthermore, some experiments in the system formaldehyde + water were carried out with the micro-mixer NMR probe, at conditions where these reactions are so fast that it is difficult to study them with other methods. The new experimental results are as well reported in the Appendix and confirm the reaction kinetic model of Hahnenstein *et al.* [29].

4.2 Reactions

The reaction equations have already been discussed in Section 2.2. However, it is convenient to illustrate the reactions in the reaction kinetic context using reaction kinetic constants k instead of equilibrium constants K. Reactions (I) to (IV) become

$$\underbrace{CH_2O}_{\text{FA}} + \underbrace{H_2O}_{\text{W}} \underset{k^-_{\text{MG}_1}}{\overset{k^+_{\text{MG}_1}}{\rightleftharpoons}} \underbrace{HO(CH_2O)H}_{\text{MG}_1} \tag{V}$$

$$\underbrace{CH_2O}_{\text{FA}} + \underbrace{HO(CH_2O)_{n-1}H}_{\text{MG}_{n-1}} \underset{k^-_{\text{MG}_n}}{\overset{k^+_{\text{MG}_n}}{\rightleftharpoons}} \underbrace{HO(CH_2O)_nH}_{\text{MG}_n} \qquad n > 1 \tag{VI}$$

$$\underbrace{CH_2O}_{\text{FA}} + \underbrace{H\text{–}(OCH_2)_n\text{–}O\text{–}CH_2\text{–}C{\equiv}C\text{–}CH_2\text{–}OH}_{\text{BYD}_{n.0}} \underset{k^-_{n.0\leftrightarrow n.1}}{\overset{k^+_{n.0\leftrightarrow n.1}}{\rightleftharpoons}}$$
$$\underbrace{H\text{–}(OCH_2)_n\text{–}O\text{–}CH_2\text{–}C{\equiv}C\text{–}CH_2\text{–}O\text{–}CH_2\text{–}OH}_{\text{BYD}_{n.1}} \qquad n \geq 0 \tag{VII}$$

$$\underbrace{CH_2O}_{\text{FA}} + \underbrace{H\text{–}(OCH_2)_{n-1}\text{–}O\text{–}CH_2\text{–}C{\equiv}C\text{–}CH_2\text{–}O\text{–}(CH_2O)_m\text{–}H}_{\text{BYD}_{n-1.m}} \underset{k^-_{n-1.m\leftrightarrow n.m}}{\overset{k^+_{n-1.m\leftrightarrow n.m}}{\rightleftharpoons}}$$
$$\underbrace{H\text{–}(OCH_2)_n\text{–}O\text{–}CH_2\text{–}C{\equiv}C\text{–}CH_2\text{–}O\text{–}(CH_2O)_m\text{–}H}_{\text{BYD}_{n.m}} \qquad n > 1, m \geq 0 \tag{VIII}$$

In the study of the chemical equilibrium, two types of reactions were distinguished in the scheme shown in Figure 1 - and this classification is kept here: firstly, the addition of an unoccupied end to formaldehyde (displayed as solid arrows in Figure 1) and secondly, the addition of an occupied end to formaldehyde (presented as dashed arrows in Figure 1). In the chemical equilibrium model, the path on which a certain molecule is formed out of formaldehyde and butynediol does not matter. However, in the reaction kinetic context the path does matter so that all possible reactions need to be considered.

The superscripts above the reaction arrows in Reactions (VII) to (VIII) denote the rate constants $k^+_{n-1.m\leftrightarrow n.m}$ and $k^-_{n-1.m\leftrightarrow n.m}$ of the forward and backward reactions and their subscript denote which molecules are involved. Obviously, n and m can be exchanged so that $k^+_{n-1.m\leftrightarrow n.m}$ is equal to $k^+_{m.n-1\leftrightarrow m.n}$. All of them are expressed as functions of

four general rate constants $k^+_{\mathrm{BYD},1}$, $k^-_{\mathrm{BYD},1}$, $k^+_{\mathrm{BYD},2}$, and $k^-_{\mathrm{BYD},2}$, the subscript denoting the reaction type (Reactions (VII) and (VIII)). The type of reaction and the symmetry relations depicted in Figure 1, cf. Section 2.2 are used to relate the rate constants $k^+_{n-1.m\leftrightarrow n.m}$ and $k^-_{n-1.m\leftrightarrow n.m}$ on the one side to the rate constants $k^+_{\mathrm{BYD},1}$, $k^-_{\mathrm{BYD},1}$, $k^+_{\mathrm{BYD},2}$, and $k^-_{\mathrm{BYD},2}$ on the other side:

$$k^+_{n.0\leftrightarrow n.1} = 2\cdot k^+_{\mathrm{BYD},1} \quad \text{for} \quad n = 0 \tag{31}$$

$$k^+_{n.0\leftrightarrow n.1} = k^+_{\mathrm{BYD},1} \quad \text{for} \quad n \geq 1 \tag{32}$$

$$k^-_{n.0\leftrightarrow n.1} = 2\cdot k^-_{\mathrm{BYD},1} \quad \text{for} \quad n = 1 \tag{33}$$

$$k^-_{n.0\leftrightarrow n.1} = k^-_{\mathrm{BYD},1} \quad \text{for} \quad n \neq 1 \tag{34}$$

$$k^+_{n-1.m\leftrightarrow n.m} = 2\cdot k^+_{\mathrm{BYD},2} \quad \text{for} \quad (n-1=m)\wedge(m\geq 1) \tag{35}$$

$$k^+_{n-1.m\leftrightarrow n.m} = k^+_{\mathrm{BYD},2} \quad \text{for} \quad (n-1>m)\wedge(m\geq 0) \tag{36}$$

$$k^-_{n-1.m\leftrightarrow n.m} = 2\cdot k^-_{\mathrm{BYD},2} \quad \text{for} \quad (n=m)\wedge(m\geq 2) \tag{37}$$

$$k^-_{n-1.m\leftrightarrow n.m} = k^-_{\mathrm{BYD},2} \quad \text{for} \quad (n-1>m)\wedge(m\geq 0) \tag{38}$$

The rate constants are related to the chemical equilibrium constants K_j by

$$K_j = \frac{k^+_j}{k^-_j} \tag{39}$$

This is consistent with the definition of the chemical equilibrium constants in Eqs. (8) to (13). In the present work, Eq. (39) was used to calculate the backward reaction constants k^-_j from the forward reaction constants k^+_j and the equilibrium constants K_j. In the formaldehyde + butynediol system, $K_{\mathrm{BYD},1}$ and $K_{\mathrm{BYD},2}$ from Chapter 2 are used as shown in the following example for the first reaction in Figure 1:

$$K_{0.0\leftrightarrow 1.0} = \frac{k^+_{0.0\leftrightarrow 1.0}}{k^-_{0.0\leftrightarrow 1.0}} = \frac{2\cdot k^+_{\mathrm{BYD},1}}{k^-_{\mathrm{BYD},1}} = 2\cdot K_{\mathrm{BYD},1} \tag{40}$$

The task of this work is finding an expression for $k^+_{\mathrm{BYD},1}$ and $k^+_{\mathrm{BYD},2}$.

4.3 Kinetic model

The rate equations used here to calculate time-dependent component amounts n_i are formulated similar to previous works [18, 29, 47, 48]:

$$\frac{\mathrm{d}n_i}{\mathrm{d}t} = n_{\mathrm{tot}}\cdot\sum_{j=1}^{2R}\left(\nu_{i,j}\ k^x_j\prod_{l\in E_j} x_l^{|\nu_{l,j}|}\right) \tag{41}$$

In this rate expression, the equilibrium reactions shown in the previous section are separated into forward and backward reactions and R is the number of equilibrium reactions, n_{tot} is the total molar amount of substance, $\nu_{i,j}$ is the stoichiometric coefficient of component i in reaction j, k_j^x the rate constant of the model for reaction j, and x_l the mole fraction of component l. E_j is the set of the components on the reactant side in reaction j. As an example, the change of the amount of $\mathrm{BYD}_{1.0}$ is given in Eq. (42):

$$\begin{aligned}\frac{1}{n_{\mathrm{tot}}} \cdot \frac{\mathrm{d}n_{\mathrm{BYD}_{1.0}}}{\mathrm{d}t} =& 2 \cdot k^+_{\mathrm{BYD},1} \cdot x_{\mathrm{FA}} \cdot x_{\mathrm{BYD}_{0.0}} - \frac{k^+_{\mathrm{BYD},1}}{K_{\mathrm{BYD},1}} \cdot x_{\mathrm{BYD}_{1.0}} \\ & - k^+_{\mathrm{BYD},1} \cdot x_{\mathrm{FA}} \cdot x_{\mathrm{BYD}_{1.0}} + 2 \cdot \frac{k^+_{\mathrm{BYD},1}}{K_{\mathrm{BYD},1}} \cdot x_{\mathrm{BYD}_{1.1}} \\ & - k^+_{\mathrm{BYD},2} \cdot x_{\mathrm{FA}} \cdot x_{\mathrm{BYD}_{1.0}} + \frac{k^+_{\mathrm{BYD},2}}{K_{\mathrm{BYD},2}} \cdot x_{\mathrm{BYD}_{2.0}} \end{aligned} \tag{42}$$

Analogously to the equilibrium model, the components considered in the model are FA, W, MG_n with $1 \le n \le 10$, and $\mathrm{BYD}_{n.m}$ with $0 \le n+m \le 10$. Longer oligomers are not considered since their concentrations can be neglected. Chemical equilibrium constants and rate constants for the reactions of formaldehyde with water yielding poly(oxymethylene) glycols, cf. Reactions (V) and (VI), were taken from Hahnenstein *et al.* [29, 30] who have used three independent chemical equilibrium constants, namely $K^x_{\mathrm{MG}_1}$, $K^x_{\mathrm{MG}_2}$, and $K^x_{\mathrm{MG}_n}$ with $n \ge 3$, as well as two independent rate constants $k^{+,x}_{\mathrm{MG}_1}$ and $k^{+,x}_{\mathrm{MG}_n}$ with $n \ge 2$. Here, the superscript x indicates that the constants refer to the model based on mole-fractions. However, as the mechanism of the addition reactions in the formaldehyde + water system is formulated differently in this work than in that of Hahnenstein *et al.* [29, 30], the parameters of the literature model had to be converted. How this was done is shown in Section 4.7.5. The converted parameters are reported in Table 8. The chemical equilibrium constants of the reactions of formaldehyde with water and formaldehyde with butynediol were calculated using an Arrhenius type equation [10, 30]:

$$K_j = \exp\left(A_j - \frac{B_j}{T/\mathrm{K}}\right) \tag{43}$$

The rate constants depend also on the pH value. The rate constants of the forward reactions in the formaldehyde + water system were calculated using the following equation [29]:

$$k^+_j/\mathrm{s}^{-1} = \left(1 + C_{1,j} \cdot 10^{-\mathrm{p}H} + \exp\left(C_{2,j} - \frac{C_{3,j}}{T/\mathrm{K}}\right) \cdot 10^{+\mathrm{p}H}\right) \cdot \exp\left(A_j - \frac{B_j}{T/\mathrm{K}}\right) \tag{44}$$

Table 8: Parameters of the reaction kinetic model for mixtures of formaldehyde + water + butynediol. Parameters from literature models were converted to fit into the present model as explained in the Appendix.

	Equation	A	B	C_1	C_2	C_3	Source
$K^x_{\mathrm{MG}_1}$	(43)	-2.325	-2579				[29]
$K^x_{\mathrm{MG}_2}$		-2.31051	-3139.9				[29]
$K^x_{\mathrm{MG}_n}$		-2.4334	-3039.4				[29]
$K^x_{\mathrm{BYD},1}$		-2.225	-3392.6				[10]
$K^x_{\mathrm{BYD},2}$		-2.334	-3032.4				[10]
$k^{+,x}_{\mathrm{MG}_1}$	(44)	8.962	1913	870	-16.5801	0	[29]
$k^{+,x}_{\mathrm{MG}_n}$		20.795	5972	247.3	-0.838	3102	[29]
$k^{+,x}_{\mathrm{BYD},1}$	(47)	16.5248	4443.23	9.486E-03	4.00		this work
$k^{+,x}_{\mathrm{BYD},2}$		21.8238	6584.64	0.2691	3		this work

4.4 Experiments

4.4.1 Chemicals

Aqueous stock solutions of formaldehyde were created by dissolution of paraformaldehyde (95-100 %, Merck) in ultrapure water at high temperatures. The overall formaldehyde concentration in the stock solutions was always around 0.33 g g^{-1}. High formaldehyde concentrations are needed to get high amounts of long-chained oligomers. The overall concentration of formaldehyde in the aqueous solution was determined by the sodium sulfite method [61] (uncertainty usually below 2 %). For the individual experiments the pH value of the formaldehyde solution taken from stock was adjusted to the desired value using small amounts of formic acid or sodium hydroxide.

The ultrapure water was produced using the Milli-Q integral water purification system from MerckMillipore, Darmstadt, Germany. Butynediol (99 %, Sigma-Aldrich) was recristallized with diethyl ether from an ethyl acetate solution, following the methodology described by Pyatnitsyna *et al.* [51]., to achieve purification. In the experiments, butynediol was used in aqueous solution at concentrations of about 0.67 g g^{-1}. The solutions can be stored at room temperature without precipitation of butynediol. The solutions were prepared gravimetrically using a high precision balance (Mettler Toledo XS603S). The uncertainty in the butynediol concentration in the stock solution is below 1 %.

4.4.2 Experimental setup and procedure

The experimental investigations of reaction kinetics were carried out using ^{1}H-NMR spectroscopy. In principle, quantitative ^{13}C{^{1}H}-NMR spectroscopy would have been

attractive due to its higher dispersion, but the acquisition time is too high to monitor the fast reactions that are of interest here. $^{13}C\{^1H\}$-NMR spectroscopy was only applied for a single test measurement that was carried out at conditions where the reaction kinetics in the studied system are slow. This experiment is described in Section 4.7.6 in the Appendix.

The reactions were started by dilution of aqueous formaldehyde solutions with aqueous butynediol solutions. In most experiments this was done outside the NMR spectrometer and the reacting sample was inserted in the NMR spectrometer in a 5 mm NMR sample tube to monitor the kinetics. These experiments are described here. A few additional experiments were carried out using a micro-mixer NMR probe that allows to reduce the delay time between the mixing and the start of the kinetic monitoring. These experiments are discussed in Section 4.7.1 in the Appendix.

An NMR spectrometer with a proton resonance frequency of 399.83 MHz (Unity Inova 400, Varian, Palo Alto, USA) was used for all experiments. For the experiments with the sample tubes, it was equipped with a Varian 400 AutoSW PFG 4 nuclei probe. The acquisition parameters were: acquisition time 2.5 s, relaxation delay $\geq$ 2.5 s, pulse width 10°, 1 scan per spectrum. The temperature measurement in the spectrometer was calibrated by chemical shift difference with methanol and ethylene glycol respectively [7]. The uncertainty of the temperature measurement is 1 K.

The liquid mixtures of formaldehyde + water and water + butynediol were stored in closed glass vessels that were placed in a thermostatted bath on a magnetic stirrer for at least one hour before starting the experiment. The mixing mass ratio of the aqueous formaldehyde solution and the aqueous butynediol solution was chosen based on preliminary NMR experiments to ensure reasonable accuracy of the quantitative evaluation of the signals. Small amounts of formic acid or sodium hydroxide were added to the formaldehyde + water mixture to adjust the pH value.

To start the reactions, the water + butynediol mixture was added to the formaldehyde + water mixture by a syringe. After 5 s of magnetic stirring, about 0.7 mL of the reacting mixture were filled into a NMR tube using a syringe and put into the spectrometer immediately. The NMR tube and the syringes were preheated in an oven at reaction temperature. The time between the mixing of the two substances and the start of the NMR measurement was measured by a stop watch. This procedure may have caused temperature shifts beyond the experimental uncertainty of the temperature measurement. They level out in the thermostatted NMR probe but may have influenced the starting phase of the kinetic measurements. The mass of both mixtures was determined by differential weighing. The resulting uncertainty of the overall mole fractions of formaldehyde and butynediol in initial solution is below 2 % and 1 %, respectively.

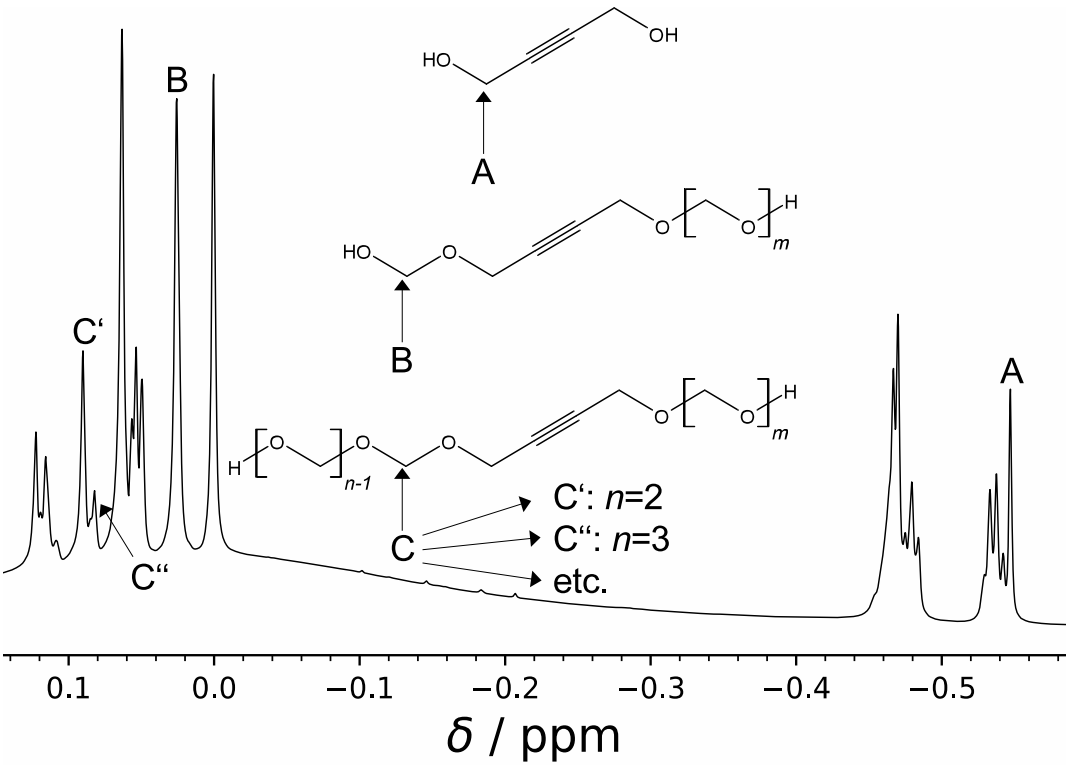

Figure 11: ^{1}H-NMR spectrum of a mixture of formaldehyde + water + butynediol in chemical equilibrium ($\tilde{x}_{\mathrm{FA}}^{(\mathrm{m})}$ = 0.27 g g^{-1}, $\tilde{x}_{\mathrm{W}}^{(\mathrm{m})}$ = 0.53 g g^{-1}, $\tilde{x}_{\mathrm{BYD}}^{(\mathrm{m})}$ = 0.20 g g^{-1}, T = 293 K, pH = 6.8, reference: TMSP). The peaks designated with A, B, and C' and C" were used for the quantification. C"' is between C' and C". C' and C" cannot be deconvoluted and were evaluated together.

After the kinetic measurement, the pH value was measured (pH Meter 713; electrode: LL Unitrode Pt 1000, Metrohm). The uncertainty due to small changes in the pH value during the measurements is about ±0.2.

4.4.3 Quantitative analysis of the NMR spectra

^{1}H and ^{13}C-NMR spectra for the system formaldehyde + water + butynediol have been discussed in detail in Chapter 2 and all peaks have been assigned [10]. Therefore, only those aspects of the spectra that are relevant for their quantitative evaluation in the present work are discussed here. Figure 11 shows a ^{1}H-NMR spectrum of a mixture of formaldehyde + water + butynediol in chemical equilibrium. In Figure 11, two signals A and B and a group of signals C are labeled that were used for the quantification.

Peak A is the signal of the methylene groups in butynediol. Peaks B, and the peak group C stem from methylene groups in oligomers that are located next to the butynylene core: peak B stems from oligomers with n = 1 methylene group bound to the considered side of the core, the peak group C stems from oligomers for which $n > 1$. In the spectrum in Figure 2 two peaks can be distinguished in that group: C' for which n = 2 and C" for

which n = 3. Also signals from oligomers with $n > 3$ lie in the spectral region C. Due to the strong overlap, it is difficult to deconvolute the individual peaks in the area, which is why they were lumped into the signal C that was integrated as a whole.

The peaks A, B and C contain reaction kinetic information about the decay of the butynediol concentration and the formation of oligomers. The areas were quantified using the software PEAXACT (version: 4.0.0, S-PACT GmbH, Aachen, Germany) with indirect hard modeling (IHM) [40]. With the IHM method, parametrized peak functions (Lorentz/Gauss curves) are fitted to the spectra. The number of fitted functions was determined from the spectrum of the mixture at the end of the experiment. The parameters of the peak functions were then fitted to each spectrum individually.

From the peak areas A_A, A_B, and A_C, peak area fractions $\zeta_\mathrm{BYD,1}$ and $\zeta_\mathrm{BYD,2}$ were calculated and related to mole fractions of individual species, taking into account the number of hydrogen atoms that cause the corresponding signals:

$$\zeta_\mathrm{BYD,1} = \frac{A_\mathrm{B}}{A_\mathrm{A}} = \frac{x_{\mathrm{BYD}_{1.1}} + \sum_{n=0}^{10} x_{\mathrm{BYD}_{n.1}}}{2 \cdot x_{\mathrm{BYD}_{0.0}}} \tag{45}$$

$$\zeta_\mathrm{BYD,2} = \frac{A_\mathrm{C}}{A_\mathrm{A}} = \frac{\sum_{n=2}^{10} \sum_{m=0}^{10-n} x_{\mathrm{BYD}_{n.m}} + \sum_{n=2}^{5} x_{\mathrm{BYD}_{n.n}}}{2 \cdot x_{\mathrm{BYD}_{0.0}}} \tag{46}$$

4.5 Determination of the model parameters

The rate constants $k^+_\mathrm{BYD,1}$ and $k^+_\mathrm{BYD,2}$ were fitted to the time-dependent experimental peak area ratios $\zeta_\mathrm{BYD,1}(t)$ and $\zeta_\mathrm{BYD,2}(t)$ for each experiment individually using the software gPROMS. In the fits, also the chemical equilibrium constants $K_\mathrm{BYD,1}$ and $K_\mathrm{BYD,2}$, cf. Eq. (39), were adjusted, as even small differences in the representation of the equilibria can lead to large errors in the fit of the kinetic constants. The four fit parameters $k^+_\mathrm{BYD,1}$, $k^+_\mathrm{BYD,2}$, $K_\mathrm{BYD,1}$, and $K_\mathrm{BYD,2}$ were obtained by minimizing the sum of squared absolute deviations between the experimental ζ_i^exp and the calculated ζ_i^mod using the least squares method. Thereby, the initial amounts of species in the reacting mixture were calculated from the true composition of the initial formaldehyde + water mixture assuming equilibrium taking into account the dilution with the water + butynediol mixture. Hence, at $t = 0$, there are no butynediol oligomers.

4.6 Results and discussion

A typical result of a kinetic measurement in the system formaldehyde + water + butynediol is depicted in Figure 12. The experimental results for $\zeta_\mathrm{BYD,1}$ and $\zeta_\mathrm{BYD,2}$ are

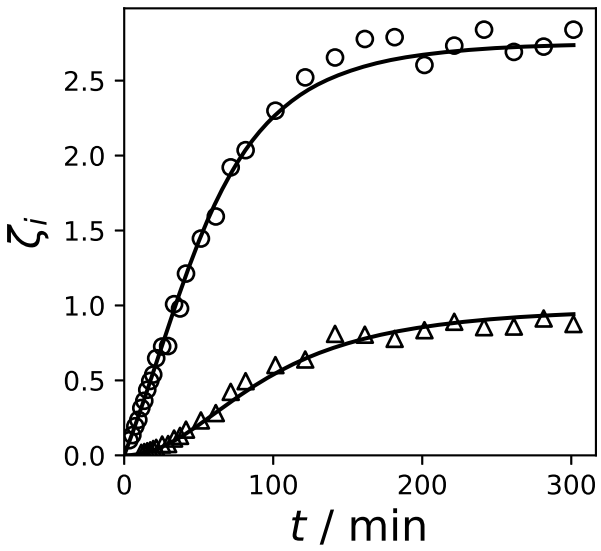

Figure 12: Experimental and calculated peak area fractions after mixing an equilibrated formaldehyde solution ($\tilde{x}^{(\mathrm{m})}_{\mathrm{FA,stock}}$ = 0.3367 g g^{-1}) with aqueous butynediol ($x^{(\mathrm{m})}_{\mathrm{BYD}}$ = 0.6006 g g^{-1}); mass ratio = 2.275:1. T = 293.15 K, pH = 4.35. (∘) $\zeta_{\mathrm{BYD},1}$, (△) $\zeta_{\mathrm{BYD},2}$ see Eqs. (45) and (46), (——) reaction kinetic model.

compared to model results obtained using the correlations for all of the four fit parameters, cf. Table 8. The correlations for $k^{+}_{\mathrm{BYD},1}$ and $k^{+}_{\mathrm{BYD},2}$ are introduced later in this section. Both curves start in the origin of the diagram, as there is only butynediol but no butynediol oligomers. The curve shape of $\zeta_{\mathrm{BYD},2}$ differs from that of $\zeta_{\mathrm{BYD},1}$. Since initially formaldehyde-free reaction sites of BYD react with formaldehyde, cf. Reaction (VII), the chain propagation reactions represented by Reaction (VIII) are delayed. This results in a sigmoid curve shape for $\zeta_{\mathrm{BYD},2}$. The corresponding figures for all other experiments are presented in the Supporting Information. The Supporting Information also contains a table showing the full set of specification of all experiments.

Table 9 gives an overview of the results for the kinetic constants and the equilibrium constants obtained from the fits. Figure 13 shows a comparison between the equilibrium constants determined from the individual fits to the kinetic ^{1}H-NMR spectroscopic data from the present work and the equilibrium model that was established in our previous work [10] based on dedicated equilibrium experiments with ^{13}C-NMR spectroscopy. As can be seen from Figure 13, the agreement between the two sets of results is generally good. Remaining deviations should not be over-interpreted as the goal of the present study was not to get new data on the equilibrium constants - they were obtained as a collateral result. As a consequence, the equilibrium constants from the present work are subject to considerable uncertainties, especially when small peaks had to be quantified, as it is the case for $K^{x}_{\mathrm{BYD},2}$. All in all, the comparison shown in Figure 13 confirms both

the results from the previous work, cf. Chapter 2 or Ref. 10 as well as the experimental method and the evaluation method used here. For completeness, Figure 13 also shows the results that were obtained in the present work in the kinetic experiments with the micro-mixer NMR probe. These results are discussed in the Appendix.

Figure 14 shows the results for the rate constants $k^{+,x}_{\mathrm{BYD},1}$ and $k^{+,x}_{\mathrm{BYD},2}$ obtained from the individual fits to the reaction kinetic data from the present work. The results obtained from the experiments in the NMR tubes as well as those from the experiments with the micro-mixer NMR probe are shown. They cover temperatures between 293 K and 328 K, the pH value is between 3 and 6. The observed dependence of the rate constant on the pH value with a minimum is typical for oligomerization reactions of formaldehyde [18, 25, 29, 48]. The data scatter, especially those for $k^{+,x}_{\mathrm{BYD},2}$ that were obtained from data on small overlapping peaks, but clear trends can be discerned. A quadratic expression for modeling the dependence of the data on the pH value combined

Table 9: Overview of experimental conditions and results of the fits of the reaction kinetic constants and equilibrium constants to the individual experiments.

NMR probe	T / K	pH	$k^{+,x}_{\mathrm{BYD},1}$	$k^{+,x}_{\mathrm{BYD},2}$	$K^{+,x}_{\mathrm{BYD},1}$	$K^{+,x}_{\mathrm{BYD},2}$
tube	293.15	3.09	4.62	0.40	11507	3063
		3.283	4.39	0.57	12068	2147
		3.514	3.50	0.40	10991	3661
		4.35	3.61	0.39	12544	6029
		4.717	4.01	1.61	12025	3515
		4.8	4.31	1.08	12205	5190
	303.15	3.54	6.76	1.94	7614	1968
		4.53	6.51	2.88	8429	2448
		4.87	8.81	6.96	8944	2228
	313.15	3.33	12.49	1.58	6026	2017
		3.88	10.30	4.05	5768	1689
		4.51	10.57	6.47	5986	1719
micro-mixer	313.15	3.61	9.24	2.03	3995	1468
		4.2	9.27	3.28	4189	1562
		5.864	12.81	14.92	3648	1475
tube	323.15	3.04	15.85	3.65	4390	1292
		3.3	16.29	2.72	4536	1379
		4.36	17.68	8.63	4088	1260
micro-mixer	323.15	4.5	16.42	8.63	2844	1041
		5.755	22.76	18.45	2680	757
tube	328.15	3.32	22.38	4.07	3995	999
		4.29	19.24	14.59	3800	1137

with an Arrhenius type expression for modeling the temperature dependence was used:

$$k^{+,x}_{\mathrm{BYD},i} = \exp\left(A - \frac{B}{T/\mathrm{K}} + C_1 \cdot (\mathrm{p}H - C_2)^2\right) \tag{47}$$

The parameters A, B, C_1, and C_2 of Eq. (47) were determined from a fit to the data by multiple linear regression of $\ln k^{+,x}_{\mathrm{BYD},i}$. The results are reported in Table 8. The results of the correlation are shown in Figure 14 as solid lines. Fair agreement within the strong scattering of the data is observed. The mean average percentage deviation (MAPD) is 7 % for $k^{+,x}_{\mathrm{BYD},1}$ and 36 % for $k^{+,x}_{\mathrm{BYD},2}$. A summary of the model parameter values is given in Table 8.

As stated above and described in more detail in the Appendix, a single kinetic experiment was carried out in a test tube with quantitative $^{13}\mathrm{C}\{^1\mathrm{H}\}$-NMR spectroscopy. The results of this experiment are shown in Figure 15 and were not used for the model development. Excellent agreement of the measured and the calculated species distribution is found. In particular, also the maximum in the concentration of $\mathrm{BYD}_{1.0}$ and the minimum in the concentration of MG_1 is correctly predicted. The shown maximum in the concentration of $\mathrm{BYD}_{1.0}$ and the minimum in the MG_1 concentration cannot be observed in the peak area fractions that were used for the model development, cf. also Figure 12. This is because the individual species are lumped together into $\zeta_{\mathrm{BYD},1}$ and $\zeta_{\mathrm{BYD},2}$.

4.7 Appendix Chapter 4

4.7.1 Experiments with the micro-mixer NMR probe

Figure 16 shows the experimental setup that was used for the experiments with the micro-mixer NMR probe to extend the database for the systems formaldehyde + water and formaldehyde + water + butynediol. The two solutions which are to be mixed were filled into two syringe pumps (260D, Teledyne Isco) that were connected to the micro-mixer NMR probe which was placed in the same NMR spectrometer that was used also for the other experiments (see Section Experiments). For a detailed description of the probe, see Refs. 12, 13, 32. Pumps, capillaries, as well as the micro-mixer NMR probe were thermostatted to the desired temperature. At the outlet, the mixture was either discarded or led to a thermostatted vessel for the pH measurement. Two Coriolis flow meters (mini CORI-FLOW™ M12, Bronkhorst High-Tech) were installed in the feed lines to obtain data on the mass flows of the mixtures from which their mass ratio was

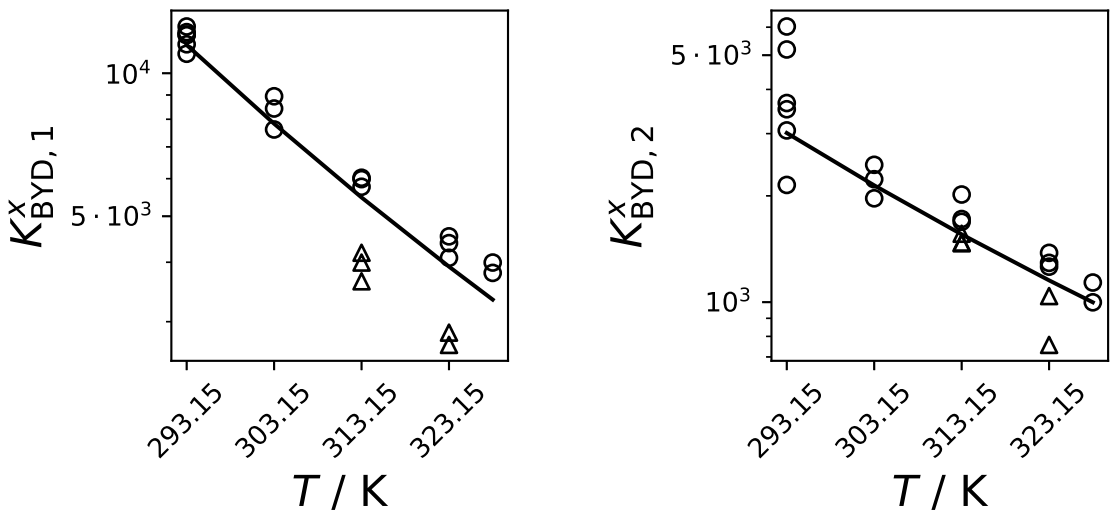

(a) (b)

Figure 13: Chemical equilibrium constants. a) $K^x_{\mathrm{BYD},1}$ and b) $K^x_{\mathrm{BYD},2}$. Symbols: values obtained from the fits to the reaction kinetic experiments, (∘) tube experiments, (△) micro-mixer experiments, (——) equilibrium model [10].

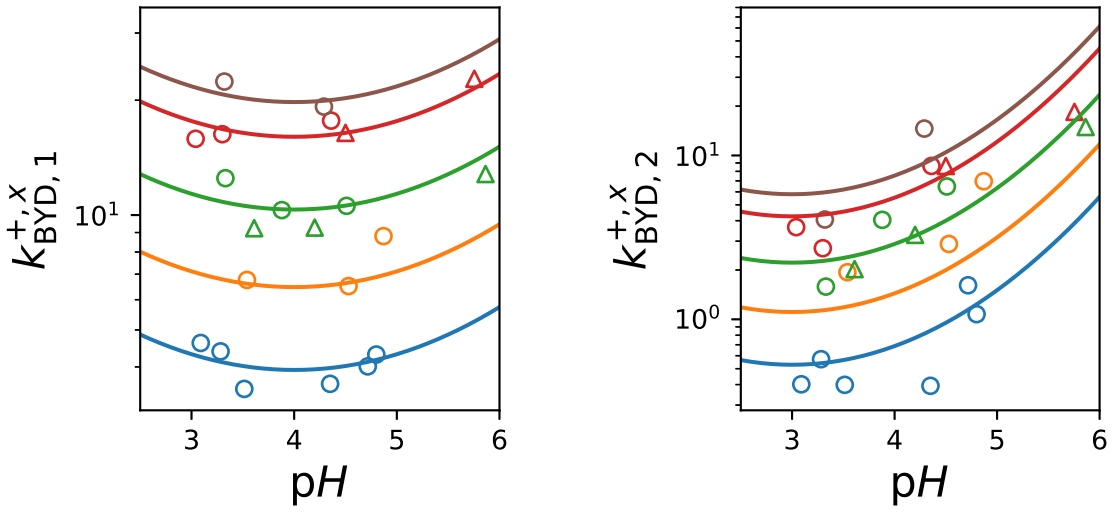

(a) (b)

Figure 14: Rate constants for the reactions of formaldehyde with butynediol. (a) reaction with an unoccupied end according to Eq. (VII), (b) reaction with an occupied end according to Eq. (VIII); (blue) 293 K, (orange) 303 K, (green) 313 K, (red) 323 K, (brown) 328 K, (∘) tube experiments, (△) micro-mixer experiments, (——) reaction kinetic model.

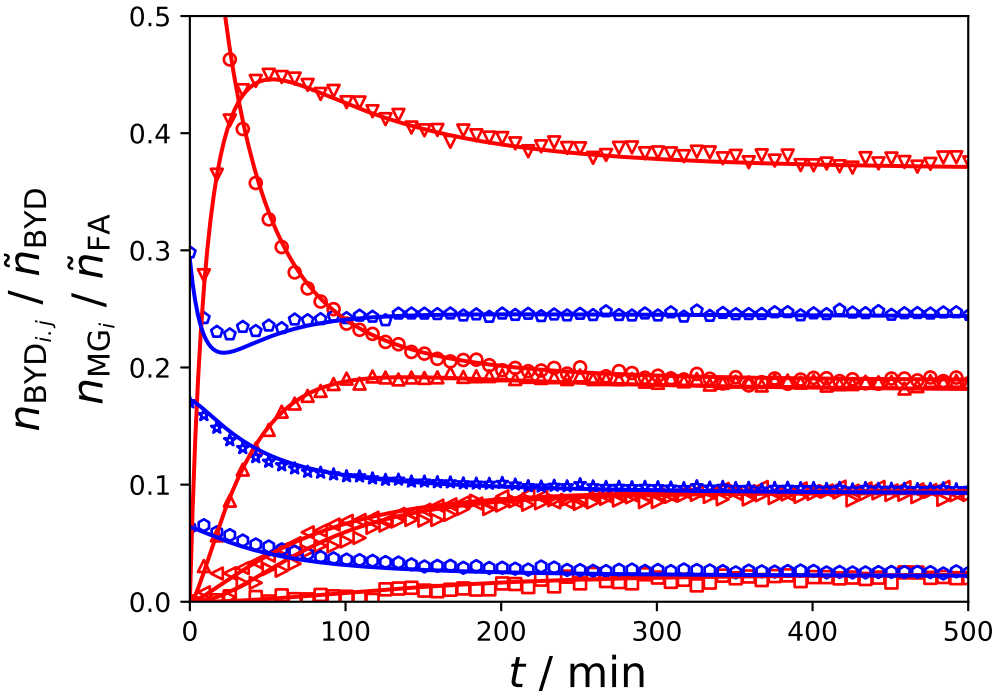

Figure 15: Results from a test measurement carried out with ^{13}C-NMR spectroscopy. Ratios of true amounts to overall amounts for butynediol and reaction products of butynediol with formaldehyde (red) and reaction products of water with formaldehyde (blue). An equilibrated aqueous formaldehyde solution ($\tilde{x}_{FA}^{(m)}$ = 0.2955 g g^{-1}) was diluted with aqueous butynediol ($x_{BYD}^{(m)}$ = 0.6526 g g^{-1}), the mass ratio was 2.414:1. T = 293.15 K, pH = 4.18. (∘) $BYD_{0.0}$, (▽) $BYD_{1.0}$, (△) $BYD_{1.1}$, (◁) $BYD_{2.0}$, (▷) $BYD_{2.1}$, (□) $BYD_{3.0}$, (⬠) MG_1, (⋆) MG_2, (⬡) MG_3, (——) reaction kinetic model.

calculated. The temperature was measured in the probe with a calibrated platinum resistance thermometer with an uncertainty of 0.2 K.

The feed mixtures were stored in the thermostatted pumps for at least one hour to ensure equilibration. After switching on the pumps, the system was purged for about 10 min. During this time, the mixture leaving the probe is first discarded; then, it is collected for the pH measurement. High feed flow rates were used to obtain a short time delay between the mixing and the detection in the NMR coil. The total flow rate of the two pumps was 1 mL min^{-1} in all experiments. The kinetic measurements were carried out after stopping the flow. This was done by swithching the four-way valve and stopping the pumps. The time at which this was done is considered as t = 0 of the experiment. The pressure in the system was controlled by a nitrogen reservoir connected to the liquid outlet and measured at several points in the system. The pressure was about 2 bar and is not reported for the individual experiments as its influence on the results for the liquid phase reaction kinetics is small. The following acquisition parameters were used

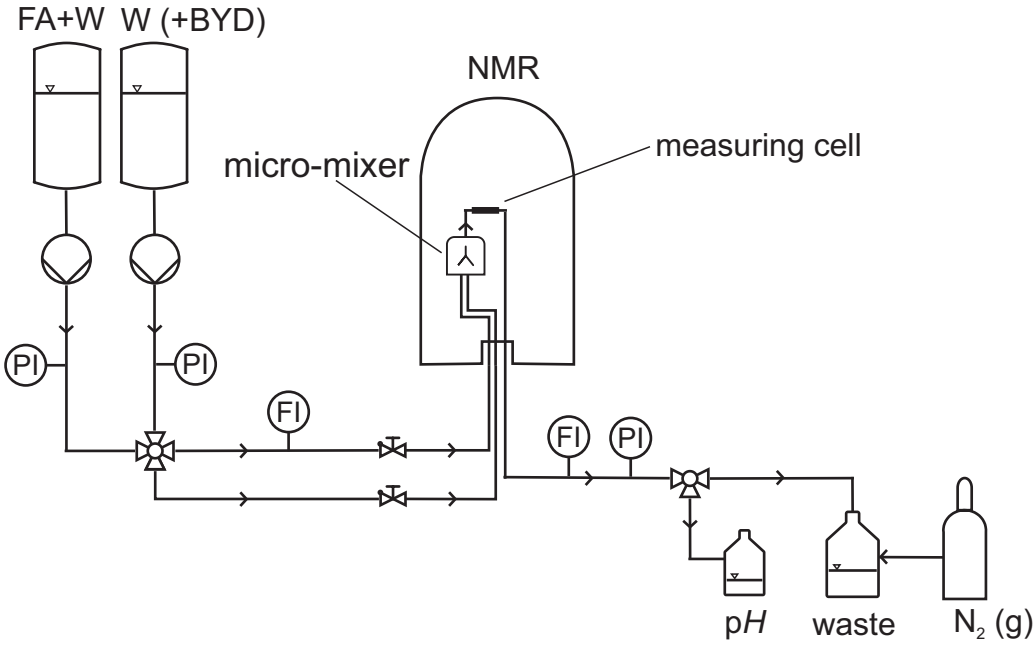

Figure 16: Experimental setup of NMR experiments with the micro-mixer NMR probe.

to generate ^{1}H-NMR spectra: acquisition time 0.5 s, relaxation delay ≥ 1.5 s, pulse width 10°, 1 scan per spectrum.

4.7.2 Analysis of the NMR spectra obtained with the micro-mixer NMR probe

^{1}H and ^{13}C-NMR spectra of the mixtures formaldehyde + water and formaldehyde + water + butynediol are well understood, cf. for example Refs. 10, 29, 44. However, ^{1}H-NMR spectra generated with the micro-mixer NMR probe show broader signals due to field inhomogeneities which result in strong signal overlapping. Therefore, examples of spectra of the studied systems taken with the micro-mixer NMR probe are shown in Figure 17. The spectra are dominated by a large, broad peak from hydrogen nuclei of water and all hydroxyl groups. The position of this peak strongly depends on the temperature and the pH value.

The used nomenclature for the non-interchangeable hydrogen is also depicted in Figure 17. The methylene groups in the butynylene group ($-CH_2-C\equiv C-CH_2-$) are labeled with a superscript β. Methylene groups in the CH_2O chain on both sides of the butynylene group are indicated with superscript Arabic numbers. The position of the superscript indicates the location of the nuclei in $BYD_{n.m}$. A superscript on the left side represents the n-side of the molecule, while a superscript on the right side represents the m-side. These sides are equivalent because exchanging corresponding indices does not change the molecule. However, in unsymmetrical molecules, the location of a

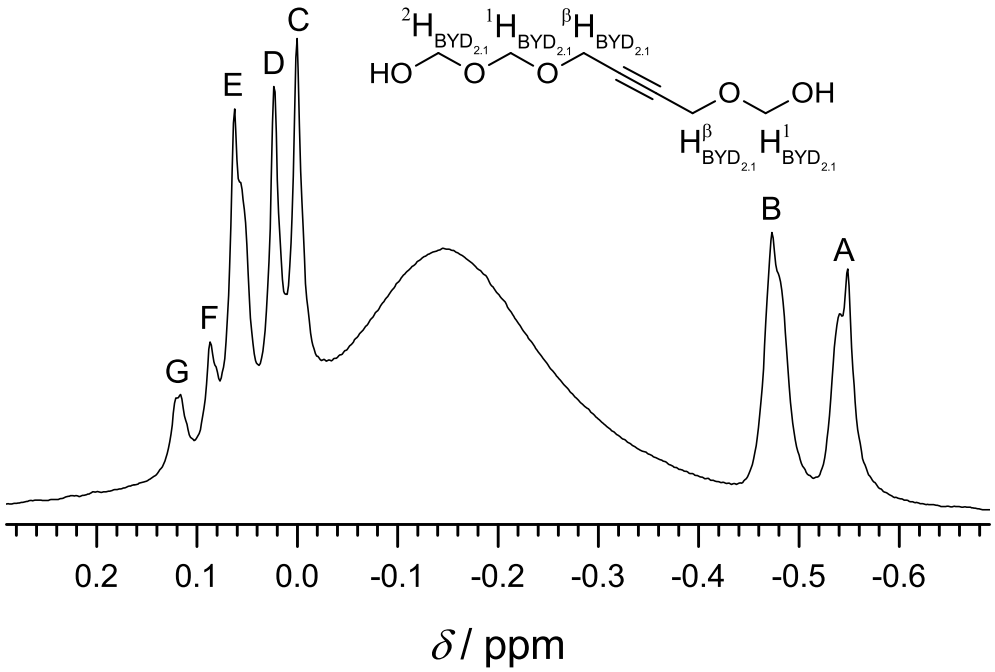

(a)

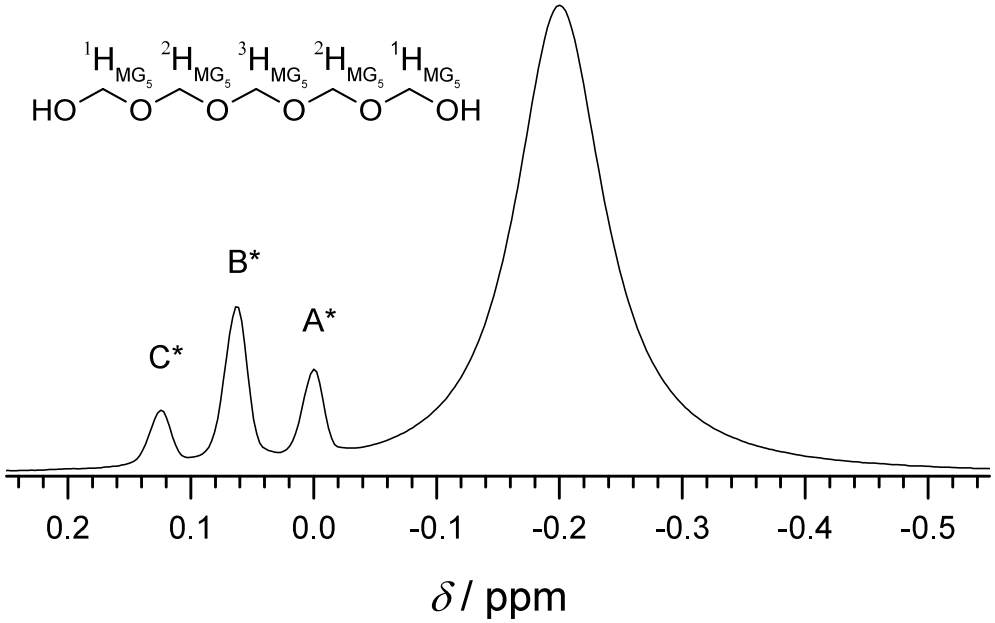

(b)

Figure 17: ^{1}H-NMR spectra taken with the micro-mixer NMR probe. (a) Mixture formaldehyde + water + and butynediol; $\tilde{x}^{(m)}_{FA}$ = 0.229 g g^{-1}, $\tilde{x}^{(m)}_{W}$ = 0.568 g g^{-1}, $\tilde{x}^{(m)}_{BYD}$ = 0.203 g g^{-1}, T = 313.15 K, pH = 4.2, reference: $\delta(^{1}H_{MG_1}) = 0$ ppm. (b) Mixture formaldehyde + water; $\tilde{x}^{(m)}_{FA}$ = 0.178 g g^{-1}, $\tilde{x}^{(m)}_{W}$ = 0.822 g g^{-1}, T = 323 K, pH = 4.0, reference: $\delta(^{1}H_{MG_1}) = 0$ ppm. The labels A-G and A*-C* are explained in Tables 10 and 11.

Table 10: ^{1}H chemical shifts for a mixture of formaldehyde and water ($\tilde{x}_{\mathrm{FA}}^{(\mathrm{m})}$ = 0.178 g g^{-1}, $\tilde{x}_{\mathrm{W}}^{(\mathrm{m})}$ = 0.822 g g^{-1}, T = 323 K, pH = 4.0, reference: $\delta(^1\mathrm{H}_{\mathrm{MG}_1})$ = 0 ppm). All peaks stem from methylene groups: A* from MG_1, B* from chain ends of MG_n, $n > 1$ and C* from middle groups in MG_n, $n > 2$, that are not connected to hydroxyl groups.

^{1}H (400.40 MHz)		
Peak	δ / ppm	Assignment
A*	0.00	$^1\mathrm{H}_{\mathrm{MG}_1}$
B*	0.06	$^1\mathrm{H}_{\mathrm{MG}_n}$, $n \geq 2$ (end)
C*	0.12	$^i\mathrm{H}_{\mathrm{MG}_n}$, $n \geq 3,\ n/2+1 > i \geq 2$ (middle)

Table 11: ^{1}H chemical shifts for a mixture of formaldehyde + water + butynediol ($\tilde{x}_{\mathrm{FA}}^{(\mathrm{m})}$ = 0.229 g g^{-1}, $\tilde{x}_{\mathrm{W}}^{(\mathrm{m})}$ = 0.568 g g^{-1}, $\tilde{x}_{\mathrm{BYD}}^{(\mathrm{m})}$ = 0.203 g g^{-1}, T = 313.15 K, pH = 4.2, reference: $\delta(^1\mathrm{H}_{\mathrm{MG}_1})$ = 0 ppm). An explanation of the nomenclature used for the peak assignment is given in the text.

^{1}H (400.40 MHz)		
Peak	δ / ppm	Assignment
A	–0.55	$\mathrm{H}^{\beta}_{\mathrm{BYD}_{n.0}}$, $n \geq 0$
B	–0.47	$^{\beta}\mathrm{H}^{\beta}_{\mathrm{BYD}_{n.m}}$, $n,\ m \geq 1$
C	0.00	$^1\mathrm{H}_{\mathrm{MG}_1}$
D	0.02	$\mathrm{H}^{1}_{\mathrm{BYD}_{n.1}}$, $n \geq 0$
E	0.06	$^1\mathrm{H}_{\mathrm{MG}_n}$, $n \geq 2$ (end)
		$^n\mathrm{H}_{\mathrm{BYD}_{n.m}}$, $n \geq 2,\ m \geq 0$ (end)
F	0.09	$^1\mathrm{H}_{\mathrm{BYD}_{n.m}}$, $n \geq 2,\ m \geq 0$ (inner)
G	0.12	$^i\mathrm{H}_{\mathrm{MG}_n}$, $n \geq 3,\ n/2+1 > i \geq 2$ (middle)
		$^j\mathrm{H}_{\mathrm{BYD}_{n.m}}$, $n \geq 3,\ m \geq 0,\ n > j \geq 2$ (middle)

specific group matters. A more detailed discussion of the peak assignments has already been given in Ref. 10 or part A of the Supporting Information, so that here only an overview of the resulting peak assignments for the micro-mixer NMR probe is given in Tables 10 and 11.

The peak area fractions $\zeta_{\mathrm{BYD},1}$ and $\zeta_{\mathrm{BYD},2}$ were calculated and related to mole fractions of individual species, taking into account the number of hydrogen atoms that cause the corresponding signals:

$$\zeta_{\mathrm{BYD},1} = \frac{A_{\mathrm{B}}}{A_{\mathrm{A}}} = \frac{x_{\mathrm{BYD}_{1.1}} + \sum_{n=0}^{10} x_{\mathrm{BYD}_{n.1}}}{2 \cdot x_{\mathrm{BYD}_{0.0}} + \sum_{i=1}^{10} x_{\mathrm{BYD}_{i.0}}} \tag{48}$$

$$\zeta_{\mathrm{BYD},2} = \frac{A_{\mathrm{C}}}{A_{\mathrm{A}}} = \frac{\sum_{n=2}^{10} \sum_{m=0}^{10-n} x_{\mathrm{BYD}_{n.m}} + \sum_{n=2}^{5} x_{\mathrm{BYD}_{n.n}}}{2 \cdot x_{\mathrm{BYD}_{0.0}} + \sum_{i=1}^{10} x_{\mathrm{BYD}_{i.0}}} \tag{49}$$

In the system formaldehyde + water, cf. Figure 17b and Table 10, peak A* is the methylene signal obtained from MG_1. Peak B* contains the signals of the methylene groups at the chain ends of longer oligomers. Peak C* contains the methylene signals of the methylene groups that are not connected to hydroxyl groups.
The peak area fractions were calculated and related to mole fractions as follows:

$$\zeta_{A^*} = \frac{\zeta_{A^*}}{\zeta_{A^*} + \zeta_{B^*} + \zeta_{C^*}} = \frac{x_{MG_1}}{\sum_{n=1}^{10}(n \cdot x_{MG_n})} \tag{50}$$

$$\zeta_{B^*} = \frac{\zeta_{B^*}}{\zeta_{A^*} + \zeta_{B^*} + \zeta_{C^*}} = \frac{2 \cdot \sum_{n=2}^{10} x_{MG_n}}{\sum_{n=1}^{10}(n \cdot x_{MG_n})} \tag{51}$$

$$\zeta_{C^*} = 1 - \zeta_{A^*} - \zeta_{B^*} \quad = \frac{\sum_{n=3}^{10}((n-2) \cdot x_{MG_n})}{\sum_{n=1}^{10}(n \cdot x_{MG_n})} \tag{52}$$

4.7.3 Results for the system formaldehyde + water + butynediol obtained with the micro-mixer NMR probe

The numerical results of the 5 kinetic experiments in the system (formaldehyde + water + butynediol) that were carried out with the micro-mixer NMR probe are presented in the Supporting Information. Also plots showing $\zeta_{BYD,1}$ and $\zeta_{BYD,2}$ as a function of time for all experiments are given in the Supporting Information. The evaluation of these results was done as described in the previous section and the kinetic and equilibrium constants obtained from that evaluation are included in Table 9 well as in Figures 13 and 14. In general, they fit together well with the results obtained from the experiments in the sample tubes. The exception are the results for the equilibrium constant $K^x_{BYD,1}$ that are systematically below the results from the literature and those from the sample tube (cf. Figure 13a). A detailed analysis of these deviations has not been carried out as the main goal of the experiments was the determination of rate constants and the equilibrium constants are only a collateral result of the fit. It is not claimed that the micro-mixer NMR probe is a particularly useful instrument for measuring chemical equilibrium constants.

4.7.4 Results for the system formaldehyde + water obtained with the micro-mixer NMR probe

The micro-mixer NMR probe is useful for studying fast reaction kinetics. Therefore, it was used for experiments in the system formaldehyde + water at conditions where the reactions are so fast that no quantitative data on the reaction kinetics was available so far. In all experiments, aqueous formaldehyde solutions were diluted with water and the resulting shift of the oligomer distribution towards smaller oligomers was monitored.

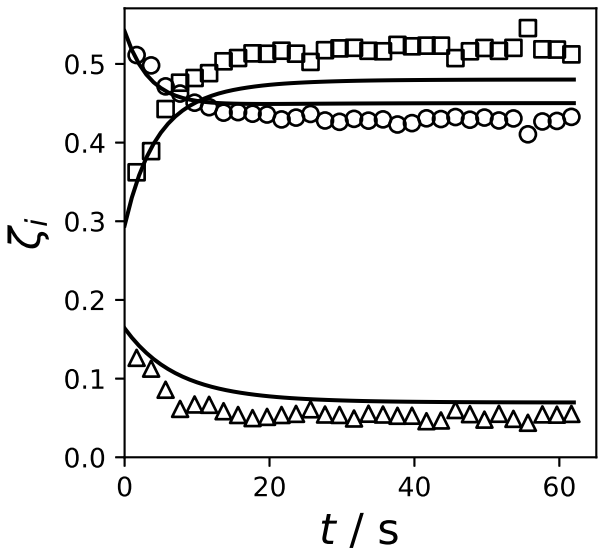

Figure 18: Results from a reaction kinetic experiment in the system formaldehyde + water carried out with the micro-mixer NMR probe. Dilution of a formaldehyde solution ($\tilde{x}_{\mathrm{FA}}^{(\mathrm{m})}$ = 0.3401 g g^{-1}) with water (mass ratio 1.1:1); T = 343 K, pH = 4.6. (□) ζ_{A^*}, (○) ζ_{B^*}, (△) ζ_{C^*}, (——) reaction kinetic model. The peak area fractions refer to signals of methylene groups in MG_1 (ζ_{A^*}), at the end of MG_n $n \geq 2$ (ζ_{B^*}) and in the middle of MG_n $n \geq 3$ (ζ_{C^*}).

The experiments were carried out as described in Section 4.7.1. The numerical results of the 10 kinetic experiments in the system formaldehyde + water are presented in the Supporting Information. An example for the results is presented in Figure 18, where the peak area fractions of methylene groups in MG_1 (ζ_{A^*}), at the end of MG_n $n \geq 2$ (ζ_{B^*}) and in the middle of MG_n $n \geq 3$ (ζ_{C^*}) are shown as a function of time. It is remarkable that good quantitative kinetic data could be obtained for a kinetic process with a time constant of the order of only 10 s. Additionally, Figure 18 shows the result of the converted model of Hahnenstein *et al.* [29]. The model describes the experimental data very well. Similar plots for the other experiments are presented in the Supporting Information.

The rate constants of the poly(oxymethylene) glycol formation, cf. Reaction (VI), obtained from the fits to the new experimental data are shown in Figure 19 where they are compared to experimental results from the literature as well as the model of Hahnenstein *et al.* [29]. It can be seen from Figure 19 that the new data substantially extend the range for which experimental reaction kinetic data in the system formaldehyde + water are available. It also becomes clear that the new data fully confirm the predictions by the model of Hahnenstein *et al.* [29] that was based on a fit to the other data shown in Figure 19. The new data is also in line with the previous data. This is also confirmed by

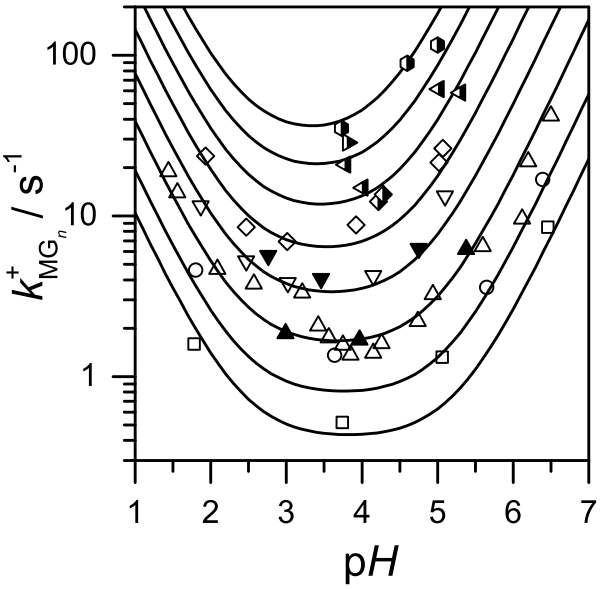

Figure 19: Rate constants for the formation of poly(oxymethylene) glycols using mole fractions. Empty and filled symbols are converted rate constants taken from Hahnenstein *et al.* [29]. Empty symbols: rate constants from density measurements. Filled symbols: rate constants from NMR measurements. Half-filled symbols: new measurements with micro-mixer NMR probe this work. (□) 275 K, (○) 283 K, (△) 293 K, (▽) 303 K, (◇) 313 K, (◁) 323 K, (▷) 333 K, (⬡) 343 K, (——) reaction kinetic model.

the results for 313 K, where data from the present work and from Hasse and Maurer [35] are available.

4.7.5 Conversion of parameters of models of the system formaldehyde + water

Hahnenstein *et al.* [29] have modeled the oligomerization reactions in the system formaldehyde + water not with monomeric formaldehyde as reacting species but have used methylene glycol instead. I.e., instead of Reaction (VI), the following reaction was used:

$$\mathrm{MG}_{n-1} + \mathrm{MG}_1 \underset{k^{-,*}_{\mathrm{MG}_n}}{\overset{k^{+,*}_{\mathrm{MG}_n}}{\rightleftharpoons}} \mathrm{MG}_n + \mathrm{W} \tag{IX}$$

For describing the chemical equilibria, both approaches are equivalent, and the equilibrium constants can be converted using Eq. (53):

$$K^x_{\mathrm{MG}_n} = K^{x,*}_{\mathrm{MG}_n} \cdot K^x_{\mathrm{MG}_1} \tag{53}$$

where $K^{x}_{\mathrm{MG}_n}$ is the equilibrium constant used in the present work and refers to Reaction (VI), $K^{x,*}_{\mathrm{MG}_n}$ is the equilibrium constant used by Hahnenstein *et al.* [29] and refers to Reaction (VI), and $K^{x}_{\mathrm{MG}_1}$ is the equilibrium constant of Reaction (V), which is the same in both models.

Not only the equilibrium model but also the kinetic models of Hahnenstein *et al.* [29] and that from the present work can be mapped onto each other assuming that the Reaction (V) is much faster than the other reactions and can be considered to be in equilibrium. For an equivalence of the two kinetic models, the following equation must be fulfilled:

$$k^{+,x,*}_{\mathrm{MG}_n} \cdot x_{\mathrm{MG}_{n-1}} \cdot x_{\mathrm{MG}_1} = k^{+,x}_{\mathrm{MG}_n} \cdot x_{\mathrm{FA}} \cdot x_{\mathrm{MG}_{n-1}} \tag{54}$$

Assuming that Reaction (V) is in equilibrium, one can find that:

$$k^{+,x}_{\mathrm{MG}_n} = k^{+,x,*}_{\mathrm{MG}_n} \cdot K^{x}_{\mathrm{MG}_1} \cdot x_{\mathrm{W}} \tag{55}$$

Taking into account that the experiments that were used for the parameterization of the model of Hahnenstein *et al.* [29] were carried out at comparatively low overall formaldehyde concentrations, Eq. (55) can be simplified further:

$$k^{+,x}_{\mathrm{MG}_n} \approx k^{+,x,*}_{\mathrm{MG}_n} \cdot K^{x}_{\mathrm{MG}_1} \tag{56}$$

Eq. (56) was used for the calculation of the kinetic constants of the present model $k^{+,x}_{\mathrm{MG}_n}$ as they are reported in Table 8 from those of the model of Hahnenstein *et al.* [29] $k^{+,x,*}_{\mathrm{MG}_n}$.

4.7.6 Kinetic experiment with ^{13}C-NMR spectroscopy

For testing the kinetic model developed in the present work, a single kinetic experiment was carried out in a test tube using quantitative $^{13}\mathrm{C}\{^{1}\mathrm{H}\}$-NMR spectroscopy with inverse gated decoupling, which yields spectra with much more structural information than the ^{1}H-NMR spectra - however at the expense of long acquisition times or signal to noise ratio. Therefore, this experiment was carried out at conditions, where the reaction kinetics are slow (293 K and pH 4). Acquisition parameters for this experiment were: acquisition time 2.5 s, relaxation delay ≥ 27.5 s, pulse width 65°, 2 scans per spectrum. The analysis of the spectra was similar as described in Section 2.3.5.

5 Conclusions

The occuring species in mixtures of formaldehyde, water, and butynediol were elucidated by NMR spectroscopy. Only poly(oxymethylene) glycols and poly(oxymethylene) hemiformals have been observed. Acetals or other condensation products were not found under the conditions of the performed experiments.

Two models were developed to describe the chemical equilibrium in these mixtures: one based on mole fractions and the other on activities. Quantitative ^{13}C-NMR spectra were the basis of the models. These models use two independent chemical equilibrium constants: one constant for the addition of an initially formaldehyde-free hydroxyl group of butynediol to formaldehyde and one constant for chain propagation reactions. The models are based on statistical considerations as butynediol contains two chemically identical hydroxyl groups. The activity-based model has also been used successfully in the second chapter to predict vapor-liquid equilibria without the need of fitting any parameters to the measured vapor-liquid equilibrium data from this work.

It was observed that the chemical equilibrium constants for the chain propagation reactions are all very similar regardless of the alcohol present in the hemiformal. This was the basis to start a general approach of modeling chemical equilibrium constants [38].

Free butynediol has a strong ability to bind formaldehyde into oligomers due to its two hydroxyl groups, which increase the probability of a successful reaction to form oligomers. The value of the chemical equilibrium constant for the reaction of formaldehyde and butynediol can be compared to that for the reaction of formaldehyde with methanol although from the homologous series of monoalcohols a decreasing ability can be observed [38].

These effects have an impact on the vapor-liquid behavior in the system. Long-chained oligomers are formed with high formaldehyde concentrations, while strongly bound formaldehyde is formed with high butynediol concentrations. High pressures and temperatures are required to shift the equilibrium towards monomeric formaldehyde for separation.

Finally, the model has been extended with expressions for the reaction kinetics of the oligomer formation reactions of formaldehyde with butynediol on the basis of ^{1}H-NMR

spectroscopic experiments. The developed model is compatible with a previous model of the reaction kinetics of formaldehyde with water and with methanol [29]. Despite the low resolution of components in the ^{1}H-NMR spectra compared to the ^{13}C-NMR spectra, the results of the model are remarkably good. The results presented here contribute to the data basis for developing a unified approach for describing reaction kinetics in formaldehyde solutions of water and alcohols, for which Kircher et al. [38] have recently laid the foundations by describing a unified equilibrium model. The extension of that model to reaction kinetics is still an open task to be tackled in future work.

The new micro-mixer NMR probe [9, 12, 13, 32] was found to be useful for reaction kinetic studies with time constants down to about 10 s. The ^{1}H-NMR spectra from this probe do not have the quality of spectra acquired with standard ^{1}H-NMR probes but are sufficient for a quantification, even in complex systems as the one studied here. In particular, this probe was also used for reaction kinetic experiments in the system formaldehyde + water, which extend the previously available data to faster processes. The new data confirm the reaction kinetic model of Hahnenstein *et al.* [29].

Literature

[1] M. Albert, B. Coto García, C. Kuhnert, R. Peschla, G. Maurer: Vapor-Liquid Equilibrium of Aqueous Solutions of Formaldehyde and Methanol, AIChE J. 46 (2000) 1676–1687. doi:10.1002/aic.690460818.

[2] M. Albert, B.C. García, C. Kreiter, G. Maurer: Vapor-Liquid and Chemical Equilibria of Formaldehyde-Water Mixtures, AIChE J. 45 (1999) 2024–2033. doi:10.1002/aic.690450919.

[3] M. Albert, I. Hahnenstein, H. Hasse, G. Maurer: Vapor-liquid equilibrium of formaldehyde mixtures: New data and model revision, AIChE J. 42 (1996) 1741–1752. doi:10.1002/aic.690420625.

[4] M. Albert, I. Hahnenstein, H. Hasse, G. Maurer: Vapor-Liquid and Liquid-Liquid Equilibria in Binary and Ternary Mixtures of Water, Methanol, and Methylal, J. Chem. Eng. Data 46 (2001) 897–903. doi:10.1021/je0003521.

[5] M. Albert, H. Hasse, C. Kuhnert, G. Maurer: New experimental results for the vapor-liquid equilibrium of the binary system (trioxane plus water) and the ternary system (formaldehyde plus trioxane plus water), J. Chem. Eng. Data 50 (2005) 1218–1223. doi:10.1021/je050015i.

[6] J. Aldrich: R. A. Fisher and the Making of Maximum Likelihood 1912-1922, Stat. Sci. 12 (1997) 162–176.

[7] C. Ammann, P. Meier, A. Merbach: A simple multinuclear NMR thermometer, J. Magn. Reson. 46 (1982) 319 – 321. doi:10.1016/0022-2364(82)90147-0.

[8] A. Balashov, S. Danov, V. Krasnov, A. Chernov, T. Ryabova: Association of Formaldehyde in Aqueous-Alcoholic Systems, Russ. J. Gen. Chem. 72 (2002) 744–747. doi:10.1023/A:1019512419592.

[9] R. Behrens, M. Dyga, G. Sieder, E. von Harbou, H. Hasse: NMR spectroscopic method for studying homogenous liquid phase reaction kinetics in systems used in reactive gas absorption and application to monoethanolamine-water-carbon dioxide, Chem. Eng. J. 374 (2019) 1127–1137. doi:10.1016/j.cej.2019.05.189.

[10] J. Berje, J. Baldamus, J. Burger, H. Hasse: NMR Spectroscopic Study of Chemical Equilibria in Solutions of Formaldehyde, Water, and Butynediol, AIChE J. 63 (2017) 4442–4450. doi:10.1002/aic.15788.

[11] Berufsgenossenschaft Rohstoffe und chemische Industrie (BG RCI): Datenblatt: 2-Butin-1,4-diol, 2016. URL: www.gischem.de.

[12] A. Brächer, R. Behrens, E. von Harbou, H. Hasse: Application of a new micro-reactor ^{1}H NMR probe head for quantitative analysis of fast esterification reactions, Chem. Eng. J. 306 (2016) 413 – 421. doi:10.1016/j.cej.2016.07.045.

[13] A. Brächer, S. Hoch, K. Albert, H. Kost, B. Werner, E. von Harbou, H. Hasse: Thermostatted micro-reactor NMR probe head for monitoring fast reactions, J. Magn. Reson. 242 (2014) 155 – 161. doi:10.1016/j.jmr.2014.02.013.

[14] S. Brandani, V. Brandani, G. Di Giacomo: The System Formaldehyde-Water-Methanol: Thermodynamics of Solvated and Associated Solutions, Ind. Eng. Chem. Res. 31 (1992) 1792–1798. doi:10.1021/ie00007a026.

[15] S. Brandani, V. Brandani, I. Tarquini: Vapor-Liquid Equilibrium of Formaldehyde Mixtures Containing Methanol, Ind. Eng. Chem. Res. 37 (1998) 3485–3489. doi:10.1021/ie980020y.

[16] C.F. Breitkreuz, J. Burger, H. Hasse: Solid-Liquid Equilibria and Kinetics of the Solid Formation in Binary and Ternary Mixtures Containing (Formaldehyde + Water + Methanol), Ind. Eng. Chem. Res. 61 (2022) 1871–1884. doi:10.1021/acs.iecr.1c04275.

[17] J. Burger, E. Ströfer, H. Hasse: Chemical Equilibrium and Reaction Kinetics of the Heterogeneously Catalyzed Formation of Poly(oxymethylene) Dimethyl Ethers from Methylal and Trioxane, Ind. Eng. Chem. Res. 51 (2012) 12751–12761. doi:10.1021/ie301490q.

[18] B. Coto, R. Peschla, C. Kreiter, G. Maurer: Reaction Kinetics in Liquid Mixtures of Formaldehyde and 1-Butanol from ^{13}C NMR Spectroscopy, Ind. Eng. Chem. Res. 42 (2003) 2934–2939. doi:10.1021/ie030119r.

[19] M. Detcheberry, P. Destrac, X.M. Meyer, J.S. Condoret: Phase equilibria of aqueous solutions of formaldehyde and methanol: Improved approach using UNIQUAC coupled to chemical equilibria, Fluid Phase Equilibr. 392 (2015) 84 – 94. doi:10.1016/j.fluid.2015.02.011.

[20] J.O. Drunsel, M. Renner, H. Hasse: Experimental study and model of reaction kinetics of heterogeneously catalyzed methylal synthesis, Chem. Eng. Res. Des. 90 (2012) 696–703. doi:10.1016/j.cherd.2011.09.014.

[21] M. Dyga, A. Keller, H. Hasse: ^{13}C-NMR Spectroscopic Study of the Kinetics of Formaldehyde Oligomerization Reactions in the System (Formaldehyde + Water + Isoprenol), Ind. Eng. Chem. Res. 61 (2022) 224–235. doi:10.1021/acs.iecr.1c03911.

[22] D. Emeis, W. Anker, K.P. Wittern: Quantitative C-13 NMR Spectroscopic Studies on the Equilibrium of Formaldehyde with Its Releasing Cosmetic Preservatives, Anal. Chem. 79 (2007) 2096–2100. doi:10.1021/ac0619985.

[23] R.A. Fisher: Theory of statistical estimation, Math. Proc. Cambridge 22 (1925) 700–725. doi:10.1017/S0305004100009580.

[24] Å. Fredenslund, R.L. Jones, J.M. Prausnitz: Group-Contribution Estimation of Activity Coefficients in Nonideal Liquid Mixtures, AIChE J. 21 (1975) 1086–1099. doi:10.1002/aic.690210607.

[25] L.H. Funderburk, L. Aldwin, W.P. Jencks: Mechanisms of general acid and base catalysis of the reactions of water and alcohols with formaldehyde, J. Am. Chem. Soc. 100 (1978) 5444–5459. doi:10.1021/ja00485a032.

[26] K.Z. Gaca, J.A. Parkinson, L. Lue, J. Sefcik: Equilibrium Speciation in Moderately Concentrated Formaldehyde-Methanol Water Solutions Investigated Using ^{13}C and ^{1}H Nuclear Magnetic Resonance Spectroscopy, Ind. Eng. Chem. Res. 53 (2014) 9262–9271. doi:10.1021/ie403252x.

[27] J. Gmehling, B. Kolbe, M. Kleiber, J. Rarey: Chemical Thermodynamics for Process Simulation, 1 ed., WILEY-VCH, Weinheim, 2012.

[28] J. Gmehling, P. Rasmussen, Å. Fredenslund: Vapor-Liquid Equilibria by UNIFAC Group Contribution. Revision and Extension. 2, Ind. Eng. Chem. Process Des. Dev. 21 (1982) 118–127. doi:10.1021/i200016a021.

[29] I. Hahnenstein, M. Albert, H. Hasse, C.G. Kreiter, G. Maurer: NMR Spectroscopic and Densimetric Study of Reaction Kinetics of Formaldehyde Polymer Formation in Water, Deuterium Oxide, and Methanol, Ind. Eng. Chem. Res. 34 (1995) 440–450. doi:10.1021/ie00041a003.

[30] I. Hahnenstein, H. Hasse, C.G. Kreiter, G. Maurer: ^{1}H- and ^{13}C-NMR Spectroscopic Study of Chemical Equilibria in Solutions of Formaldehyde in Water,

Deuterium Oxide, and Methanol, Ind. Eng. Chem. Res. 33 (1994) 1022–1029. doi:10.1021/ie00028a033.

[31] H.K. Hansen, P. Rasmussen, Å. Fredenslund, M. Schiller, J. Gmehling: Vapor-Liquid Equilibria by UNIFAC Group Contribution. 5. Revision and Extension, Ind. Eng. Chem. Res. 30 (1991) 2352–2355. doi:10.1021/ie00058a017.

[32] E. von Harbou, R. Behrens, J. Berje, A. Brächer, H. Hasse: Studying Fast Reaction Kinetics with Online NMR Spectroscopy, Chem. Ing. Tech. 89 (2017) 369–378. doi:10.1002/cite.201600068.

[33] H. Hasse: Dampf-Flüssigkeits-Gleichgewichte, Enthalpien und Reaktionskinetik in formaldehydhaltigen Mischungen, Ph.D. thesis, University of Kaiserslautern, Kaiserslautern, Germany, 1990.

[34] H. Hasse, I. Hahnenstein, G. Maurer: Revised vapor-liquid equilibrium model for multicomponent formaldehyde mixtures, AIChE J. 36 (1990) 1807–1814. doi:10.1002/aic.690361204.

[35] H. Hasse, G. Maurer: Kinetics of the poly(oxymethylene) glycol formation in aqueous formaldehyde solutions, Ind. Eng. Chem. Res. 30 (1991) 2195–2200. doi:10.1021/ie00057a022.

[36] R. Huang, J. Liu, S. Ji: Vapor-liquid equilibrium of water and butynediol at constant temperature, Huaxue Gongcheng 17 (1989) 64–68.

[37] É.J. Kibrik, O. Steinhof, G.D. Scherr, W.R. Thiel, H. Hasse: On-Line NMR Spectroscopic Reaction Kinetic Study of Urea- Formaldehyde Resin Synthesis, Ind. Eng. Chem. Res. 53 (2014) 12602–12613.

[38] R. Kircher, N. Schmitz, J. Berje, K. Münnemann, W.R. Thiel, J. Burger, H. Hasse: Generalized Chemical Equilibrium Constant of Formaldehyde Oligomerization, Ind. Eng. Chem. Res. 59 (2020) 11431–11440. doi:10.1021/acs.iecr.0c00974.

[39] L.V. Kogan: State of the Vapor Phase Above Solutions of Formaldehyde in Water and Methanol, Zhur. Prikl. Khim. 52 (1979) 2722–2725.

[40] E. Kriesten, F. Alsmeyer, A. Bardow, W. Marquardt: Fully automated indirect hard modeling of mixture spectra, Chemom. Intell. Lab. Syst. 91 (2008) 181 – 193. doi:10.1016/j.chemolab.2007.11.004.

[41] C. Kuhnert: Dampf-Flüssigkeits-Gleichgewichte in mehrkomponentigen formaldehydhaltigen Systemen, Ph.D. thesis, University of Kaiserslautern, Kaiserslautern, Germany, 2003.

[42] C. Kuhnert, M. Albert, S. Breyer, I. Hahnenstein, H. Hasse, G. Maurer: Phase Equilibrium in Formaldehyde Containing Multicomponent Mixtures: Experimental Results for Fluid Phase Equilibria of (Formaldehyde + (Water or Methanol) + Methylal)) and (Formaldehyde + Water + Methanol + Methylal) and Comparison with Predictions, Ind. Eng. Chem. Res. 45 (2006) 5155–5164. doi:10.1021/ie060131u.

[43] M. Maiwald, H. Fischer, M. Ott, R. Peschla, C. Kuhnert, C. Kreiter, G. Maurer, H. Hasse: Quantitative NMR Spectroscopy of Complex Liquid Mixtures: Methods and Results for Chemical Equilibria in Formaldehyde-Water-Methanol at Temperatures up to 383 K, Ind. Eng. Chem. Res. 42 (2003) 259–266. doi:10.1021/ie0203072.

[44] M. Maiwald, H.H. Fischer, Y.K. Kim, K. Albert, H. Hasse: Quantitative high-resolution on-line NMR spectroscopy in reaction and process monitoring, J. Magn. Reson. 166 (2004) 135 – 146. doi:10.1016/j.jmr.2003.09.003.

[45] M. Maiwald, T. Grützner, E. Ströfer, H. Hasse: Quantitative NMR spectroscopy of complex technical mixtures using a virtual reference: chemical equilibria and reaction kinetics of formaldehyde-water-1,3,5-trioxane, Anal. Bioanal. Chem. 385 (2006) 910–917. doi:10.1007/s00216-006-0477-3.

[46] G. Maurer: Vapor-Liquid Equilibrium of Formaldehyde- and Water-Containing Multicomponent Mixtures, AIChE J. 32 (1986) 932–948. doi:10.1002/aic.690320604.

[47] M. Ott: Reaktionskinetik und Destillation formaldehydhaltiger Mischungen, Ph.D. thesis, University of Kaiserslautern, Kaiserslautern, Germany, 2004.

[48] M. Ott, H.H. Fischer, M. Maiwald, K. Albert, H. Hasse: Kinetics of oligomerization reactions in formaldehyde solutions: NMR experiments up to 373 K and thermodynamically consistent model, Chem. Eng. Process. Process Intensif. 44 (2005) 653 – 660. doi:10.1016/j.cep.2003.07.004.

[49] M. Ott, H. Schoenmakers, H. Hasse: Distillation of formaldehyde containing mixtures: laboratory experiments, equilibrium stage modeling and simulation, Chem. Eng. Proces. 44 (2005) 687–694. doi:10.1016/j.cep.2003.09.011.

[50] R. Peschla, B.C. García, M. Albert, C. Kreiter, G. Maurer: Chemical equilibrium and liquid-liquid equilibrium in aqueous solutions of formaldehyde and 1-butanol, Ind. Eng. Chem. Res. 42 (2003) 1508–1516. doi:10.1021/ie020743o.

[51] E. Pyatnitsyna, M. El'chaninov, A. Savost'yanov: Procedures for Recovery of Crystalline 2-Butyne-1,4-diol from Industrial Aqueous Solutions and for Its Purification, Russ. J. Appl. Chem. 82 (2009) 1428–1430. doi:10.1134/S1070427209080205.

[52] W. Reppe: Äthinylierung III, Justus Liebigs Ann. Chem. 596 (1955) 25–38.

[53] M. Rivlin, U. Eliav, G. Navon: Nmr studies of the equilibria and reaction rates in aqueous solutions of formaldehyde, J. Phys. Chem. B 119 (2015) 4479–4487. doi:10.1021/jp513020y.

[54] R. Rowley, W. Wilding, J. Oscarson, Y. Yang, N. Zundel, T. Daubert, R. Danner: DIPPR Information and Data Evaluation Manager for the Design Institute for Physical Properties, Version 10.0.1, AIChE, 2016.

[55] N. Schmitz, J. Burger, H. Hasse: Reaction kinetics of the formation of poly(oxymethylene) dimethyl ethers from formaldehyde and methanol in aqueous solutions, Ind. Eng. Chem. Res. 54 (2015) 12553–12560. doi:10.1021/acs.iecr.5b04046.

[56] N. Schmitz, F. Homberg, J. Berje, J. Burger, H. Hasse: Chemical equilibrium of the synthesis of poly(oxymethylene) dimethyl ethers from formaldehyde and methanol in aqueous solutions, Ind. Eng. Chem. Res. 54 (2015) 6409–6417. doi:10.1021/acs.iecr.5b01148.

[57] M.I. Siling, B.Y. Akselrod: Spectrophotometric Determination of Equilibrium Constants of the Hydration and Protonation of formaldehyde, Russ. J. Phys. Chem. 42 (1968) 1479–1482.

[58] O. Steinhof, É.J. Kibrik, G. Scherr, H. Hasse: Quantitative and qualitative ^{1}H, ^{13}C, and ^{15}N NMR spectroscopic investigation of the urea-formaldehyde resin synthesis, Magn. Reson. Chem. 52 (2014) 138–162. doi:10.1002/mrc.4044.

[59] O. Steinhof, G. Scherr, H. Hasse: Investigation of the reaction of 1,3-dimethylurea with formaldehyde by quantitative on-line NMR spectroscopy: a model for the urea-formaldehyde system, Magn. Reson. Chem. 54 (2016) 457–476. doi:10.1002/mrc.4274.

[60] S. Ung, M.F. Doherty: Calculation of residue curve maps for mixtures with multiple equilibrium chemical reactions, Ind. Eng. Chem. Res. 34 (1995) 3195–3202. doi:10.1021/ie00037a003.

[61] J.F. Walker: Formaldehyde, ACS Monograph Series, 2 ed., Reinhold, New York, 1953.

[62] S. Widagdo, W.D. Seider: Journal review. azeotropic distillation, AIChE J. 42 (1996) 96–130. doi:10.1002/aic.690420110.

[63] R. Wittig, J. Lohmann, J. Gmehling: Vapor-Liquid Equilibria by UNIFAC Group Contribution. 6. Revision and Extension, Ind. Eng. Chem. Res. 42 (2003) 183–188. doi:10.1021/ie020506l.

Supporting Information

A Chemical equilibrium

A.1 Overall and true mole fractions

In this work overall mole fractions $\tilde{x}_i$ and true mole fractions x_i are used in the calculations. The overall mole fractions describe the composition neglecting the true species that occur in the system. The relation between overall and true mole fractions is as follows:

$$\tilde{x}_{\mathrm{FA}} = \frac{x_{\mathrm{FA}} + \sum_{i>0}(i \cdot x_{\mathrm{MG}_i}) + \sum_{i>0}\sum_{0\leq j\leq i}((i+j)\cdot x_{\mathrm{BYD}_{i.j}})}{s} \tag{57}$$

$$\tilde{x}_{\mathrm{W}} = \frac{x_{\mathrm{W}} + \sum_{i>0}(x_{\mathrm{MG}_i})}{s} \tag{58}$$

$$\tilde{x}_{\mathrm{BYD}} = \frac{x_{\mathrm{BYD}_{0.0}} + \sum_{i>0}\sum_{0\leq j\leq i}(x_{\mathrm{BYD}_{i.j}})}{s} \tag{59}$$

$$s = 1 + \sum_{i>0}(i \cdot x_{\mathrm{MG}_i}) + \sum_{i>0}\sum_{0\leq j\leq i}((i+j)\cdot x_{\mathrm{BYD}_{i.j}}) \tag{60}$$

A.2 Activity-based modeling

In the activity-based model, the chemical equilibrium constants are calculated not using mole fractions but activities a_i which are the product of the mole fractions x_i and the activity coefficients γ_i. The following equations replace Eqs. (1) to (4):

$$K^a_{\mathrm{MG}_1} = \frac{x_{\mathrm{MG}_1}}{x_{\mathrm{W}} \cdot x_{\mathrm{FA}}} \cdot \frac{\gamma_{\mathrm{MG}_1}}{\gamma_{\mathrm{W}} \cdot \gamma_{\mathrm{FA}}} \tag{61}$$

$$K^a_{\mathrm{MG}_n} = \frac{x_{\mathrm{MG}_n}}{x_{\mathrm{MG}_{n-1}} \cdot x_{\mathrm{FA}}} \cdot \frac{\gamma_{\mathrm{MG}_n}}{\gamma_{\mathrm{MG}_{n-1}} \cdot \gamma_{\mathrm{FA}}} \quad \text{for} \quad n \geq 2 \tag{62}$$

$$K^a_{n.0 \leftrightarrow n.1} = \frac{x_{\mathrm{BYD}_{n.1}}}{x_{\mathrm{BYD}_{n.0}} \cdot x_{\mathrm{FA}}} \cdot \frac{\gamma_{\mathrm{BYD}_{n.1}}}{\gamma_{\mathrm{BYD}_{n.0}} \cdot \gamma_{\mathrm{FA}}} \quad \text{for} \quad n \geq 0 \tag{63}$$

$$K^a_{n-1.m \leftrightarrow n.m} = \frac{x_{\mathrm{BYD}_{n.m}}}{x_{\mathrm{BYD}_{n-1.m}} \cdot x_{\mathrm{FA}}} \cdot \frac{\gamma_{\mathrm{BYD}_{n.m}}}{\gamma_{\mathrm{BYD}_{n-1.m}} \cdot \gamma_{\mathrm{FA}}} \quad \text{for} \quad n \geq 2 \wedge m \geq 0 \tag{64}$$

The constants $K^a_{\mathrm{MG}_1}$ and $K^a_{\mathrm{MG}_n}$ are adopted from Kuhnert *et al.* [42] who also give a UNIFAC [24] model of the activity coefficients γ_i. Parameters and details concerning the UNIFAC model are given in a following section. The interdependency of the constants $K^a_{n.0 \leftrightarrow n.1}$ and $K^a_{n-1.m \leftrightarrow n.m}$ is in full analogy to the mole fraction-based model according to Eqs. (8) to (13) using two independent constants $K^a_{\mathrm{BYD},1}$ and $K^a_{\mathrm{BYD},2}$ and a respective temperature function according to Eq. (24).

A.3 Conversion of chemical equilibrium constants for the reactions of formaldehyde + water

In the literature [2, 5, 8, 18, 26, 29, 30, 41–43, 45, 46, 50, 53, 61] commonly a condensation mechanism for the formation of poly(oxymethylene) glycols MG_n is used. This mechanism differs from the addition mechanism in Reactions I and II in the way that the chain propagation reactions are formed by the reaction of MG_{n-1} and MG_1:

$$\underbrace{\mathrm{CH_2O}}_{\mathrm{FA}} + \underbrace{\mathrm{H_2O}}_{\mathrm{W}} \overset{K_{\mathrm{MG}_1}}{\rightleftharpoons} \underbrace{\mathrm{HO(CH_2O)H}}_{\mathrm{MG}_1} \tag{X}$$

$$\underbrace{\mathrm{HO(CH_2O)H}}_{\mathrm{MG}_1} + \underbrace{\mathrm{HO(CH_2O)_{n-1}H}}_{\mathrm{MG}_{n-1}} \overset{K^*_{\mathrm{MG}_n}}{\rightleftharpoons} \underbrace{\mathrm{HO(CH_2O)_nH}}_{\mathrm{MG}_n} + \underbrace{\mathrm{H_2O}}_{\mathrm{W}} \tag{XI}$$

Ott [47] combined kinetic models for the systems formaldehyde + water and formaldehyde + methanol for the ternary system formaldehyde + water + methanol and showed that the addition mechanism gives better results for the modeling of reaction kinetics. The addition mechanism is selected for the later extension of the model by reaction kinetics. Since the literature [42] only gives the activity-based equilibrium constants for the condensation mechanism, they have to be converted as described by Ott [47].

The activity-based chemical equilibrium constant for the addition of water to formaldehyde $K^a_{\mathrm{MG}_1}$ in the liquid phase is calculated from the chemical equilibrium constant in the vapor phase $K^{\mathrm{vap}}_{\mathrm{MG}_1}$. These constants are linked by the extended Raoult's Law $p \cdot y_i = p^{\mathrm{s}}_i \cdot x_i \cdot \gamma_i$ according to

$$K^{\mathrm{vap}}_{\mathrm{MG}_1} = \frac{y_{\mathrm{MG}_1}}{y_{\mathrm{FA}} \cdot y_{\mathrm{W}}} \cdot \frac{p^{\ominus}}{p} \tag{65}$$

$$= K^{p,*}_{\mathrm{MG}_1} \cdot p^{\ominus} \tag{66}$$

$$= K^{a}_{\mathrm{MG}_1} \cdot \frac{p^{\mathrm{s}}_{\mathrm{MG}_1} \cdot p^{\ominus}}{p^{\mathrm{s}}_{\mathrm{FA}} \cdot p^{\mathrm{s}}_{\mathrm{W}}} \tag{67}$$

$K^{p,*}_{\mathrm{MG}_1}$ is taken from Kogan [39] and was also used in the works of Ott [47] and Kuhnert *et al.* [42]. The chemical equilibrium constants $K^a_{\mathrm{MG}_n}$ for the chain propagation reactions are calculated according to

$$K^a_{\mathrm{MG}_n} = K^{a,*}_{\mathrm{MG}_n} \cdot K^a_{\mathrm{MG}_1} \tag{68}$$

where $K^{a,*}_{\mathrm{MG}_n}$ is taken from Kuhnert *et al.* [42]. The correlations of the vapor pressures are given in Table 12.

Table 12: Vapor pressure of pure components according to $\ln(p^s_i/\mathrm{kPa}) = A_i + B_i/(T/\mathrm{K} + C_i) + D_i \cdot \ln(T/\mathrm{K}) + E_i \cdot (T/\mathrm{K})^{F_i}$.

component i	A_i	B_i	C_i	D_i	E_i	F_i
formaldehyde [42]	14.4625	-2204.13	-30.15	0	0	0
water [42]	16.2886	-3816.44	-46.13	0	0	0
methylene glycol [42]	17.4364	-4762.07	-51.21	0	0	0
butynediol [54]	136.6922	-16190.00	0	-16.119	$6.81 \cdot 10^{-18}$	6

A.4 Peak assignment

In the ^{1}H-NMR spectrum (see Figure 2, top), the peaks from 4.28 to 4.30 ppm result from methylene hydrogen next to triple-bonded carbon on a side where no addition to formaldehyde occurs, namely $\mathrm{H}^{\beta}_{\mathrm{BYD}_{n.0}}$ with $n \geq 0$. The main signals in this region are a singlet at 4.28 ppm which belongs to $\mathrm{BYD}_{0.0}$ and a triplet at 4.29 ppm with a ^5J-coupling constant of 1.8 Hz which belongs to $\mathrm{BYD}_{1.0}$. All $\mathrm{H}^{\beta}_{\mathrm{BYD}_{n.0}}$ signals with $n \geq 2$ are below this triplet but with lower intensities. All other signals of methylene hydrogen

next to the triple-bonded carbon are localized between 4.34 and 4.38 ppm. The triplet of ${}^{\beta}\mathrm{H}_{\mathrm{BYD}_{1.0}}$ is recognizable but not separated from other signals.

The signals of bound formaldehyde are found above 4.80 ppm on the top of a very broad water and hydroxyl signal. At 4.83 ppm the signal of ${}^{1}\mathrm{H}_{\mathrm{MG}_1}$ is located beside a signal of $\mathrm{H}^{1}_{\mathrm{BYD}_{n.1}}$ with $n \geq 0$ at 4.85 ppm. From 4.86 to 4.90 ppm the signals of ${}^{1}\mathrm{H}_{\mathrm{MG}_n}$ with $n \geq 2$, ${}^{n}\mathrm{H}_{\mathrm{BYD}_{n.m}}$ with $n \geq 2$, and $\mathrm{H}^{m}_{\mathrm{BYD}_{n.m}}$ with $m \geq 2$ are superimposed. These are methylene hydrogen signals of the outer CH_2O units which do not differentiate significantly whether water or butynediol added to formaldehyde. At 4.92 ppm a signal of $\mathrm{H}^{1}_{\mathrm{BYD}_{n.2}}$ with $n \geq 0$ is not fully separated from a signal of $\mathrm{H}^{1}_{\mathrm{BYD}_{n.m}}$ with $n \geq 0$ and $m \geq 3$. These signals arise from the CH_2O groups which are directly connected to butynediol and are not superimposed by signals of MG_n. The peaks from 4.93 to 4.96 ppm arise from the remaining methylene groups of formaldehyde oligomers both with water and with butynediol and cannot be clearly assigned.

The carbon spectrum shown in Figure 2 (bottom) shows no baseline distortion, in contrast to the hydrogen spectrum. Furthermore, much more signals are separated from each other in the ^{13}C-NMR spectrum as compared to the ^{1}H-NMR spectrum. In the high-field part of the spectrum from 52 to 58 ppm, signals of methylene carbon nuclei next to triple-bonded carbon $\mathrm{C}^{\beta}_{\mathrm{BYD}_{n.m}}$ $(n, m \geq 0)$ are found. Peaks appear in groups of three. The three peaks from 52.34 to 52.39 ppm are assigned to carbon nuclei of poly(oxymethylene) hemiformals with one unoccupied end, on the side where no CH_2O chains are present, namely $\mathrm{C}^{\beta}_{\mathrm{BYD}_{n.0}}$. The next three peaks from 56.76 to 56.83 ppm correspond to oligomers with one CH_2O group to one side and arbitrary numbers of CH_2O groups to the other side, $\mathrm{C}^{\beta}_{\mathrm{BYD}_{n.1}}$. This argument can be continued for the next peak groups. The distance between these groups decreases with increasing chain length as the carbon nuclei become less influenced by the outer CH_2O units. This results in the overlap of signals with four and more CH_2O units to one side. Inside these groups the number of CH_2O groups on the opposite side influences the chemical shift but the resolution is less due to the larger distance inside the molecule. In the group from 52.34 to 52.39 ppm the peaks correspond to $\mathrm{C}^{\beta}_{\mathrm{BYD}_{0.0}}$, $\mathrm{C}^{\beta}_{\mathrm{BYD}_{1.0}}$, and $\mathrm{C}^{\beta}_{\mathrm{BYD}_{n.0}}$ $(n \geq 2)$ with increasing field strength. The other peak groups are assigned analogously.

The peaks from 83 to 88 ppm almost exclusively arise from triple-bonded carbon nuclei. Only the highest peak in the spectrum at 84.81 ppm belongs to ${}^{1}\mathrm{C}_{\mathrm{MG}_1}$. Due to the fact that the distance to both formaldehyde chains in $\mathrm{BYD}_{n.m}$ is relatively short, the signals of the triple-bonded carbon nuclei are influenced by both sides. In this region of the spectrum the following molecules can be distinguished: $\mathrm{BYD}_{0.0}$ (peak a), $\mathrm{BYD}_{1.0}$ (b, c), $\mathrm{BYD}_{2.0}$ (d, e), $\mathrm{BYD}_{3.0}$ (f, g), $\mathrm{BYD}_{n.0}$ with $n \geq 4$ (very small next to d and e), $\mathrm{BYD}_{1.1}$ (h), $\mathrm{BYD}_{2.1}$ (i, j), $\mathrm{BYD}_{3.1}$ (k, l), and $\mathrm{BYD}_{n.1}$ with $n \geq 4$ (very small next to k and l).

The signal of $BYD_{2.2}$ can be seen between peaks n and h but due to the low signal to noise ratio it cannot be said if signals of other oligomers are superimposed.

All peaks above 88 ppm arise from bound formaldehyde. The signal of $^1C_{MG_2}$ is located at 88.27 ppm. At about 88.8 ppm two signals of $C^2_{BYD_{n.2}}$ ($n \geq 0$) and $^1C_{MG_3}$ (p) overlap. Signals of $C^m_{BYD_{n.m}}$ ($n \geq 0$, $m \geq 3$) and $^1C_{MG_n}$ ($n \geq 4$) from 89.06 to 89.10 ppm, which are also outer CH_2O units, are not separable from each other. These carbon nuclei which have at least one CH_2O group between the β-carbon are no more influenced by the chain length of the other side. While the β-carbon signals in the high-field part show a slight differentiation of the chain length to the opposite side (groups of three signals), it can be generally concluded that the chemical shift of signals from bound formaldehyde with a superscript above 1, namely $C^i_{BYD_{n.m}}$ ($n \geq 0$, $m \geq 2$, $i \geq 2$), is not influenced by the chain length of the opposite side. The first CH_2O carbon in the chain ($^1C_{BYD_{n.m}}$) can at least differentiate if there is a formaldehyde chain on the other side or not. The signals of $^1C_{BYD_{1.0}}$, $^1C_{BYD_{2.0}}$, and $^1C_{BYD_{3.0}}$ are at 89.82 (m), 93.00, and 93.56 ppm respectively. The signals with formaldehyde on the other side, namely $^1C_{BYD_{1.m}}$, $^1C_{BYD_{2.m}}$, and $^1C_{BYD_{3.m}}$ each are about 0.05 ppm in the low-field direction. The peaks ranging from 91.38 to 92.64 ppm belong to formaldehyde bound in chains both with water and butynediol and include all formaldehyde carbon which is bound in the middle of the chains.

A.5 UNIFAC groups and interaction parameters

The group assignment and the parameters for the calculation of activity coefficients with UNIFAC are shown in Tables 13 and 14 respectively. All values of the interaction parameters a_{ij}, the size parameters R_i, and the surface parameters Q_i with $i, j \leq 5$ were taken from Kuhnert *et al.* [42]. The extension of the formaldehyde + water system to include butynediol results in the addition of the C≡C group to the parameter matrix. Interaction parameters for the water group with the C≡C group ($a_{4,6}$ and $a_{6,4}$) were fitted to binary VLE data [36] in the system water + butynediol. The literature data and the fit results are shown in Figure 20. As proposed by Maurer [46], the methylene glycol group ($HO(CH_2O)H$) is assumed to behave like water so that

$$a_{5,6} = a_{4,6} \qquad a_{6,5} = a_{6,4} \tag{69}$$

All remaining UNIFAC parameters were taken from further literature [28, 31, 63].

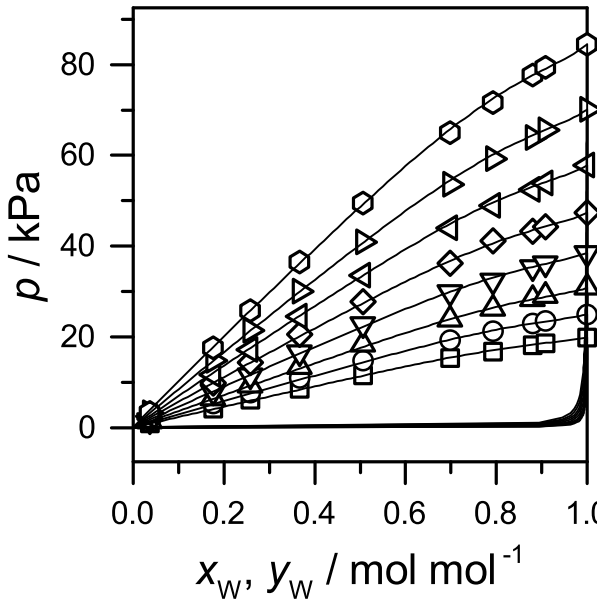

Figure 20: Experimental [36] and calculated vapor-liquid equilibrium in the system water + butynediol with new interaction parameters. (⬡) 368.15 K, (▷) 363.15 K, (◁) 358.15 K, (◇) 353.15 K, (▽) 348.15 K, (△) 343.15 K, (○) 338.15 K, (□) 333.15 K, (—) UNIFAC model.

A.6 Parameter fit and results

The chemical equilibrium constants $K^a_{\mathrm{BYD},1}$ and $K^a_{\mathrm{BYD},2}$ were fitted in full analogy to the mole fraction-based model for every single experiment. The temperature dependence of the equilibrium constants was regressed with Microsoft Excel according to Eq. (24) in a subsequent step. The results of the fitting are shown in Figure 21 and Table 15. The mean absolute percentage deviation (MAPD) of the temperature correlation to the single experiments are 5 % for $K^a_{\mathrm{BYD},1}$ and 8 % for $K^a_{\mathrm{BYD},2}$ which is comparable to the

Table 13: UNIFAC interaction parameters a_{ij} / K for the system formaldehyde + water + butynediol.

i \ j	1	2	3	4	5	6
1	0	28.06	156.4	353.5	353.5	727.8 [a]
2	237.7	0	83.36	867.8	189.21	-156.57 [b]
3	986.5	251.5	0	1318	1318	298.9 [c]
4	-229.1	-254.51	300	0	189.52	88.35 [d]
5	-229.1	59.2	300	-191.82	0	88.35 [d]
6	68.95 [a]	173.77 [b]	-72.88 [c]	321.52 [d]	321.52 [d]	0

[a] Hansen *et al.* [31] [b] Wittig *et al.* [63] [c] Gmehling *et al.* [28]
[d] this work

Table 14: UNIFAC group assignment with size (R_i) and surface (Q_i) parameters. [42]

group number	1	2	3	4	5	6
group i	OH	CH_2O	CH_2	H_2O	$HO(CH_2O)H$	C≡C
R_i	1	0.9183	0.6744	0.92	2.674	1.0613 [a]
Q_i	1.2	0.78	0.54	1.4	2.94	0.784 [a]
FA		1				
W				1		
BYD	2		2			1
MG_1					1	
MG_n	2	$n-1$	1			
$BYD_{n,m}$	2	$n+m$	2			1

[a] Gmehling *et al.* [28]

results of the mole fraction-based model. The uncertainty in $K^a_{\mathrm{BYD},1}$ and $K^a_{\mathrm{BYD},2}$ is estimated to be in the same order as $K^x_{\mathrm{BYD},1}$ and $K^x_{\mathrm{BYD},2}$ (25 % and 75 % respectively between 293 K and 393 K).

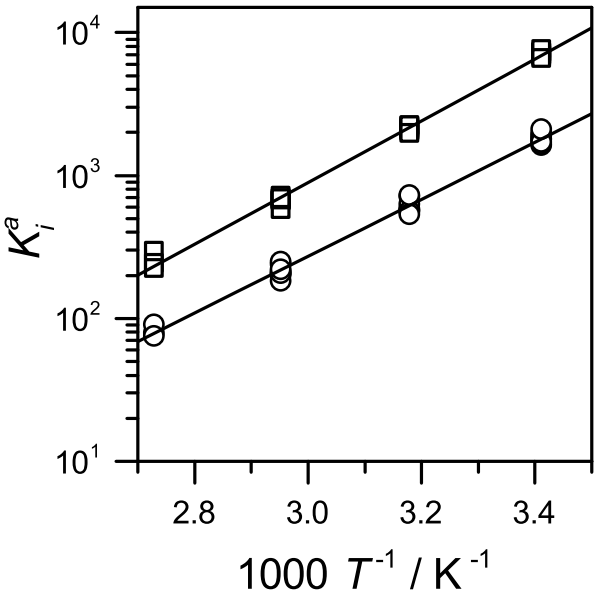

Figure 21: Chemical equilibrium constants from parameter fittings: (□) $K^a_{\mathrm{BYD},1}$, (∘) $K^a_{\mathrm{BYD},2}$, (——) temperature dependent fit.

Figures 22a and b show the peak area ratios obtained from the correlations for $K^a_{\mathrm{BYD},1}$ and $K^a_{\mathrm{BYD},2}$ over the corresponding experimental peak area ratios. The MAPD of the calculated to the experimental peak area ratios are 5 % for $\zeta_{\mathrm{BYD}_{1.0}}$, 7 % for $\zeta_{\mathrm{BYD}_{2.0}}$, 20 % for $\zeta_{\mathrm{BYD}_{3.0}}$, 8 % for $\zeta_{\mathrm{BYD}_{1.1}}$, 11 % for $\zeta_{\mathrm{BYD}_{2.1}}$, 17 % for $\zeta_{\mathrm{BYD}_{3.1}}$, 6 % for ζ_{MG_1}, 9 % for ζ_{MG_2}, and 17 % for ζ_{MG_3} respectively.

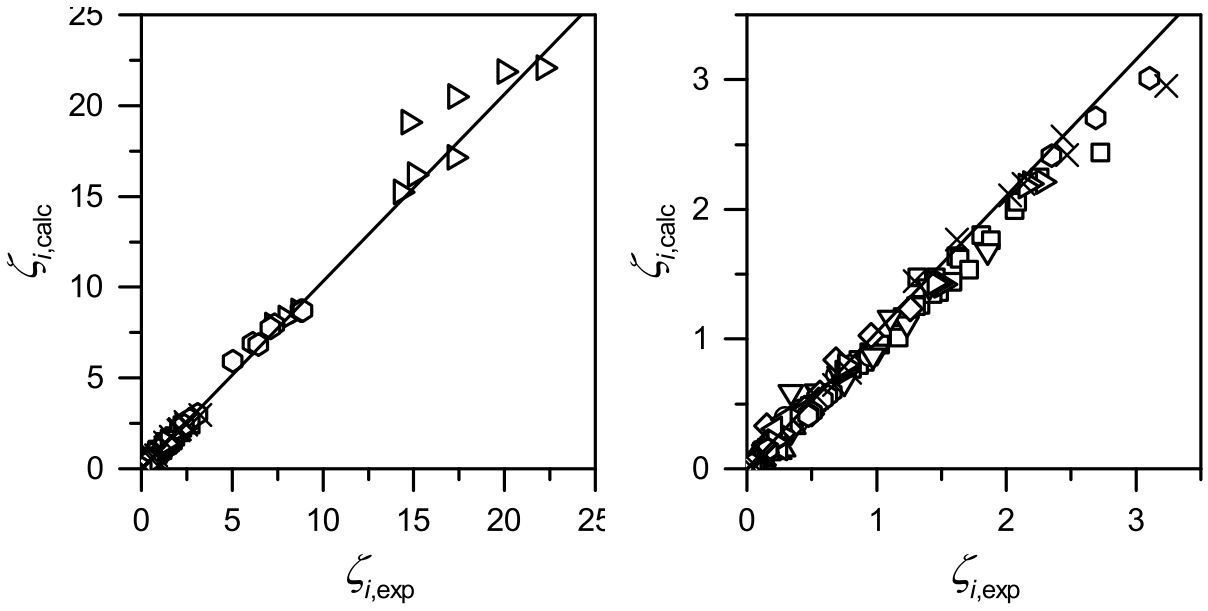

(a) **(b)**

Figure 22: Calculated vs. experimental peak area ratios. (□) $BYD_{1.0}$, (○) $BYD_{2.0}$, (△) $BYD_{3.0}$, (▽) $BYD_{1.1}$, (◇) $BYD_{2.1}$, (◁) $BYD_{3.1}$, (▷) MG_1, (⬡) MG_2, (×) MG_3. (b) Zoom of (a).

Table 15: Parameters for the calculation of chemical equilibrium constants for the system formaldehyde + water + butynediol according to Eq. (24).

	A	B	Ref.
$K^{p,*}_{MG_1}$	-16.984	5233.2	[39]
$K^{a,*}_{MG_2}$	$5.019 \cdot 10^{-3}$	834.5	[42]
$K^{a,*}_{MG_n}$	$1.312 \cdot 10^{-2}$	542.1	[42]
$K^{a}_{BYD,1}$	-8.136	4977.6	this work
$K^{a}_{BYD,2}$	-8.161	4589.4	this work

In the mole fraction-based approach it could be shown that the chemical equilibrium constants for chain propagation reactions are the same for all studied alcohols. This agreement is slightly disturbed when using the activity-based approach. At 293 K values of $K^{a}_{MG_n}$ = 1475, $K^{a}_{ME_n}$ = 2845, and $K^{a}_{BYD,2}$ = 1797 are obtained for the chain propagation reactions in the systems formaldehyde + water [42], formaldehyde + methanol [42], and formaldehyde + butynediol (this work) respectively. A better agreement could probably be obtained by adjusting the parameters of the UNIFAC model. Since there are several degrees of freedom, i.e. parameters that were not fitted to formaldehyde containing systems, left, it is probably possible to improve the agreement while not deteriorating the description of the vapor-liquid equilibrium.

B Reaction Kinetics

B.1 Experimental results of the tube experiments in the system formaldehyde + water + butynediol

Table 16 gives an overview of the conditions of the reaction kinetic experiments in the system formaldehyde + water + butynediol carried out in the NMR tubes. The numerical data for the time-dependent peak area fractions is given in an Excel file in the electronic part of the SI. Figures 23 to 38 show the results for $\zeta_{\mathrm{BYD},1}$ and $\zeta_{\mathrm{BYD},2}$ according to Eqs. (45) and (46) for all experiments except for experiment T4 shown in Figure 12 of the main part.

B.2 Experimental results of the micro-mixer experiments in the system formaldehyde + water + butynediol

Table 17 gives an overview of the conditions of the reaction kinetic experiments in the system formaldehyde + water + butynediol carried out with the micro-mixer probe. The numerical data for the time-dependent peak area fractions is given in an Excel file in the electronic part of the SI. Figures 39 to 43 show the results for $\zeta_{\mathrm{BYD},1}$ and $\zeta_{\mathrm{BYD},2}$ according to Eqs. (48) and (49) for all experiments.

B.3 Experimental results of the micro-mixer experiments in the system formaldehyde + water

Table 18 gives an overview of the conditions of the reaction kinetic experiments in the system formaldehyde + water carried out with the micro-mixer probe. The numerical data for the time-dependent peak area fractions is given in an Excel file in the electronic

part of the SI. Figures 44 to 52 show the results for ζ_{A^*}, ζ_{B^*}, and ζ_{C^*} according to Eqs. (50) to (52) for all experiments except for experiment FAW10 shown in Figure 18 of the main part.

Table 16: Conditions of the reaction kinetic experiments in the system formaldehyde + water + butynediol carried out in the NMR tubes.

Experiment	T / K	pH	$\tilde{x}_{\mathrm{FA}}^{(\mathrm{m})}$	$\tilde{x}_{\mathrm{BYD}}^{(\mathrm{m})}$	mass ratio (FA solution : BYD solution)
T1	293.15	4.8	0.3367	0.5998	2.327
T2		3.514			2.332
T3		3.283			2.292
T4		4.717			2.278
T5		3.09			2.289
T6		4.35			2.275
T7	303.15	3.54	0.3393	0.6686	2.395
T8		4.87		0.6656	2.323
T9		4.53		0.6667	2.403
T10	313.15	4.5		0.6656	2.358
T11		3.88			2.290
T12		3.33			2.352
T13	323.15	4.36			2.329
T14		3.3			2.303
T15		3.04			2.325
T16	328.15	3.32			2.315
T17		4.29			2.321

Table 17: Conditions of the reaction kinetic experiments in the system formaldehyde + water + butynediol carried out in the micro-mixer probe.

Experiment	T / K	pH	$\tilde{x}_{\mathrm{FA}}^{(\mathrm{m})}$	$\tilde{x}_{\mathrm{BYD}}^{(\mathrm{m})}$	mass ratio (FA solution : BYD solution)
M1	313.15	3.61	0.3274	0.6734	2.323
M2		4.2			
M3		5.864	0.3384		2.329
M4	323.15	4.5	0.3274		2.325
M5		5.755	0.3384		2.330

Table 18: Conditions of the reaction kinetic experiments in the system formaldehyde + water carried out in the micro-mixer probe.

Experiment	T / K	pH	$\tilde{x}_{\mathrm{FA}}^{(\mathrm{m})}$	mass ratio (FA solution : dilution)
FAW1	313.15	4.22	0.3401	1.104
FAW2		4.28		
FAW3	323.15	3.78		1.106
FAW4		4.01		
FAW5		5.02		
FAW6		5.3	0.3274	1.101
FAW7	333.15	3.81	0.3401	1.107
FAW8	343.15	3.73		
FAW9		4.6		
FAW10		5		

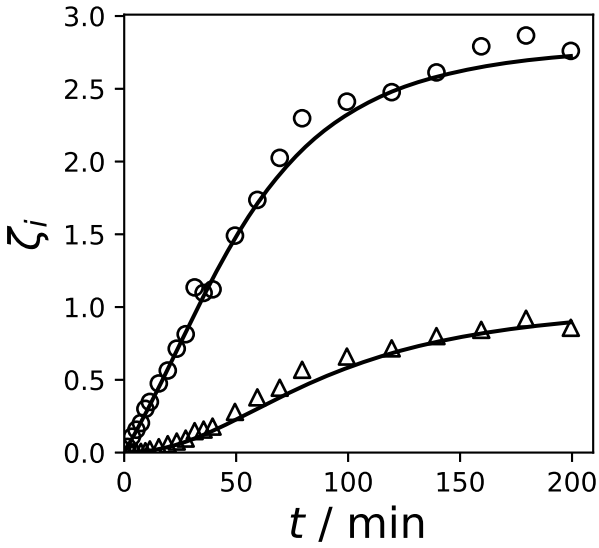

Figure 23: Experimental and calculated peak area fractions after mixing an equilibrated formaldehyde solution with aqueous butynediol. Conditions cf. Table 16 (T1) (∘) $\zeta_{\mathrm{BYD},1}$, (△) $\zeta_{\mathrm{BYD},2}$, (——) reaction kinetic model.

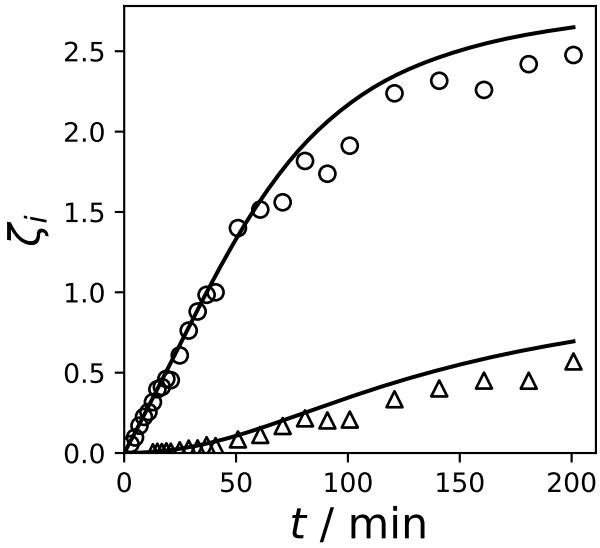

Figure 24: Experimental and calculated peak area fractions after mixing an equilibrated formaldehyde solution with aqueous butynediol. Conditions cf. Table 16 (T2) (∘) $\zeta_{\mathrm{BYD},1}$, (△) $\zeta_{\mathrm{BYD},2}$, (——) reaction kinetic model.

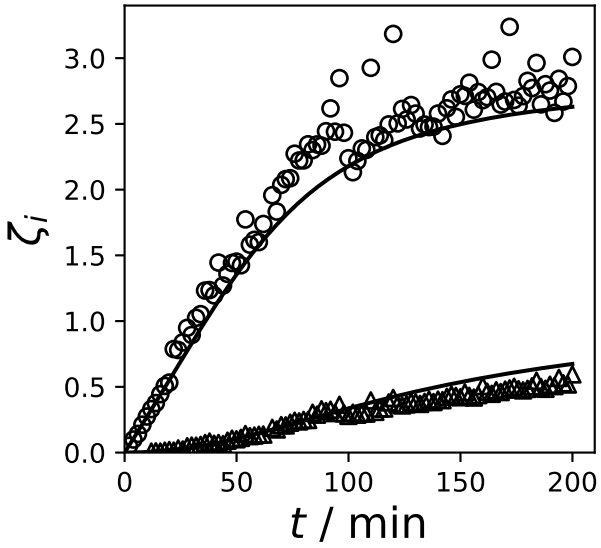

Figure 25: Experimental and calculated peak area fractions after mixing an equilibrated formaldehyde solution with aqueous butynediol. Conditions cf. Table 16 (T3) (∘) $\zeta_{\mathrm{BYD},1}$, (△) $\zeta_{\mathrm{BYD},2}$, (——) reaction kinetic model.

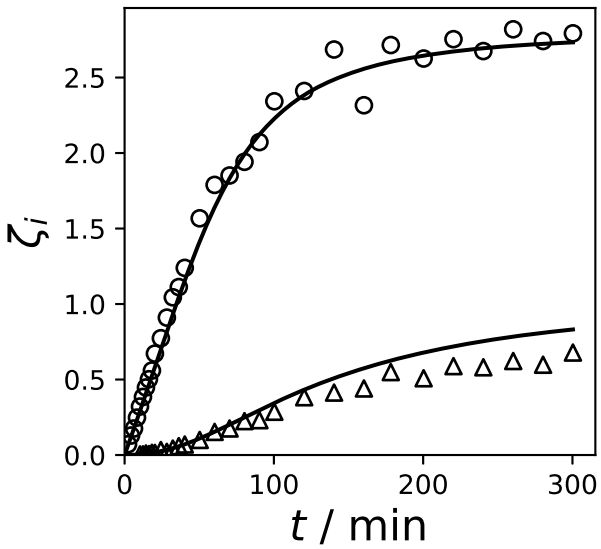

Figure 26: Experimental and calculated peak area fractions after mixing an equilibrated formaldehyde solution with aqueous butynediol. Conditions cf. Table 16 (T5) (∘) $\zeta_{\mathrm{BYD},1}$, (△) $\zeta_{\mathrm{BYD},2}$, (——) reaction kinetic model.

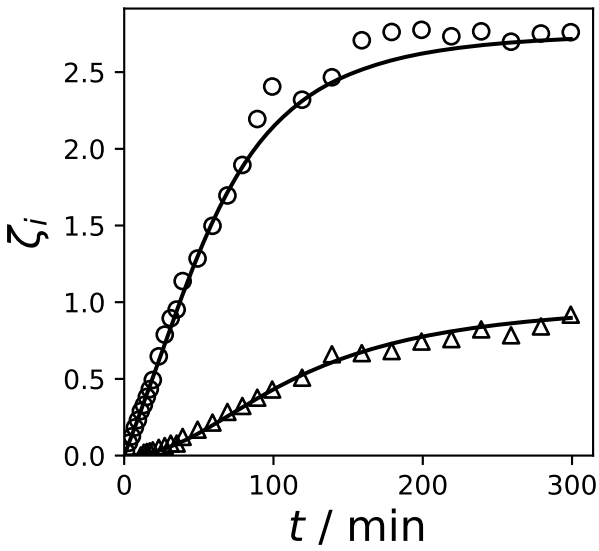

Figure 27: Experimental and calculated peak area fractions after mixing an equilibrated formaldehyde solution with aqueous butynediol. Conditions cf. Table 16 (T6) (∘) $\zeta_{\mathrm{BYD},1}$, (△) $\zeta_{\mathrm{BYD},2}$, (——) reaction kinetic model.

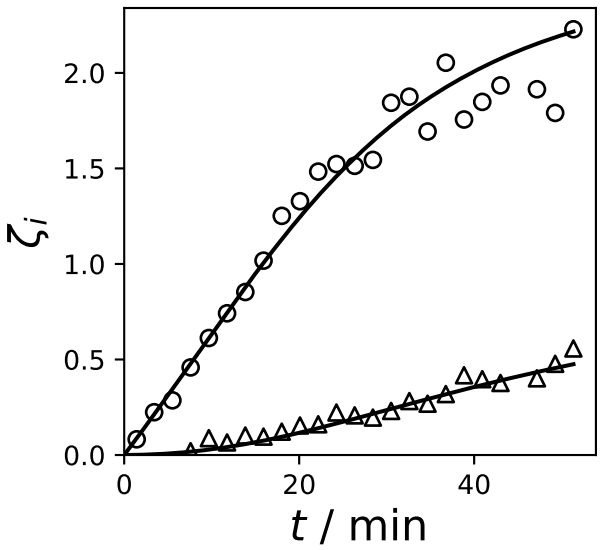

Figure 28: Experimental and calculated peak area fractions after mixing an equilibrated formaldehyde solution with aqueous butynediol. Conditions cf. Table 16 (T7) (∘) $\zeta_{\mathrm{BYD},1}$, (△) $\zeta_{\mathrm{BYD},2}$, (——) reaction kinetic model.

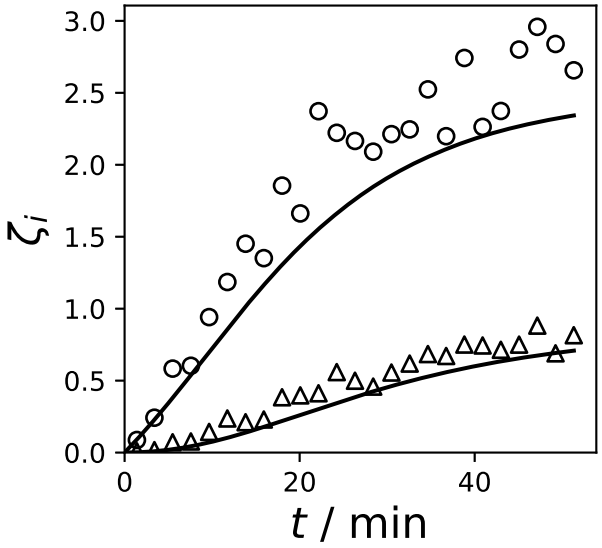

Figure 29: Experimental and calculated peak area fractions after mixing an equilibrated formaldehyde solution with aqueous butynediol. Conditions cf. Table 16 (T8) (∘) $\zeta_{\mathrm{BYD},1}$, (△) $\zeta_{\mathrm{BYD},2}$, (——) reaction kinetic model.

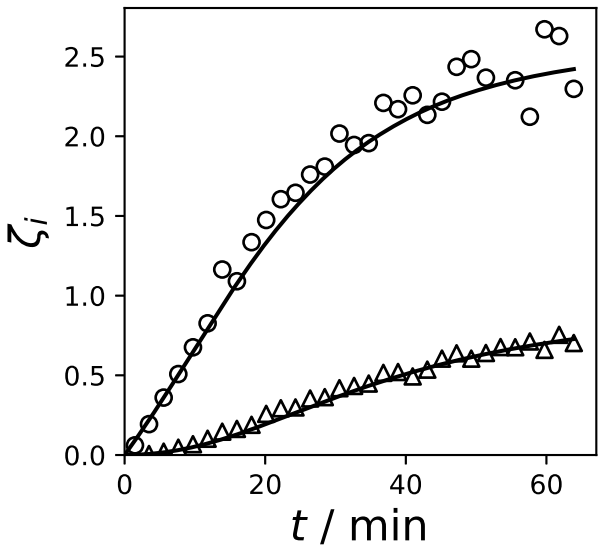

Figure 30: Experimental and calculated peak area fractions after mixing an equilibrated formaldehyde solution with aqueous butynediol. Conditions cf. Table 16 (T9) (∘) $\zeta_{\mathrm{BYD},1}$, (△) $\zeta_{\mathrm{BYD},2}$, (——) reaction kinetic model.

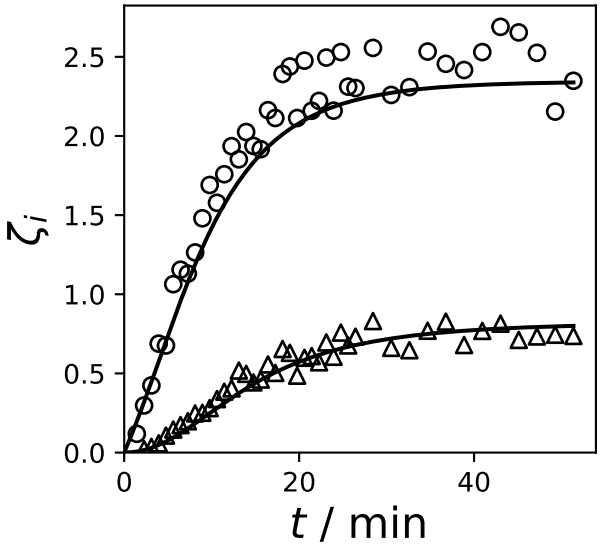

Figure 31: Experimental and calculated peak area fractions after mixing an equilibrated formaldehyde solution with aqueous butynediol. Conditions cf. Table 16 (T10) (∘) $\zeta_{\mathrm{BYD},1}$, (△) $\zeta_{\mathrm{BYD},2}$, (——) reaction kinetic model.

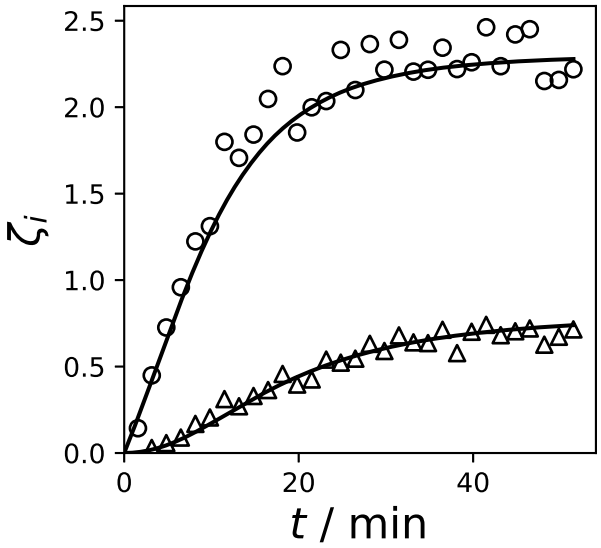

Figure 32: Experimental and calculated peak area fractions after mixing an equilibrated formaldehyde solution with aqueous butynediol. Conditions cf. Table 16 (T11) (∘) $\zeta_{\mathrm{BYD},1}$, (△) $\zeta_{\mathrm{BYD},2}$, (——) reaction kinetic model.

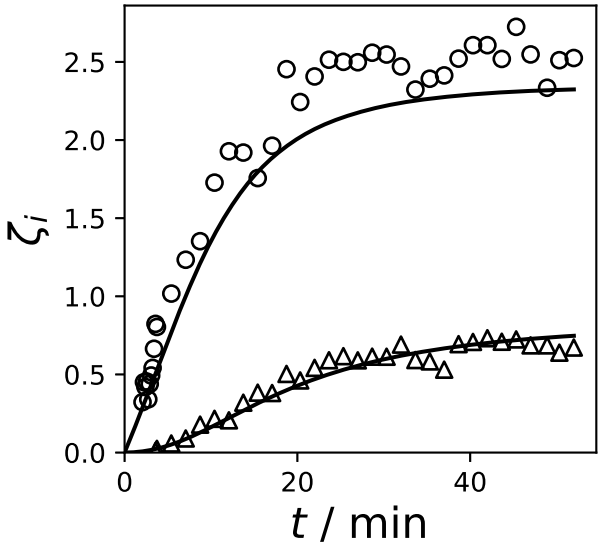

Figure 33: Experimental and calculated peak area fractions after mixing an equilibrated formaldehyde solution with aqueous butynediol. Conditions cf. Table 16 (T12) (∘) $\zeta_{\mathrm{BYD},1}$, (△) $\zeta_{\mathrm{BYD},2}$, (——) reaction kinetic model.

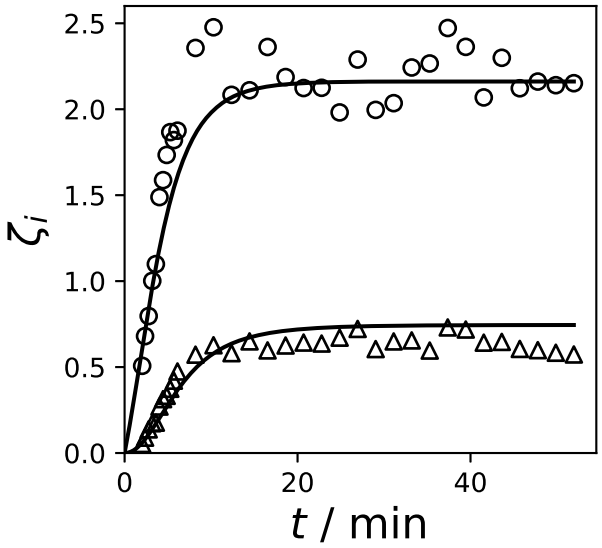

Figure 34: Experimental and calculated peak area fractions after mixing an equilibrated formaldehyde solution with aqueous butynediol. Conditions cf. Table 16 (T13) (∘) $\zeta_{\mathrm{BYD},1}$, (△) $\zeta_{\mathrm{BYD},2}$, (——) reaction kinetic model.

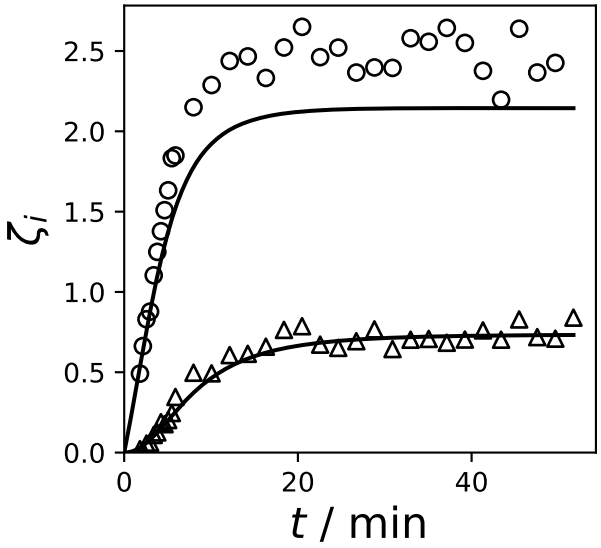

Figure 35: Experimental and calculated peak area fractions after mixing an equilibrated formaldehyde solution with aqueous butynediol. Conditions cf. Table 16 (T14) (∘) $\zeta_{\mathrm{BYD},1}$, (△) $\zeta_{\mathrm{BYD},2}$, (——) reaction kinetic model.

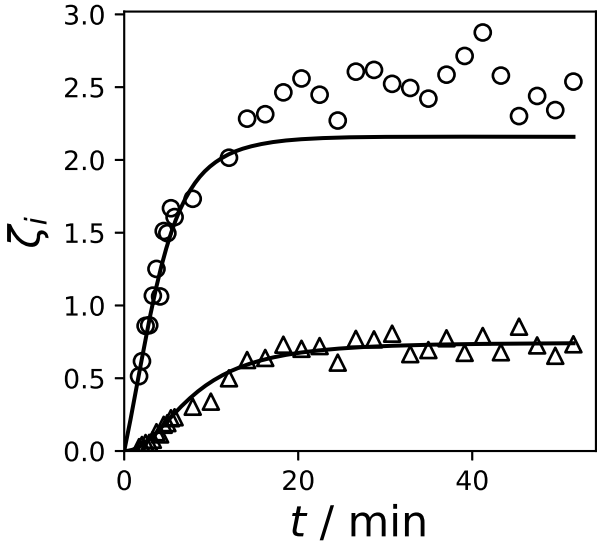

Figure 36: Experimental and calculated peak area fractions after mixing an equilibrated formaldehyde solution with aqueous butynediol. Conditions cf. Table 16 (T15) (∘) $\zeta_{\mathrm{BYD},1}$, (△) $\zeta_{\mathrm{BYD},2}$, (——) reaction kinetic model.

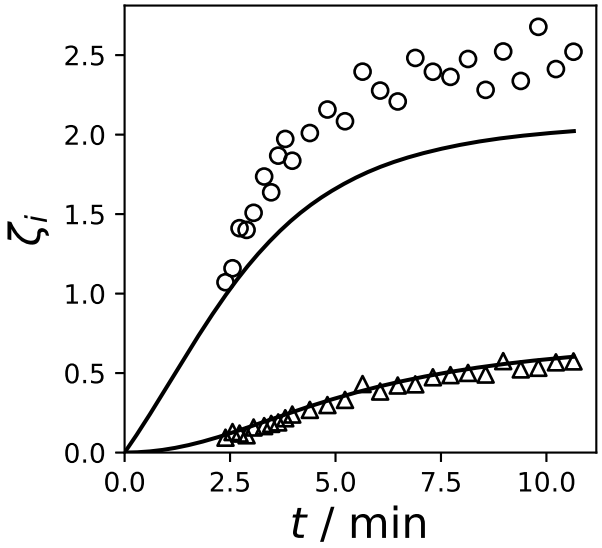

Figure 37: Experimental and calculated peak area fractions after mixing an equilibrated formaldehyde solution with aqueous butynediol. Conditions cf. Table 16 (T16) (∘) $\zeta_{\mathrm{BYD},1}$, (△) $\zeta_{\mathrm{BYD},2}$, (——) reaction kinetic model.

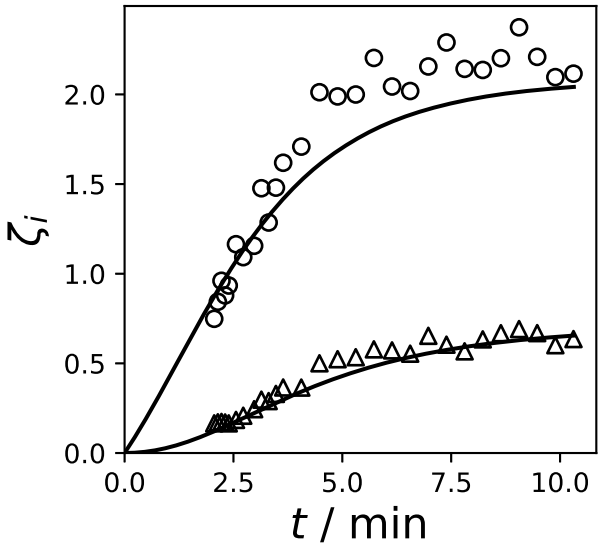

Figure 38: Experimental and calculated peak area fractions after mixing an equilibrated formaldehyde solution with aqueous butynediol. Conditions cf. Table 16 (T17) (∘) $\zeta_{\mathrm{BYD},1}$, (△) $\zeta_{\mathrm{BYD},2}$, (——) reaction kinetic model.

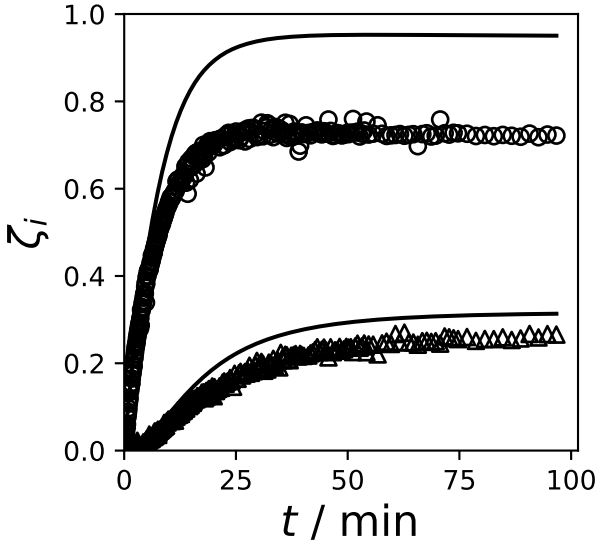

Figure 39: Experimental and calculated peak area fractions after mixing an equilibrated formaldehyde solution with aqueous butynediol. Conditions cf. Table 17 (M1) (∘) $\zeta_{\mathrm{BYD},1}$, (△) $\zeta_{\mathrm{BYD},2}$, (——) reaction kinetic model.

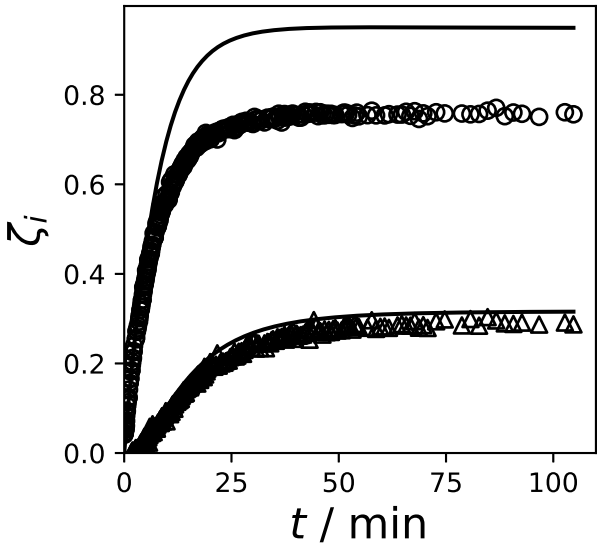

Figure 40: Experimental and calculated peak area fractions after mixing an equilibrated formaldehyde solution with aqueous butynediol. Conditions cf. Table 17 (M2) (∘) $\zeta_{\mathrm{BYD},1}$, (△) $\zeta_{\mathrm{BYD},2}$, (——) reaction kinetic model.

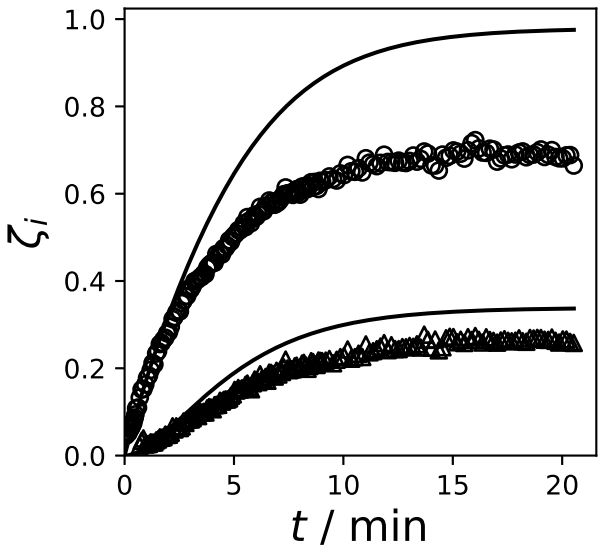

Figure 41: Experimental and calculated peak area fractions after mixing an equilibrated formaldehyde solution with aqueous butynediol. Conditions cf. Table 17 (M3) (∘) $\zeta_{\mathrm{BYD},1}$, (△) $\zeta_{\mathrm{BYD},2}$, (——) reaction kinetic model.

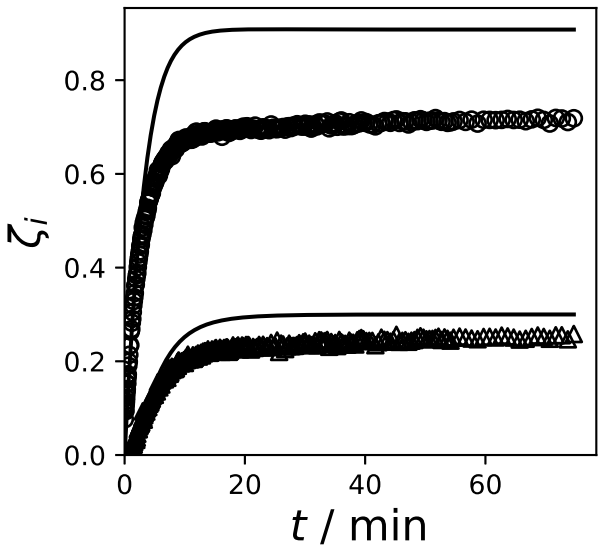

Figure 42: Experimental and calculated peak area fractions after mixing an equilibrated formaldehyde solution with aqueous butynediol. Conditions cf. Table 17 (M4) (∘) $\zeta_{\mathrm{BYD},1}$, (△) $\zeta_{\mathrm{BYD},2}$, (——) reaction kinetic model.

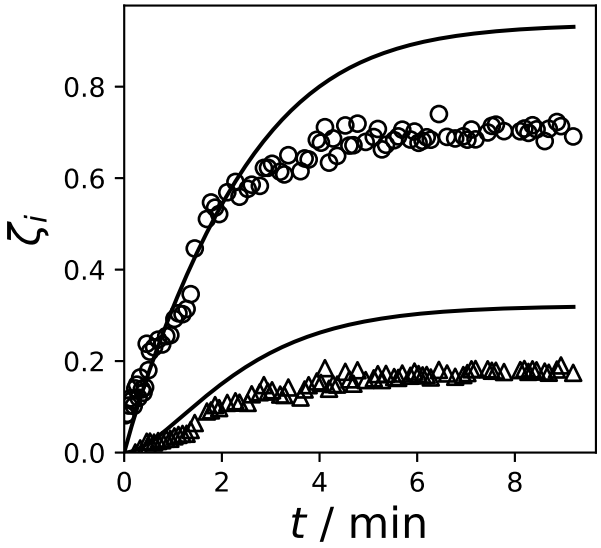

Figure 43: Experimental and calculated peak area fractions after mixing an equilibrated formaldehyde solution with aqueous butynediol. Conditions cf. Table 17 (M5) (∘) $\zeta_{\mathrm{BYD,1}}$, (△) $\zeta_{\mathrm{BYD,2}}$, (——) reaction kinetic model.

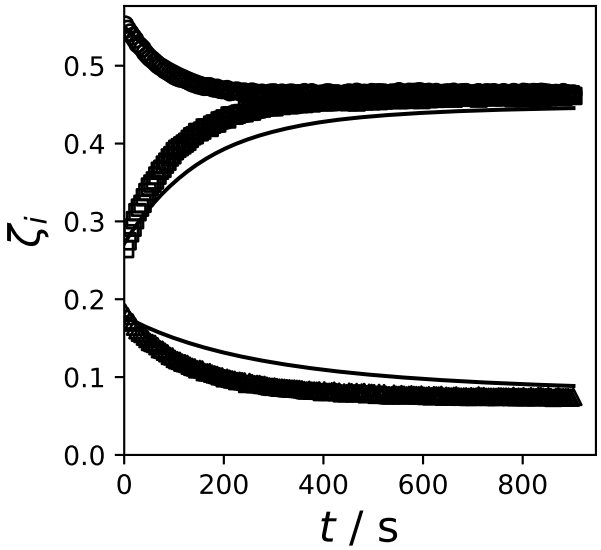

Figure 44: Experimental and calculated peak area fractions after mixing an equilibrated formaldehyde solution with aqueous butynediol. Conditions cf. Table 18 (FAW1) (□) ζ_{A^*}, (∘) ζ_{B^*}, (△) ζ_{C^*}, (——) reaction kinetic model.

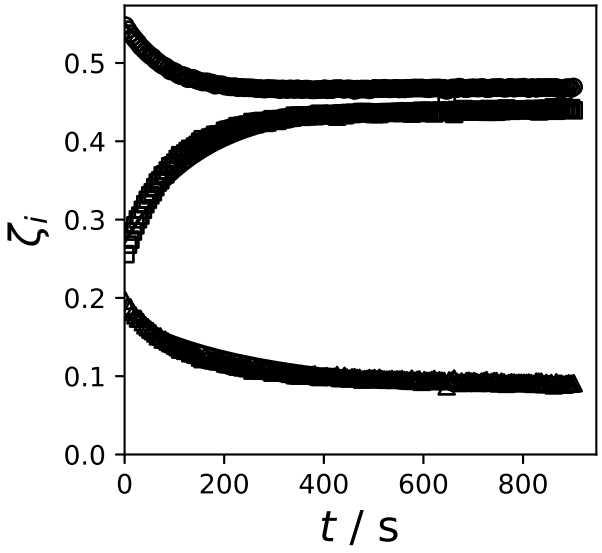

Figure 45: Experimental and calculated peak area fractions after mixing an equilibrated formaldehyde solution with aqueous butynediol. Conditions cf. Table 18 (FAW2) (□) ζ_{A^*}, (∘) ζ_{B^*}, (△) ζ_{C^*}, (——) reaction kinetic model.

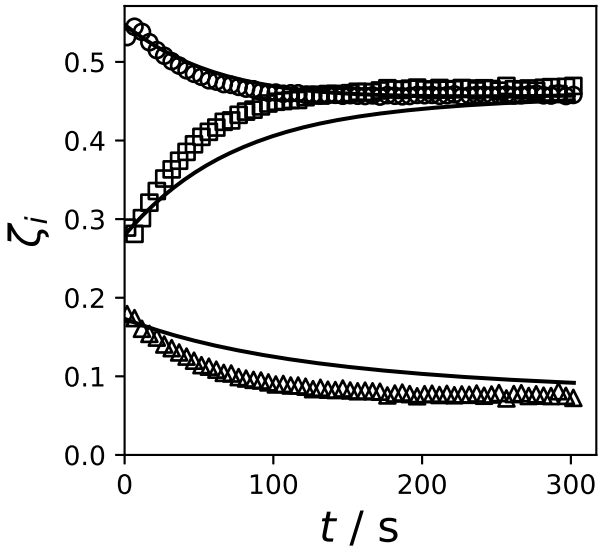

Figure 46: Experimental and calculated peak area fractions after mixing an equilibrated formaldehyde solution with aqueous butynediol. Conditions cf. Table 18 (FAW3) (□) ζ_{A^*}, (∘) ζ_{B^*}, (△) ζ_{C^*}, (——) reaction kinetic model.

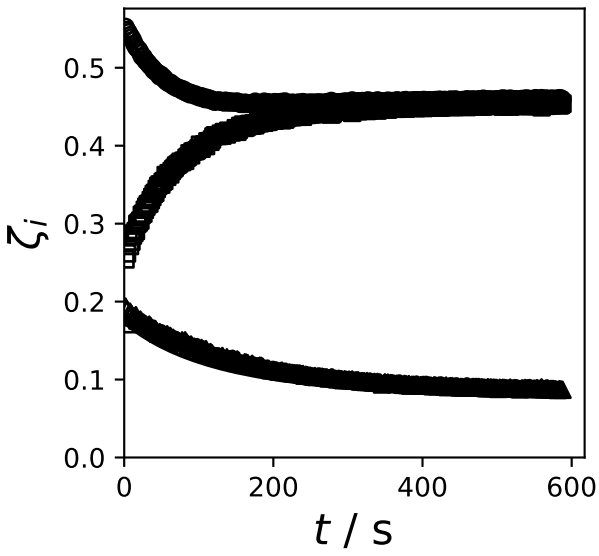

Figure 47: Experimental and calculated peak area fractions after mixing an equilibrated formaldehyde solution with aqueous butynediol. Conditions cf. Table 18 (FAW4) (□) ζ_{A^*}, (∘) ζ_{B^*}, (△) ζ_{C^*}, (——) reaction kinetic model.

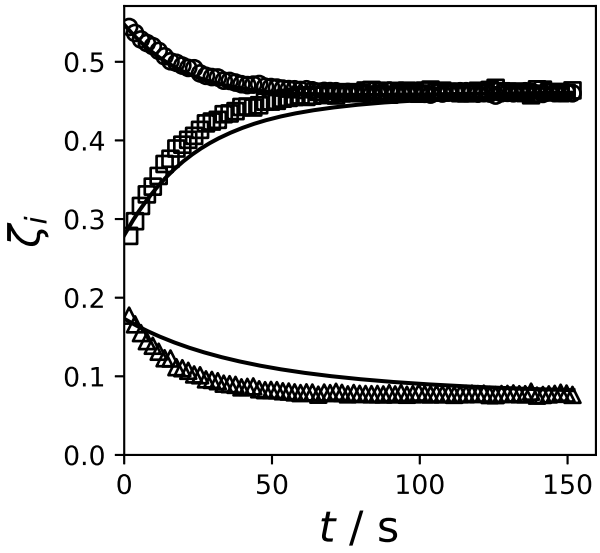

Figure 48: Experimental and calculated peak area fractions after mixing an equilibrated formaldehyde solution with aqueous butynediol. Conditions cf. Table 18 (FAW5) (□) ζ_{A^*}, (∘) ζ_{B^*}, (△) ζ_{C^*}, (——) reaction kinetic model.

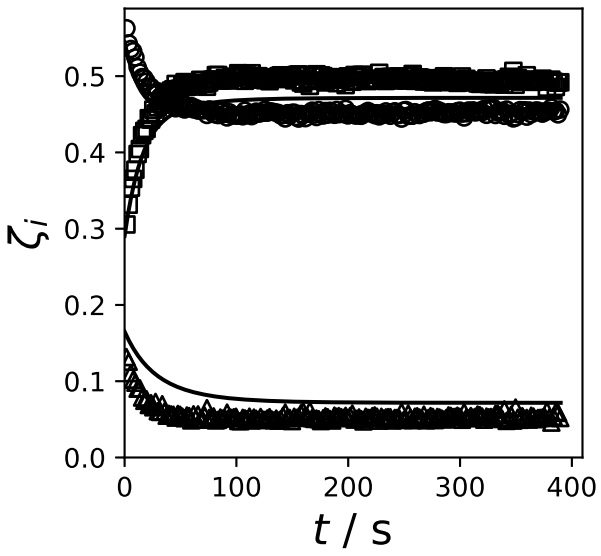

Figure 49: Experimental and calculated peak area fractions after mixing an equilibrated formaldehyde solution with aqueous butynediol. Conditions cf. Table 18 (FAW6) (□) ζ_{A^*}, (∘) ζ_{B^*}, (△) ζ_{C^*}, (——) reaction kinetic model.

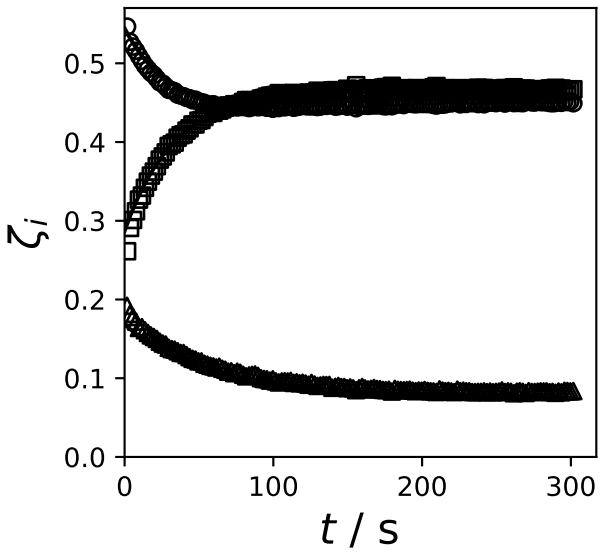

Figure 50: Experimental and calculated peak area fractions after mixing an equilibrated formaldehyde solution with aqueous butynediol. Conditions cf. Table 18 (FAW7) (□) ζ_{A^*}, (∘) ζ_{B^*}, (△) ζ_{C^*}, (——) reaction kinetic model.

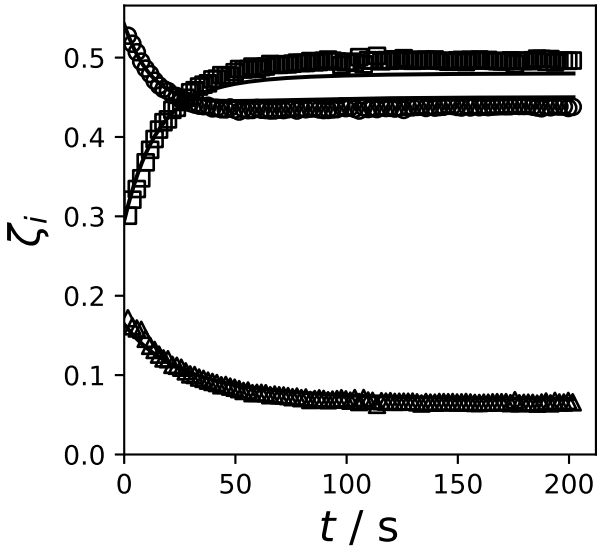

Figure 51: Experimental and calculated peak area fractions after mixing an equilibrated formaldehyde solution with aqueous butynediol. Conditions cf. Table 18 (FAW8) (□) ζ_{A^*}, (∘) ζ_{B^*}, (△) ζ_{C^*}, (——) reaction kinetic model.

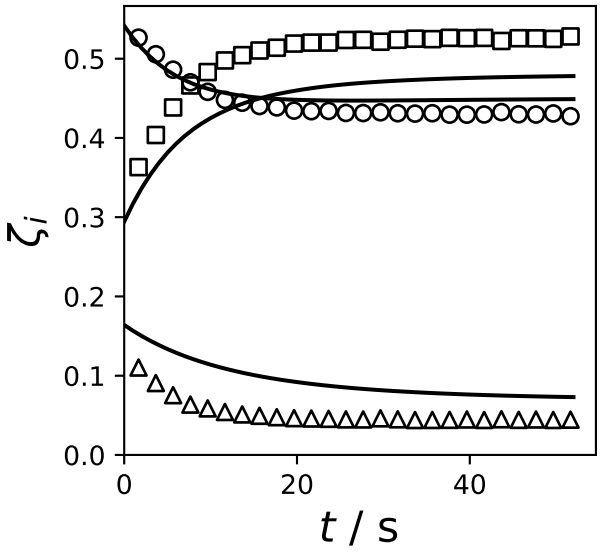

Figure 52: Experimental and calculated peak area fractions after mixing an equilibrated formaldehyde solution with aqueous butynediol. Conditions cf. Table 18 (FAW9) (□) ζ_{A^*}, (∘) ζ_{B^*}, (△) ζ_{C^*}, (——) reaction kinetic model.

Declaration

This dissertation contains material that has been published previously or that is included in submitted publications. In the following, these publications are listed together with a statement on the contributions of the author of the present dissertation.

- Berje, J., Baldamus, J., Burger, J., Hasse, H.: NMR Spectroscopic Study of Chemical Equilibria in Solutions of Formaldehyde, Water, and Butynediol. AIChE Journal 63 (10), 4442–4450 (2017)

  The author performed the experiments, developed the model and wrote the manuscript.

- Berje, J., Baldamus, J., Burger, J., Hasse, H.: Vapor-Liquid Equilibrium of Mixtures Containing Formaldehyde, Water, and Butynediol. Fluid Phase Equilibria 490 (30), 101–106 (2019)

  The author launched the thin-film evaporator after its set-up and performed or supervised the experiments and residue curve calculations, developed the predictive model and wrote the manuscript.

- Berje, J., Brächer, A., Baldamus, J., Burger, J., Hasse, H.: NMR Spectroscopic Study of Reaction Kinetics in Mixtures of Formaldehyde, Water, and Butynediol. *submitted*

  The author performed the tube experiments and supervised the experiments with the micro-mixer probe, developed the reaction kinetic model and wrote the manuscript.

Student theses

The following student theses were prepared under the supervision of the author of the present doctoral thesis in the frame of his research:

- Kolano, M.: Konzeptioneller Verfahrensentwurf der destillativen Trennung von Gemischen aus Formaldehyd, Wasser und Butindiol, Diploma thesis, Laboratory of Engineering Thermodynamics (LTD), University of Kaiserslautern (2014).
- Urich, N.: Experimentelle Untersuchung des Dampf-Flüssigkeits Gleichgewichts im System Formaldehyd + Wasser + Butindiol, Research project thesis, Laboratory of Engineering Thermodynamics (LTD), University of Kaiserslautern (2015).
- Krüger, N.: Experimentelle Untersuchung der Reaktionskinetik im System Formaldehyd + Wasser + Butindiol, Research project thesis, Laboratory of Engineering Thermodynamics (LTD), University of Kaiserslautern (2016).

Curriculum vitae

Name:	Jürgen Berje
Birth place:	Bremerhaven
Nationality:	German

Education

1992 – 1996	Grundschule Stotel
1996 – 1998	Orientierungsstufe Loxstedt
1998 – 2002	Gymnasium Loxstedt
2002 – 2005	Gymnasium Wesermünde
	Degree: Allgemeine Hochschulreife

Civilian service

2005 – 2006	Gemeinde Loxstedt

Academical education

2006 – 2009	Carl von Ossietzky Universität Oldenburg
	Major: Chemistry
	Degree: Bachelor of Science (B. Sc.)
2009 – 2012	Carl von Ossietzky Universität Oldenburg
	Major: Chemistry
	Degree: Master of Science (M. Sc.)

Professional activity

2012 – 2016	Research assistant
	Laboratory of Engineering Thermodynamics
	Technical University of Kaiserslautern
	Prof. Dr.-Ing. Hans Hasse
Since 2017	Chemical engineer
	Evonik Industries AG, Hanau (DE)